THE ASTROPHYSICAL JOURNAL SUPPLEMENT SERIES, 32:233–282, 1976 October

THE STRUCTURE OF SUPERNOVA SHOCK WAVES*†

THOMAS A. WEAVER
University of California Lawrence Livermore Laboratory; and
Physics Department, University of California, Berkeley
Received 1975 October 21; revised 1976 February 13

CONTENTS

ABSTRACT

The structure of strong shock waves is calculated over the range of shock energies (1 to 100 MeV nucleon^{-1}) and initial number densities (10^{15}–10^{22} cm^{-3}) believed likely to occur in the red-giant-like envelopes of stars undergoing Type II supernova explosions. These calculations were motivated by the proposal of Colgate and Hoyle and Fowler that the ions in such shocks could be heated to temperatures in excess of 10 MeV by hard ion-ion collisions, resulting in the spallation of helium and the subsequent formation of sufficient deuterium via neutron capture to account for the presently observed abundance, without recourse to its formation in a low-density big bang.

The general equations governing the structure of such shocks are developed on the basis of a plasma composed of ions, electrons, positrons, and photons, making use of diffusion theory to evaluate the dissipative and transfer terms. The present treatment differs from previous calculations in that the effects of radiation transport on the energy and momentum balance in the shock are taken into account, as well as the relativistic contributions to radiative emission rates due to nondipole electron-ion bremsstrahlung, electron-electron bremsstrahlung, and radiative Compton scattering. An implicit treatment of inverse Compton scattering is also developed in terms of the creation and diffusion of effective photons.

Several models of strong shock structure are formulated and solved on the basis of these equations and physical processes. First, a shock model dominated by radiation pressure and transport is considered, and criteria for its self-consistency are deduced. In particular, radiative heat transport is shown to be a sufficient shock-dissipation mechanism even for nonequilibrium radiation fields, provided that the ratio of radiation to matter pressure in the region of the final shock compression exceeds 4.45. This criterion is found to hold over the entire regime of interest, thus avoiding the necessity of the shock being mediated by hard ion-ion collisions. This fact, combined with the high rates of radiative emission and inverse Compton upscattering of the large reservoir of low-energy bremsstrahlung protons, results in peak ion temperatures approximately two orders of magnitude below those possible in a shock mediated by hard ion-ion collisions.

* Based on a portion of a Ph.D. thesis submitted to the Physics Department, University of California, Berkeley.

† Work performed in part under the auspices of the U.S. ERDA, W-7405-ENG-48.

Specifically, peak electron temperatures remain below ~ 70 keV for shock energies $\lesssim 30$–50 MeV nucleon^{-1}, depending on the initial density, while shocks with energies $\lesssim 1$ MeV nucleon^{-1} are found to be in nearly complete radiative equilibrium.

For electron temperatures above ~ 70 keV, the $\gamma\gamma \leftrightarrow e^+e^-$ reaction is found to give rise to a sufficient number of pairs to cause the principal source of shock dissipation to shift from radiative heat transport to ion-lepton Coulomb friction. The properties of such a pair-dominated model are discussed, and it is argued that the peak shock temperatures remain below ~ 200 MeV for shock energies below 100 MeV nucleon^{-1}.

The role of viscosity in supernova shock waves is examined in the context of a sequence of shock-structure models that become progressively more realistic and complex. The final general model includes the effects of ion viscosity, electron heat conduction, and multiple ion species, as well as an accurate treatment of the radiation field. The resulting shock structures agree with the previous radiation diffusion-dominated solutions to within 3–5 percent, and are shown to be stable. Hot, ion viscosity-mediated shocks, produced by artificially lowering radiative emission rates one hundredfold, are shown to relax to cool radiation-dominated shocks when these rates are returned to normal. It is concluded that a cosmologically significant amount of deuterium is unlikely to be produced in supernova shock waves.

The applications of these concepts and results to the problems of cosmic-ray composition, neutron star accretion, and protogalaxy formation are briefly considered.

Subject headings: plasmas — shock waves — stars: supernovae

I. INTRODUCTION

It is sufficient in most cases of physical and astrophysical interest to treat a shock as a discontinuous transition, since, in general, the final postshock state is uniquely determined by the preshock conditions, *independent* of the details of the dissipation mechanism involved (Zel'dovich and Raizer 1966). Exceptions can occur, however, if nonequilibrium processes (e.g., nuclear reactions or radiation or neutrino loss) take place within the shock that cannot be relaxed in the final postshock state, and in these cases a detailed shock-structure calculation is necessary.

The structure of strong shocks thus plays an important role in a variety of astrophysical situations, including the proposed production of deuterium and cosmic rays in supernova explosions (Colgate 1974; Colgate and Johnson 1960), the radiation spectrum resulting from the accretion of matter onto a neutron star (Alme and Wilson 1973; Zel'dovich and Shakura 1969), and the formation of protogalaxies in the early universe (Silk 1974).

In this study we shall deal primarily with the question of whether the shocks traversing the extended outer envelopes ($\sim 10^{12}$–10^{13} cm in radius) postulated for Type II supernovae (Shklovsky 1968) can reach sufficiently high temperatures to cause deuterium, boron, and other light elements to be produced via nuclear spallation and subsequent neutron capture as Colgate (1973, 1974, 1975*a*) and Hoyle and Fowler (1973) have predicted. They postulate that as the shock formed in the mantle of a star undergoing a supernova explosion moves down the steep density gradient at the mantle's edge, it is accelerated to energies in excess of 10 MeV nucleon^{-1} and gradually increases in strength as it traverses the extended envelope at densities $\sim 10^{-4}$ to 10^{-7} g cm^{-3}. Since the details of supernova hydrodynamics are not fully understood, we will examine the structure of such shocks over a very broad range of initial densities (10^{15}–10^{22} cm^{-3}) and initial energies (1–100 MeV nucleon^{-1}) to determine if the ion temperatures of $\gtrsim 10$ MeV needed for deuterium production, or those of $\gtrsim 1$ MeV required for the production of other light elements, can in fact occur. A brief account of a portion of this calculation was given in Weaver and Chapline (1974).

The magnitude of the shock temperature that will occur is principally determined by the degree of equilibration of the radiation field. If no radiation is present in the shock, the only dissipation mechanism capable of generating the amount of entropy required by the Hugoniot relations for a strong shock (Zel'dovich and Raizer 1966) is ion viscosity. This results in a shock a few ion-ion mean free paths thick in which "hard" ion-ion collisions transform the kinetic energy of the incoming ions (in the frame of the postshock material) directly into ion thermal energy. The hot ions then heat the electrons by Coulomb friction, and the electrons in turn lose their energy to radiation in a relatively large postshock relaxation layer.

On the other hand, for nonrelativistic shocks, if the ratio of radiation to matter pressure exceeds 4.45 in the region of final compression, the dissipation due to radiative heat conduction, which typically occurs on the scale of many Compton lengths, is sufficient to satisfy the Hugoniot relations and prevents the shock from steepening further into the regime where ion viscosity is important. (Belokon' 1959; and § V below.) In such "radiation-dominated" shocks the photons diffuse ahead, creating sufficient pressure to decelerate the electrons (as viewed from the frame in which the shock front is fixed). The ions are then decelerated by a combination of a charge-separation-induced electric field and Coulomb friction with the electrons. The kinetic energy of the ions is thus directly transformed into electron and photon thermal energy. The ions are only weakly heated by Coulomb friction, and by the generally small amount of viscous heating that can still take place over gradients of many Compton lengths. For preshock kinetic energies and densities of less than 100 MeV nucleon^{-1} and 10^{21} cm^{-3}, the peak temperature of a radiation-dominated shock ranges from less than 10 keV if the radiation field is every-

where in blackbody equilibrium, to at most 4 MeV at the point where the criterion for radiation dominance is no longer satisfied. This is in sharp contrast to the up to 50–70 MeV temperatures that would occur in a viscous ion shock. Figure 1 illustrates qualitatively these various possible types of shock structure. In addition, we shall see that the presence of electron-positron pairs in the shock front can result in a shock structure in which dissipation occurs principally by ion-pair Coulomb friction.

The essential object of the calculations that follow is to decide which of these structures in fact occurs at a given initial energy and density. Our treatment differs from that of Colgate (1974) in that we include the effect of photon diffusion on energy and momentum balance in the shock, while Colgate considered only the postshock radiative equilibration. In addition, we include the effects of electron-electron bremsstrahlung, radiative Compton scattering, electron-positron pair creation, and a more accurate treatment of inverse Compton scattering. As we shall see, these effects substantially increase the rate of radiative equilibration. Further, the suggestions of Colgate (1975*a*) that radiation-dominated shocks may be unstable, or that self-consistent hot-ion shocks may also exist, are found to be invalid when examined in the context of a shock model which contains both viscous and radiative effects and takes into account the presence of helium.

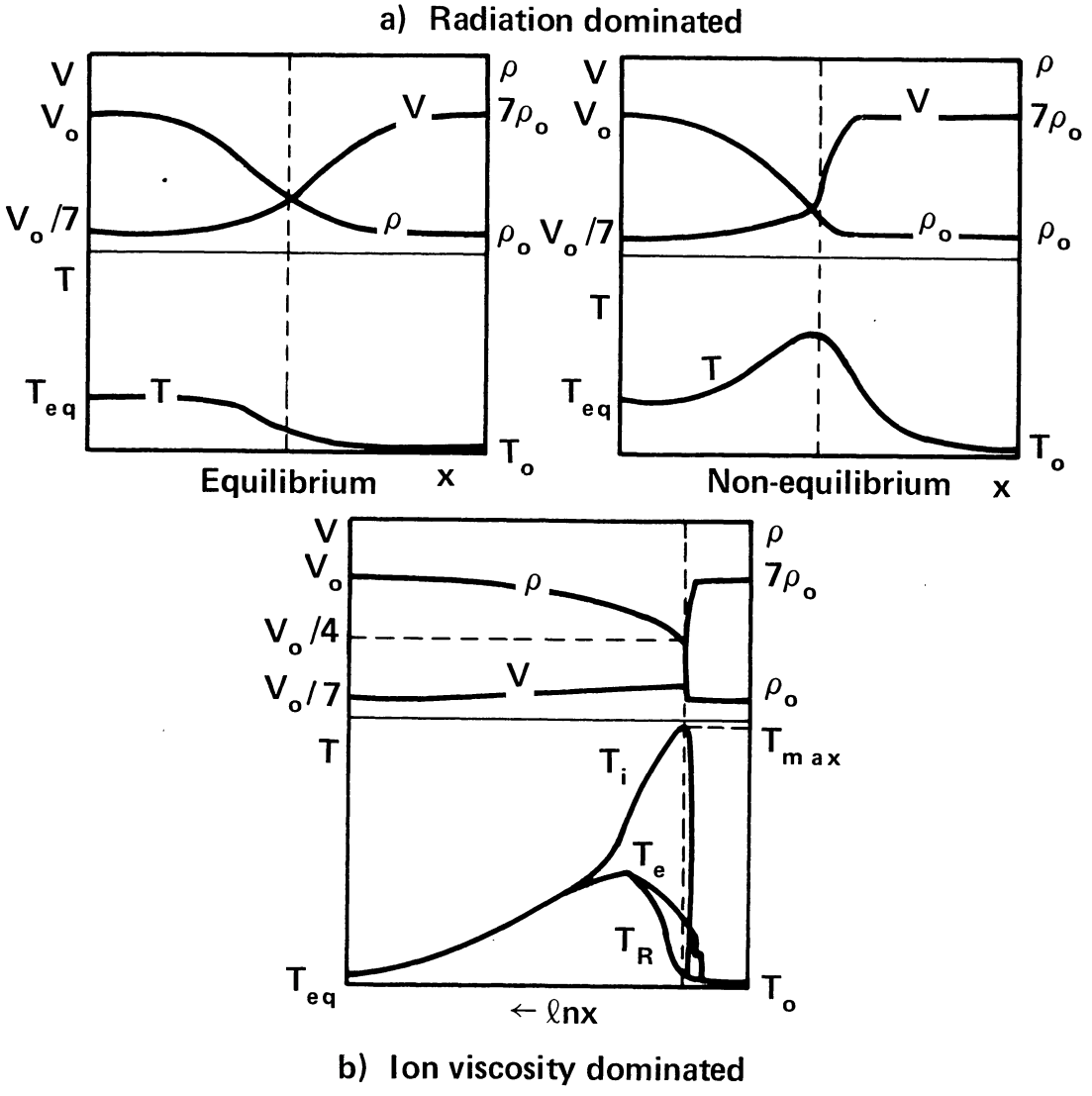

FIG. 1.—Types of shock structure. Shock waves mediated by radiative heat transport and dominated by radiation pressure are shown in (*a*) for the cases when the radiation field always remains in equilibrium and when a substantial departure from equilibrium exists near the shock front. The case when ion viscosity provides the shock dissipation is shown in (*b*). These shocks are schematic and are shown in their comoving frame, where the matter moves with velocity v to the left. T_i, T_e, T_R, and T are the ion, electron, radiation, and mean temperatures, respectively, while ρ is the matter density and x the spatial coordinate; v_0, ρ_0, and T_0 are the preshock values of v, ρ, and T, while T_{eq} is the final postshock equilibrium temperature. Note that, except in the equilibrium case, a temperature peak develops that may cause nuclear processing if it is sufficiently hot and broad.

In § II, we derive the hydrodynamic equations governing shock structure in sufficiently general form to treat both viscous and radiation-dominated shocks, and in § III discuss and develop the physical processes that determine the parameters in these equations. Section IV describes an approximate treatment of the radiation field in terms of a Bose-Einstein distribution of "effective photons" that substantially simplifies the shock equations, while including inverse Compton processes implicitly.

The radiation-dominated shock model is formulated and solved in § V, and is shown to result in shocks whose peak temperatures remain below ~ 100 keV for shock energies $\lesssim 40$–50 MeV nucleon^{-1}, while the effect of pairs is explored in § VI. Section VII develops shock models containing viscosity, and in § VIII these are merged with a realistic treatment of the radiation field. These models verify the consistency and stability of the radiation-dominated shock structures found in § V, while no self-consistent "hot-ion" shocks are found. The implications of these results for deuterium synthesis and the applications of such strong-shock-structure calculations to other astrophysical phenomena are discussed in § IX.

Unless explicitly stated otherwise, cgs-Gaussian units will be used throughout this study. A list of the symbols employed, with their definitions and units, is given in Appendix A.

II. SHOCK-STRUCTURE EQUATIONS

a) Basic Hydrodynamic Equations

The general hydrodynamic equations governing the structure of a multispecies shock assumed to be one-dimensional and to have reached a steady state in its comoving frame can be obtained by requiring the conservation of momentum, energy, and particle number for each species, and can be written in the form

$$\frac{dP_{xx}{}^{i}}{dx} = \sum_{j} \mathcal{P}^{ij}, \tag{2.1}$$

$$\frac{dE_{x}{}^{i}}{dx} = \sum_{j} \mathcal{E}^{ij}, \tag{2.2}$$

$$\frac{d(n^{i}v^{i})}{dx} = Q^{i}, \tag{2.3}$$

where $P_{xx}{}^{i}$, $E_{x}{}^{i}$, v^{i}, and n^{i} are the pressure and energy components of the stress-energy tensor, and the macroscopic velocity and number density, respectively, of the ith particle species or energy group. Here $\mathcal{P}^{ij}$ and $\mathcal{E}^{ij}$ are the rates of momentum and energy transfer from group or particle j to group or particle i, and Q^{i} is the rate at which particles of type or energy group i are "created" or "destroyed." All of the above quantities, including the spatial coordinate x, are to be measured in the frame in which the shock is at rest.

If we neglect external electric and magnetic fields, the electrical properties of the shocked plasma are given by the one-dimensional Poisson's equation

$$\frac{d\Sigma_{x}}{dx} = 4\pi\rho, \tag{2.4}$$

where Σ_x is the x component of the electric field, and ρ, the charge density.

In their present form equations (2.1)–(2.3) are relativistically correct (cf. Johnson and McKee 1971) and can be most readily evaluated by Lorentz transforming the various stress tensor, transfer, and source terms from the rest frame of each particle species to the shock frame. The resulting relativistic shock equations and shock models will be the subject of a later paper. For the purposes of the present study, however, we shall restrict ourselves to nonrelativistic shock velocities and in addition make the following general assumptions (the validity and self-consistency of these assumptions in the context of supernova shocks or other astrophysical applications are discussed in the sections or papers noted):

1. The shocked material is a fully ionized hydrogen plasma and its associated radiation and electron-positron pair fields. (The effect of helium and high-Z components will be discussed in § VIII*b*.)
2. The electrons and ions can be characterized macroscopically by temperatures T_e and T_i, velocities v_e and v_i, and densities n_e and n_i (§ IX).
3. Except for the very small differences giving rise to electrical effects, the positrons share the velocity and temperature of the electrons and their number density, n_+, is included in n_e (§§ V*d*, VI).
4. The radiation field is allowed to have an arbitrary energy spectrum, but radiation transport in x-space is assumed to be adequately described in terms of the diffusion approximation (§ III), and to take place in an optically thick region (§ IX).
5. Viscosity, heat conduction, and momentum and energy transfer among the ions and electrons are given by the usual Navier-Stokes relations (see, e.g., Landau and Lifshitz 1959; Jaffrin and Probstein 1964; § IX of this paper).

With these assumptions, equations (2.1)–(2.4) can be written in the more explicit form

$$\frac{d}{dx}\left[n_e kT_e + E_\gamma/3 + m_e n_e v_e^2 - \mu_e \frac{dv_e}{dx}\right] = \mathscr{P}_{ei}' + \rho_e \Sigma_x , \tag{2.5}$$

$$\frac{d}{dx}\left[n_e v_e(1+\alpha_e)kT_e + \tfrac{1}{2}m_e n_e v_e^3 + n_e v_e m_e c^2 + \tfrac{4}{3}E_\gamma v_e + S_\gamma - \kappa_e \frac{dT_e}{dx} - v_e \mu_e \frac{dv_e}{dx}\right] = \mathscr{E}_{ei}' + j_e \Sigma_x , \tag{2.6}$$

$$\frac{d}{dx}\left[n_i kT_i + m_i n_i v_i^2 - \mu_i \frac{dv_i}{dx}\right] = -\mathscr{P}_{ei}' + e n_i \Sigma_x , \tag{2.7}$$

$$\frac{d}{dx}\left[\tfrac{5}{2}n_i v_i kT_i + \tfrac{1}{2}m_i n_i v_i^3 - \kappa_i \frac{dT_i}{dx} - v_i \mu_i \frac{dv_i}{dx}\right] = -\mathscr{E}_{ei}' + e v_i n_i \Sigma_x , \tag{2.8}$$

$$\frac{d}{dx}[v_e n_\gamma(\epsilon_\gamma)] - \frac{d}{dx}\left[D_\gamma(\epsilon_\gamma)\frac{dn_\gamma(\epsilon_\gamma)}{dx}\right] = n_e c \int_0^\infty [n_\gamma(\epsilon_\gamma') - n_\gamma(\epsilon_\gamma)]\sigma(\epsilon_\gamma \to \epsilon_\gamma')d\epsilon_\gamma' + Q_\gamma(\epsilon_\gamma) , \tag{2.9}$$

$$\frac{d}{dx}[n_i v_i] = 0 , \tag{2.10}$$

$$\frac{d}{dx}[n_e v_e] = 2Q_\pm , \tag{2.11}$$

$$\frac{d\Sigma_x}{dx} = 4\pi[\rho_e + e n_i] . \tag{2.12}$$

Here m_j, μ_j, κ_j are the mass and coefficients of viscosity and heat conduction, respectively, for species j; E_γ and S_γ are the energy density and flux of the radiation field in frame of the electrons; $\mathscr{P}_{ei}'$ and $\mathscr{E}_{ei}'$ are the portions of the total momentum and energy transfer terms not involving the electric field; $n_\gamma(\epsilon_\gamma)$ is the number density of photons in an energy group centered on photon energy ϵ_γ; $\sigma(\epsilon_\gamma \to \epsilon_\gamma')$ is the cross section for a photon to be Compton scattered from ϵ_γ to ϵ_γ'; $Q_\gamma(\epsilon_\gamma)$ is the rate at which photons are emitted into energy group ϵ_γ; $Q_\pm$ is the production rate for electron-positron pairs; $D_\gamma(\epsilon_\gamma)$ is the diffusion coefficient for photons; ρ_e and j_e are the charge and current density of the electron-positron fluid as viewed from the shock frame; α_e is the ratio of the energy density to pressure of the electrons (assumed $\frac{3}{2}$ for the ions); and as usual c, k, and e are the velocity of light, Boltzmann's constant, and the protonic charge.

Equations (2.5), (2.6), and (2.11) describe momentum, energy, and lepton-number conservation for the electrons and positrons, including the effects of radiation energy density, energy transport, and pressure. Radiation momentum transport and all higher transport moments are neglected, due to the assumed nonrelativistic bulk velocity and optical thickness of the shocked material. Equations (2.7), (2.8), and (2.10) describe momentum, energy, and particle conservation for the ions, while equation (2.9) describes the diffusion, creation, and scattering of photons. Note that the distribution function $n_\gamma(\epsilon_\gamma)$ is defined in the rest frame of shock and not in the frame comoving with the electrons. Finally, equation (2.12) is Poisson's equation.

The form of the parameters in equations (2.5)–(2.12) depends on the energy and density regime of interest, and will be the topic of § III.

b) Boundary Conditions and Integrated Shock Equations

In order for equations (2.5)–(2.12) to describe a shock, appropriate boundary conditions must be introduced. Specifically, we shall assume that as $x \to -\infty$, $v_e \to v_i \to v_0$, $n_e \to n_i \to n_0$, $T_e \to T_i \to T_0$, $n_\gamma(\epsilon_\gamma) \to n_{\gamma 0}(\epsilon_\gamma)$, $n_+ \to 0$, $\Sigma_x \to 0$, and the gradients of T_i, T_e, v_i and v_e vanish; and, in addition, that $n_\gamma(\epsilon_\gamma) \to n_{\gamma 1}(\epsilon_\gamma)$ as $x \to +\infty$. Here we have associated the subscript "0" with the preshock condition of the fluid and the subscript "1" with its postshock condition, thus assuming a fluid flow from $-\infty$ ("upstream") to $+\infty$ ("downstream"). The singular nature of the shock equations at $\pm\infty$ prevents these boundary conditions from being sufficient, and we must also require that the temperature and velocity gradients vanish at $+\infty$, and that $v = v_s$ at some finite point $x = x_s$. The last condition is necessary to fix the location of the shock; and, as we shall see, the range of v_s must be restricted to obtain physically realizable shocks.

Utilizing these conditions, we note that equations (2.10) and (2.11) imply that net electrical currents vanish. We can then obtain integral momentum and energy conservation equations for the entire plasma by adding (2.5) to (2.7) and (2.6) to (2.8), making use of (2.12), and integrating. Continuity equation (2.10) can also be immediately

integrated, while equation (2.8) can be simplified by subtracting v_i times equation (2.7). The resulting set of shock structure equations becomes

$$n_e kT_e + n_i kT_i + \tfrac{1}{3}E_\gamma - \mu_e \frac{dv_e}{dx} - \mu_i \frac{dv_i}{dx} - \frac{\Sigma_x^2}{8\pi} = m_i n_0 v_0 (v_0 - v_i) + m_e (n_0 v_0^2 - n_e v_e^2) + P_0 , \tag{2.13}$$

$$n_e v_e (1 + \alpha_e) kT_e + \tfrac{5}{2} n_0 v_0 kT_i + \tfrac{4}{3} E_\gamma v_e + S_\gamma - \kappa_e \frac{dT_e}{dx} - \kappa_i \frac{dT_i}{dx} - v_e \mu_e \frac{dv_e}{dx} - v_i \mu_i \frac{dv_i}{dx}$$
$$= \tfrac{1}{2} m_i n_0 v_0 (v_0^2 - v_i^2) + \tfrac{1}{2} m_e (n_0 v_0^3 - n_e v_e^3) + m_e c^2 (n_0 v_0 - n_e v_e) + S_0 , \tag{2.14}$$

$$n_i k \frac{dT_i}{dx} - \frac{n_0 v_0}{v_i^2} kT_i \frac{dv_i}{dx} + m_i n_0 v_0 \frac{dv_i}{dx} - \frac{d}{dx}\left[\mu_i \frac{dv_i}{dx}\right] = -\mathscr{P}_{ei}' + e n_i \Sigma_x , \tag{2.15}$$

$$\tfrac{3}{2} n_0 v_0 k \frac{dT_i}{dx} + n_i kT_i \frac{dv_i}{dx} - \mu_i \left(\frac{dv_i}{dx}\right)^2 - \frac{d}{dx}\left[\kappa_i \frac{dT_i}{dx}\right] = -(\mathscr{E}_{ei}' - v_i \mathscr{P}_{ei}') , \tag{2.16}$$

$$n_i v_i = n_0 v_0 \approx (n_e - 2n_+) v_e , \tag{2.17}$$

$$\frac{d}{dx}[n_e v_e] = 2Q_\pm , \tag{2.18}$$

$$\frac{d\Sigma_x}{dx} = 4\pi (e n_i + \rho_e) , \tag{2.19}$$

$$\frac{d}{dx}[v_e n_e(\epsilon_\gamma)] - \frac{d}{dx}\left[D_\gamma(\epsilon_\gamma) \frac{dn_\gamma(\epsilon_\gamma)}{dx}\right] = n_e c \int_0^\infty [n_\gamma(\epsilon_\gamma') - n_\gamma(\epsilon_\gamma)] \sigma(\epsilon_\gamma \to \epsilon_\gamma') d\epsilon_\gamma' + Q_\gamma(\epsilon_\gamma) , \tag{2.20}$$

where P_0 is the preshock pressure, and S_0, the energy flux due to the initial internal energy density and pressure.

III. PHYSICAL PROCESSES

a) Radiative Emission Processes

i) *Bremsstrahlung*

The photon emission spectrum from a hot plasma due to electron-ion bremsstrahlung is given in the nonrelativistic limit by Drummond (1961) as

$$J_{ei}^{\mathrm{NR}}(\epsilon_\gamma, \theta_e) d\epsilon_\gamma = \frac{16}{3}\left(\frac{2}{m_e \pi \theta_e}\right)^{1/2} Z_i^2 \alpha r_0^2 n_e n_i m_e c^2 \exp(-\epsilon_\gamma / 2\theta_e) K_0\left(\frac{\epsilon_\gamma}{2\theta_e}\right) \frac{d\epsilon_\gamma}{\epsilon_\gamma} , \tag{3.1}$$

where K_0 is the zeroth-order modified Bessel function of the second kind, α is the fine-structure constant, r_0 is the classical electron radius, $\theta_e = kT_e$, and Z_i is the ionic charge.

It is evident from the form of equation (3.1) that the *number* density of photons, $Q(\epsilon_c, \theta_e)$, emitted per unit time down to some low energy cutoff $\epsilon_c \ll \theta_e$, diverges logarithmically. While the total energy emitted in low-energy photons is small, they can contribute very substantially to the cooling and effective heat capacity of the electrons via inverse Compton scattering. The treatment of this effect is undertaken in § III*d* and § IV, and utilizes the quantity $Q(\epsilon_c, \theta_e)$, with ϵ_c taken as the lowest energy from which a photon can be effectively thermalized, which we shall term the "effective photon" emission rate. Nonrelativistically, we find from equation (3.1) that:

$$Q_{ei}^{\mathrm{NR}}(\epsilon_c, \theta_e) = 5.692 \times 10^{-12} T_e^{-1/2} n_i n_e Z_i^2 g_1(\lambda) E_1(\lambda) \quad \mathrm{cm}^{-3}\,\mathrm{s}^{-1} , \tag{3.2}$$

where $\lambda \equiv \epsilon_c / \theta_e$,

$$E_1(x) \equiv \int_x^\infty \frac{e^{-t}}{t} dt$$

is the first-order exponential integral function, and

$$g_1(\lambda) \equiv \int_{\lambda/2}^\infty e^{-x} K_0(x) \frac{dx}{x} \Big/ E_1(\lambda) . \tag{3.3}$$

The quantity g_1 is a slowly varying factor and can be expressed to an accuracy of better than one percent in the numerical form

$$g_1(\lambda) \approx 1.226 - 0.475 \ln \lambda + 0.0013 (\ln \lambda)^2 \qquad 10^{-6} \le \lambda \le 0.8 . \tag{3.4}$$

The $E_1(\lambda)$ function can also be conveniently approximated numerically (Abramowitz and Stegun 1964, p. 231) and in the limit of small λ becomes $E_1(\lambda) \approx -\ln \lambda - 0.5772$, and thus contains the logarithmic singularity expected from the $1/\epsilon_\gamma$ term in the emission spectrum.

For plasma temperatures above ~ 20 keV, electron-electron bremsstrahlung and relativistic corrections to *e-i* bremsstrahlung must be taken into account. Unfortunately, plasma emission spectra have not been calculated for these processes for most of the range between first order in θ_e/m_ec^2 and the extreme relativistic limit. At present, therefore, we must be content with making approximations to these rates, and then determining the sensitivity of our results to these approximations.

The general effect of relativistic additions to the bremsstrahlung rate is to greatly increase the high-energy portion of the spectrum while more moderately increasing emission in the low-energy tail (cf. Quigg 1968). This results in the temperature dependence of the energy emission rate increasing from $\theta_e^{1/2}$ to $\theta_e \ln (2\theta_e/m_ec^2)$ (Maxon 1972) as the transition to relativistic temperatures is made, while the mean energy-weighted emitted photon energy increases from $\frac{2}{3}\theta_e$ to $\sim 0.85\theta_e$ at $\theta_e = m_ec^2$ to $1.88\theta_e$ in the extreme relativistic limit (*e-i* case).

This behavior suggests that we take the effective photon emission rate from relativistic corrections to bremsstrahlung, $Q_{\rm RCB}$, to be:

$$Q_{\rm RCB} = \frac{W_{ei}^{\rm RC} + W_{ee}}{\epsilon_{\rm RC}\theta_e} \quad \epsilon_{\rm RC} \equiv \begin{cases} 1 & \text{if } \lambda \le 1/5, \\ 5\lambda & \text{if } \lambda > 1/5, \end{cases} \tag{3.5}$$

where W_{ee} and $W_{ei}^{\rm RC}$ are the energy emission rates for *e-e* and the relativistic correction to *e-i* bremsstrahlung. Here the form of the cutoff for large λ was determined by requiring $\epsilon_{\rm RC} = 3$ for $\lambda = 0.6$, in analogy with the nonrelativistic case. Note that this approximation is conservative in that it ignores photons with energy $\ll \theta_e$ produced by relativistic effects.

Maxon (1972) has interpolated between first-order and extreme relativistic results, to obtain bremsstrahlung energy emission rates for a plasma of arbitrary temperature. From his results, we obtain:[1]

$$W_{ei}^{\rm RC} \approx \begin{cases} W_{ei}^{\rm NR} \frac{19}{24}\tau(1 + 1.022\tau + 0.221\tau^2 - 0.239\tau^3) & \tau \le 1.5, \\ W_{ei}^{\rm NR} \frac{9}{8}\left(\frac{\pi}{2}\right)^{1/2}\tau^{1/2}(\ln 2\tau + 0.923) - 1 & \tau \ge 1.5, \end{cases} \tag{3.6}$$

$$W_{ee} \approx W_{ei}^{\rm NR} \frac{n_e}{n_i}\frac{1}{Z_i^2} \begin{cases} 3\tau(1 - 0.128\tau + 0.898\tau^2 - 0.439\tau^3) & \tau \le 1.5, \\ \frac{9}{4}\left(\frac{\pi}{2}\right)^{1/2}\tau^{1/2}(\ln 2\tau + 0.673) & \tau \ge 1.5, \end{cases} \tag{3.7}$$

where

$$W_{ei}^{\rm NR} = \tfrac{32}{2} Z_i^2 \alpha r_0^2 n_e n_i m_e c^3 \left(\frac{2\theta_e}{\pi m_e c^2}\right)^{1/2} \tag{3.8}$$

is the nonrelativistic *e-i* bremsstrahlung emission rate, and $\tau \equiv \theta_e/m_ec^2$. The interpolation errors appear to be ~ 15–20 percent. Gould (1975), however, has very recently recalculated quantum mechanically the lowest order (i.e., quadrupole) cross sections for *e-e* bremsstrahlung and found them to average roughly a factor of 2 lower than the semiclassical cross sections of Fediushin (1952) used by Maxon. The net effect of this correction is to reduce W_{ee} by ~ 65 percent for $\theta_e \ll m_ec^2$, which we shall approximate by multiplying equation (3.7) by the factor $[1 - 0.642 \exp(-\tau)]$.

ii) *Radiative Compton Scattering*

The process of radiative Compton scattering

$$e + \gamma \rightarrow e + \gamma + \gamma, \tag{3.9}$$

is expected from general quantum electrodynamics arguments to proceed at a rate $\sim\alpha(\approx 1/137)$ below that of ordinary Compton scattering at photon energies $\sim m_ec^2$, and thus be a potentially important source of photons in the extremely hot plasmas characteristic of the strong shocks under consideration. The differential cross section for this process was calculated by Mandl and Skyrme (1952) and has recently been numerically integrated by Ram and Wang (1971) to give the total cross section for photon emission for $\epsilon_\gamma > 5$ keV.

In order to average this cross section over a partially relativistic electron distribution, a general theory of relativistic reaction rates has been developed and is given in Weaver 1976. The most notable results of this theory are exact expressions for total rates involving only a single integral over the cross section for the usual case of relativistic Maxwell-Boltzmann (RMB) or Bose-Einstein distributions (RBE). This results from the fact that in the

[1] Here we have somewhat improved Maxon's interpolation by explicitly introducing the quadrupole correction to *e-i* bremsstrahlung before interpolating.

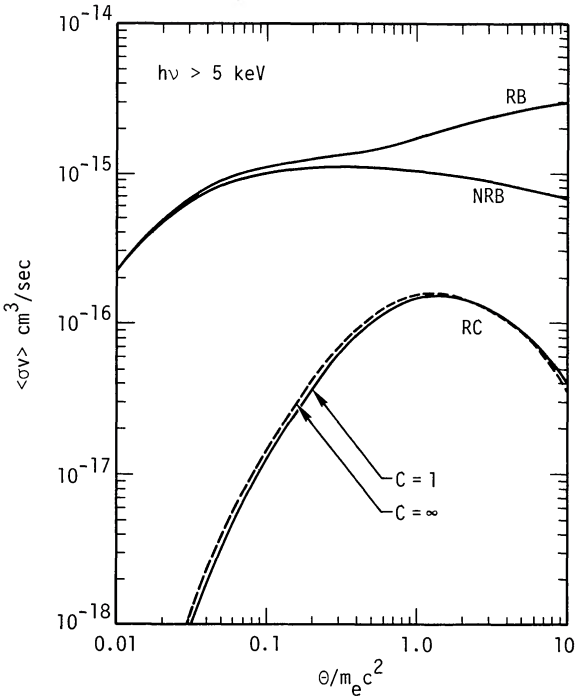

FIG. 2.—Radiative Compton (RC) scattering photon emission rate (divided by $n_\gamma n_e$) compared with the emission rates for relativistically corrected (RB) and nonrelativistic (NRB) bremsstrahlung (divided by n_e^2). These rates are for a hydrogen plasma with an electron number density n_e, effective photon number density n_γ, and temperature θ; and a low-energy cutoff of $h\nu = 5$ keV has been taken in counting the emitted photons. Here $C \equiv \exp(-\mu_\gamma/\theta)$, where μ_γ is the photon chemical potential. $C = 1$ corresponds to a blackbody distribution, while $C \to \infty$ for a nondegenerate photon distribution.

relativistic as well as the nonrelativistic case, an effective combined particle distribution function, F, can be found analytically.

For an RMB electron distribution and RBE photon distribution having the same temperature, the total photon emission rate ($\epsilon_\gamma > 5$ keV), Q_{RC}, is given in Figure 2 in density-normalized form, i.e. as $\langle \sigma v \rangle_{RC} \equiv Q_{RC}/n_\gamma n_e$. (Here n_γ is the number density of photons in the RBE distribution, which we shall associate with the effective photon number density in § IV.) As can be seen, the density-normalized radiative Compton rates for a blackbody distribution vary from ~ 15 percent below to ~ 10 percent above the nondegenerate rates as θ_e ranges from $\ll m_e c^2$ to $\gg m_e c^2$. As noted in Weaver 1976, this is due primarily to the relative augmentation of the low-energy tail of the blackbody distribution and the peak in the total cross section near $m_e c^2$. Because of this small distribution dependence, and the fact that knowledge of radiative rates is most important far from equilibrium, we shall adopt the nondegenerate rates for general use in the present work.

Also plotted in Figure 2 are the density-normalized rates for relativistically corrected (RB) and nonrelativistic (NRB) bremsstrahlung for a hydrogen plasma when a cutoff photon energy of $\epsilon_c = 5$ keV is taken. It is evident that radiative Compton scattering will dominate bremsstrahlung emission in this spectral range for $n_\gamma \gtrsim 10 n_e$ if $\theta_e \approx 500$ keV, and for $n_\gamma \gtrsim 100 n_e$ in the entire range 50 keV $\lesssim \theta_e \lesssim 5$ MeV. As we shall see below, however, Compton upscattering of low-energy bremsstrahlung photons is often the most important eventual source of thermal photons (see, e.g., Fig. 6). Above 5 MeV, the relatively unexplored processes of multiple bremsstrahlung and multiple radiative Compton scattering may become dominant.

iii) *Approach to Equilibrium*

Except in the case of the low-energy tail of the bremsstrahlung emission spectrum, we shall approximately allow for photon absorption processes by multiplying the emission rates by the factor

$$f_E = 1 - \frac{n_\gamma}{b T_e^3}, \tag{3.10}$$

where $b = 20.3\ \mathrm{cm^{-3}\ K^{-3}}$ is the radiation-equilibrium number-density constant, in analogy with the usual relation between emission and absorption for photons of a given energy (Zel'dovich and Raizer 1966). Inverse bremsstrahlung processes will be taken into account explicitly in determining the cutoff energy, ϵ_c, above which bremsstrahlung photons can be effectively thermalized (see § IV).

b) Electron-Positron Pair Production

i) *Emission Processes*

The most important means of electron-positron pair creation at electron and photon temperatures below 1 MeV are the reactions

$$\gamma + \gamma \rightarrow e^+ + e^- , \tag{3.11}$$

$$\gamma + Z \rightarrow Z + e^+ + e^- , \tag{3.12}$$

$$\gamma + e^\pm \rightarrow e^\pm + e^+ + e^- . \tag{3.13}$$

Like other second-order processes in quantum electrodynamics such as Compton scattering, γ-γ pair production has a cross section $\sim r_0^2$ in the region where it is energetically allowed. Cross sections for the third-order processes (3.12) and (3.13) are typically a factor of 1/137 below these levels (for $Z = 1$), and so for photon number densities at all comparable to the matter density, γ-γ pair production will dominate.

Jauch and Rohrlich (1955) give the relativistically correct γ-γ pair production cross section, and its integration over nondegenerate and blackbody photon distributions is carried out in Weaver 1976. The resulting rate, $Q_{\gamma\gamma}{}^{\pm}$, for the nondegenerate case of present interest is given in Figure 3 as a function of the photon temperature, T_γ. In the regime 10 keV $\lesssim kT_\gamma \lesssim$ 100 keV, this rate can be fitted numerically in the form (accurate to 2%)

$$Q_\gamma{}^{\pm} = 1.042(1 + 0.728/\phi)^{7/2} Q_{\gamma\gamma}{}^{\rm NR} , \tag{3.14}$$

where

$$Q_{\gamma\gamma}{}^{\rm NR} = \frac{n_\gamma{}^2}{2} \frac{c\pi^2 r_0{}^2}{4} \phi^3 e^{-2\phi} \tag{3.15}$$

is a nonrelativistic approximation to the reaction rate, and

$$\phi \equiv m_e c^2 / kT_\gamma . \tag{3.16}$$

ii) *Pair-Photon Relative Equilibrium*

A given number density of pairs will be in relative equilibrium with a Bose-Einstein distribution of photons (via $e^+e^- \leftrightarrow \gamma\gamma$) when

$$2\mu_\gamma = \mu_{e^+} + \mu_{e^-} + 2m_e c^2 , \tag{3.17}$$

where μ_j is the chemical potential of species j (cf. Chiu 1968, p. 134). In the case of an RMB distribution, the number density of positrons, n_+, is related to μ_{e^+} by

$$n_+ = \frac{m_e{}^3 c^3}{\pi^2 \hbar^3} \exp\left[(\mu_{e^+} + m_e c^2)/kT\right] \frac{K_2(\Phi)}{\Phi} \equiv n_{+0} \exp\left[(\mu_{e^+} + m_e c^2)/kT\right] , \tag{3.18}$$

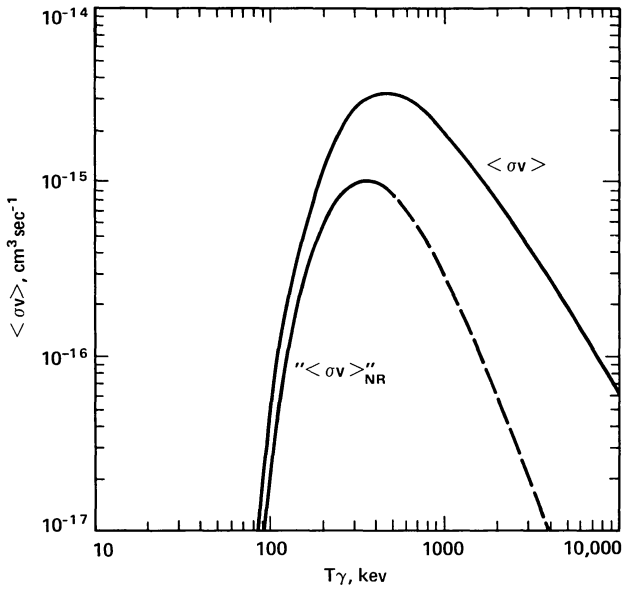

FIG. 3.—The rate ($Q_{\gamma\gamma}{}^{\pm}$) of the $\gamma\gamma \rightarrow e^+e^-$ reaction as a function of the photon temperature, T_γ. Here $\langle \sigma v \rangle \equiv 2Q_{\gamma\gamma}{}^{\pm}/n_\gamma{}^2$, where n_γ is the effective photon number density, and "$\langle \sigma v \rangle_{\rm NR}$" is a "nonrelativistic" approximation to $\langle \sigma v \rangle$.

and for nondegenerate photons, n_γ, is given by

$$n_\gamma = \frac{bT^3}{\zeta(3)} \exp(\mu_\gamma/kT) \equiv n_{\gamma 0} \exp(\mu_\gamma/kT), \tag{3.19}$$

where $\Phi = m_e c^2/kT$, $\zeta(3) = 1.2021\ldots$, and K_2 is the second-order modified Bessel function of the second kind. Since in full thermodynamic equilibrium $\mu_\gamma = 0$ and $\mu_{e^+} = -m_e c^2$, we identify n_{+0} and $n_{\gamma 0}$ with the final equilibrium density of pairs and photons, at temperature T, that would occur if these particles remained nondegenerate. Numerically we find

$$n_{+0} = 1.77 \times 10^{30} \frac{K_2(\Phi)}{\Phi} \text{ cm}^{-3} \xrightarrow[\Phi \gg 1]{} 2.22 \times 10^{30} \Phi^{-3/2} e^{-\Phi} \text{ cm}^{-3}, \tag{3.20}$$

and

$$n_{\gamma 0} = 16.9 T^3 \text{ (K) cm}^{-3} = 3.52 \times 10^{30} \Phi^{-3} \text{ cm}^{-3}. \tag{3.21}$$

Returning to equation (3.17), we find that for the case of nondegenerate distributions, $\mu_{e+} \approx \mu_{e-}$ and $T_\gamma \approx T_e$, that the pair-photon ratio is given in relative equilibrium by

$$\frac{n_+}{n_\gamma} = \frac{n_{+0}}{n_{\gamma 0}}. \tag{3.22}$$

Thus, for example, a 100 keV plasma would contain 0.04 positrons per photon. Such a relative equilibrium is expected when the $\gamma\gamma \leftrightarrow e^+ e^-$ reaction succeeds in interchanging pairs and photons much more rapidly than bremsstrahlung and radiative Compton scattering can make new photons.

c) *Transport Coefficients*

i) *Ion and Electron Viscosity and Heat Conduction*

We wish to find the transport coefficients for a plasma containing protons, electrons, and photons where the ions and electrons may have different temperatures. To do this, we shall start from a generalized diffusion approximation and then normalize our results to the case of a uniform-temperature, radiationless plasma, which has been treated more precisely.

From the diffusion approximation, we find the coefficients of viscosity and heat conduction for species j to be

$$\mu_j = C_\mu n_j m_j v_j^{\text{th}} \lambda_j, \tag{3.23}$$

$$\kappa_j = C_\kappa \alpha_j n_j k v_j^{\text{th}} \lambda_j, \tag{3.24}$$

where C_μ and C_κ are constants of order unity (usually taken equal to 1/3 [cf. Bond, Watson, and Welch 1965, pp. 240, 255]); α_j is the ratio of internal energy density to the pressure and equals 3/2 for a nonrelativistic perfect gas; and v_j^{th} and λ_j are the mean thermal velocity and "transport mean free path" for species j, given nonrelativistically by

$$v_j^{\text{th}} = \left(\frac{3\theta_j}{m_j}\right)^{1/2}, \tag{3.25}$$

$$\lambda_j \approx \left\{\sum_k [\lambda_{jk}(v_j^{\text{th}})]^{-1}\right\}^{-1}. \tag{3.26}$$

Here $\lambda_{jk}(w)$ is the transport mean free path for a particle of species j with velocity w in a gas of k-particles, defined by

$$\frac{\lambda_{jk}(w)}{w} \equiv \frac{-w}{\langle \Delta w_\parallel \rangle} \equiv t_{sjk}, \tag{3.27}$$

where $\langle \Delta w_\parallel \rangle$ is the expected initial rate of change of the parallel component of the j-particle's velocity. For interactions between charged particles, t_{sjk} is given by Spitzer (1962) as

$$t_{sjk} = \frac{w m_j^2 (v_k^{\text{th}})^2}{(1 + m_j/m_k) 12\pi e^4 n_k Z_j^2 Z_k^2 \ln \Lambda G[\sqrt{(1.5)} w/v_k^{\text{th}}]}, \tag{3.28}$$

$$G(x) = \frac{\text{erf}(x) - x(d/dx)[\text{erf}(x)]}{2x^2}, \tag{3.29}$$

$$\Lambda = \frac{3}{2 Z_j Z_k e^3} \left(\frac{\theta_e^3}{\pi n_e}\right)^{1/2}, \tag{3.30}$$

where erf (x) is the usual error function; and ln Λ, which indicates the relative importance of small-angle scatters, has been taken $\gg 1$ in deriving equations (3.28)–(3.29).

For *e-i*, *i-e*, and *j-j* Coulomb interactions, we then find (assuming $v_e^{\rm th} \gg v_i^{\rm th}$),

$$\lambda_{ei}(v_e^{\rm th}) = \frac{9}{4}\frac{\theta_e^2}{\pi Z_i^2 e^4 n_i \ln\Lambda}, \tag{3.31}$$

$$\lambda_{ie}(v_i^{\rm th}) = \frac{3}{8}\left(\frac{6m_i}{\pi m_e}\right)^{1/2}\frac{\theta_i^{1/2}\theta_e^{3/2}}{Z_i^2 e^4 n_e \ln\Lambda}, \tag{3.32}$$

$$\lambda_{jj}^{C}(v_j^{\rm th}) = 0.588\,\frac{\theta_j^2}{e^4 n_j Z_j^4 \ln\Lambda}. \tag{3.33}$$

The transport mean free path due to nuclear forces acting between protons dominates the Coulomb cross section for $\theta_i \gtrsim 1$ MeV and is given to a rough approximation by Colgate (1974) as

$$\lambda_{pp}^{N}(v_i^{\rm th}) \approx \left(\frac{\theta_i\,(\rm MeV)}{6}\right)^{1/2}\frac{10^{24}}{n_i}\ \rm cm, \tag{3.34}$$

which is most accurate when $1 < \theta_i < 10$ MeV.

For nonrelativistic electrons traveling in a photon gas, we have from § III*d* that for $T_e \approx T_\gamma$,

$$-\frac{\langle \Delta w_\parallel\rangle_{e\gamma}}{w}\bigg|_{w=v_e^{\rm th}} \approx \sigma_{\rm T} n_\gamma c\,\frac{\theta_e}{m_e c^2}, \tag{3.35}$$

implying

$$\lambda_{e\gamma}(v_e^{\rm th}) \approx \left(\frac{m_e}{3\theta_e}\right)^{1/2}\frac{3c}{\sigma_{\rm T} n_\gamma}, \tag{3.36}$$

where $\sigma_{\rm T}$ is the Thompson cross section ($\frac{8}{3}\pi r_0^2$). Using these cross sections, the nonrelativistic coefficients of electron and *proton* ($i \equiv p$) viscosity can be written in the form

$$\mu_i^{\rm NR} = \frac{1.018 C_\mu m_i^{1/2}\theta_i^{5/2}}{e^4 \ln\Lambda}\left\{1 + 0.026\,\frac{n_e}{n_i}\left(\frac{T_i}{T_e}\right)^{3/2} + 6.9\,\frac{10}{\ln\Lambda}\,[\theta_i\,(\rm MeV)]^{3/2}\right\}^{-1}, \tag{3.37}$$

$$\mu_e^{\rm NR} = \frac{1.018 C_\mu m_e^{1/2}\theta_e^{5/2}}{e^4 \ln\Lambda}\left\{1 + 0.821\,\frac{n_i}{n_e} + 1.5\,\frac{n_\gamma}{n_e}\frac{10}{\ln\Lambda}\,[\theta_e\,(\rm MeV)]^{5/2}\right\}^{-1}. \tag{3.38}$$

Setting $T_i = T_e$, $n_i = n_e$, $n_\gamma = 0$, and neglecting the nuclear contribution, we see by comparing the sum of equations (3.37) and (3.38) with Spitzer's (1962) equation (5-54) for the plasma viscosity coefficient, that $C_\mu = 0.55$, when account is taken of the factor of $\frac{4}{3}$ difference in his definition of μ. We see that for equal velocity gradients and temperatures in the Coulomb regime, the overall effects of viscosity increase as $T^{5/2}$, with ion viscosity dominating electron viscosity by a factor $(m_i/m_e)^{1/2}$. For $kT_i \gtrsim 1$ MeV, nuclear and radiation effects limit this increase.

Similarly, the nonrelativistic expressions for ion and electron heat conduction are given by

$$\kappa_j^{\rm NR} = \frac{3}{2}\frac{k}{m_j}\frac{C_\kappa}{C_\mu}\mu_j^{\rm NR}, \tag{3.39}$$

where by comparison of equation (3.39) with the result of Spitzer (1962) for a *hydrogen* plasma of uniform temperature, we find $C_\kappa = 1.14$. We see that for equal temperatures and temperature gradients in the Coulomb regime, heat conduction also increases as $T^{5/2}$, with electron heat conduction dominating ion heat conduction by a factor $(m_i/m_e)^{1/2}$.

While a precise extension of these results to allow for relativistic electron effects has not been made, and is beyond the scope of the present work, the following approximate corrections seem evident. First, the mean electron thermal velocity relativistically becomes

$$v_e^{\rm th} = c\left[1 - \left(1 + \frac{\alpha_e\theta_e}{m_e c^2}\right)^{-2}\right]^{1/2}. \tag{3.40}$$

Second, the factors of θ_e in the Coulomb mean free paths are transformed to $\frac{2}{3}\alpha_e\theta_e$ to allow for the increased electronic specific heat (see § III*e* for values of α_e); and third, σ_T in equation (3.36) goes to the Klein-Nishina cross section while the factor $(m_e/3\theta_e)^{1/2}$ is limited to $1/c$. As we shall see, electron temperatures for most cases of interest remain below $\sim$200 keV, so relativistic corrections are unlikely to become crucial, especially in view of the large temperature dependence of the Coulomb cross sections. For future convenience, we define $A_2 = \mu_i\theta_i^{-5/2}$.

ii) *Photon Diffusion and Heat Transport*

Following the diffusion approximation, we take

$$D_\gamma(\epsilon_\gamma) = \frac{c}{3} l_c \equiv \frac{c}{3} \frac{1}{n_e \sigma_c(\epsilon_\gamma)} . \tag{3.41}$$

Here l_c is the Compton transport length, and nonrelativistically (i.e., ϵ_γ, $\theta_e \ll m_e c^2$)$\sigma_c = \sigma_T$. Relativistically,

$$\sigma_c \approx \frac{m_e c^2}{\epsilon_\gamma} \sigma_T ,$$

with more precise numerical results and analytic fits being given by Cooper (1974). The use of the diffusion approximation in the form of equation (3.41) has been shown to be accurate to ~ 5 percent (cf. Alme and Wilson 1973), provided the directed photon velocity $v_\gamma \equiv S_\gamma / E_\gamma$ is much less than c. For $v_\gamma \approx c$, the diffusion approximation can be modified to give accurate results (errors $\sim 5\%$) by limiting v_γ to $\leq c$ by an appropriate multiplicative expression termed a flux limiter (Alme and Wilson 1973).

The heat transport by radiation relative to the frame of the electrons is then given by (non–flux-limited)

$$S_\gamma(\epsilon_\gamma) = -\epsilon_\gamma D_\gamma(\epsilon_\gamma) \frac{dn_\gamma(\epsilon_\gamma)}{dx} . \tag{3.42}$$

d) Transfer Processes

i) *Ion-Electron Energy and Momentum Coupling*

Burgers (1960) has calculated the momentum and energy transfer rates, $\mathscr{P}_{ei}'$ and $\mathscr{E}_{ei}'$, between ions and electrons due to Coulomb forces for arbitrary temperature and velocity differences. Assuming

$$T_i \ll \frac{m_i}{m_e} T_e , \quad |v_e - v_i| \ll v_e^{\text{th}} , \quad v_e \ll \frac{m_i}{m_e} v_i ,$$

and neglecting terms of order $(m_e/m_i)^{1/2}$, his results can be written in the form (cf. Jaffrin and Probstein 1964)

$$\mathscr{P}_{ei}' = -\frac{A_1 n_e n_i m_i (v_e - v_i)}{\theta_e^{3/2}} , \tag{3.43}$$

$$\mathscr{E}_{ei}' = -\frac{A_1 n_e n_i [3(\theta_e - \theta_i) + (v_e - v_i) v_i m_i]}{\theta_e^{3/2}} , \tag{3.44}$$

where

$$A_1 = \frac{8}{3} \left(\sqrt{\frac{\pi}{2}}\right) e^4 Z_i^2 \frac{m_e^{1/2}}{m_i} \ln \Lambda = 3.21 \times 10^{-27} Z_i^2 \ln \Lambda \text{ ergs}^{3/2} \text{ cm}^3 \text{ s}^{-1} . \tag{3.45}$$

As the electron temperatures become relativistic, two opposing effects take place to change the electron-ion coupling. First, the low-energy tail of the electron distribution to which the ions are most strongly coupled will at first remain nonrelativistic but will experience a relative depopulation as the rest of the velocity distribution becomes relativistic by a factor

$$f_{ei} = \left(\sqrt{\frac{\pi}{2}}\right) \left(\frac{\theta_e}{m_e c^2}\right)^{1/2} \frac{\exp(-m_e c^2/\theta_e)}{K_2(m_e c^2/\theta_e)} \xrightarrow{\text{NR}} 1 \Big/ \left(1 + \frac{15}{8} \frac{\theta_e}{m_e c^2}\right) \equiv f_{ei}^{\text{NR}} , \tag{3.46}$$

where the nonrelativistic form is accurate to ~ 20 percent up to $\theta_e = m_e c^2$. At the same time, however, the relativistic electrons of higher energy have a larger effective mass and thus will couple better to the ions. For lack of a definitive treatment, we will use f_{ei}^{NR} as the correction factor for $\theta_e < m_e c^2$ and correct by $f_{ei}^{\text{NR}}(m_e c^2) = 0.35$ at higher temperatures. This choice should give a *lower* limit on the electron-ion coupling, and thus an upper limit on the peak ion temperature in supernova shock waves where viscous ion heating is important. As we shall see below, however, electron temperatures for most cases of interest remain below ~ 200 keV, and thus this correction is relatively small.

ii) *Compton Scattering*

The cross sections indicated by $\sigma(\epsilon_\gamma \rightarrow \epsilon_\gamma')$ in the Compton scattering kernel in equation (2.9) have been evaluated numerically by Stone and Nelson (1966) in a relativistically correct fashion (see Stone 1971, 1973; Cooper 1971, 1974, for subsequent applications and special cases). For electron temperatures below 100 keV and photon energies

below 1 MeV, the effects of Compton scattering in changing the energy of continuum radiation can be accurately and much more conveniently represented using the Fokker-Planck approximation (Cooper 1971) according to which:

$$\frac{\partial n(\epsilon_\gamma, t)}{\partial t} = \frac{1}{\epsilon_\gamma^2}\frac{\partial}{\partial \epsilon_\gamma}\left[\left[\alpha_{\rm FP}(\epsilon_\gamma, T_e)\left\{n(\epsilon_\gamma, t)[1 + n(\epsilon_\gamma, t)] + \theta_e \frac{\partial n(\epsilon_\gamma, t)}{\partial \epsilon_\gamma}\right\}\right]\right], \tag{3.47}$$

where $n(\epsilon_\gamma, t)$ is the dimensionless photon distribution function, normalized by requiring

$$\int_0^\infty n(\epsilon_\gamma, t)\epsilon_\gamma^2 d\epsilon_\gamma = \frac{(hc)^3}{8\pi} n_\gamma ,$$

as a function of photon energy, ϵ_γ, and time, and $\alpha_{\rm FP}(\epsilon_\gamma, T_e)$ is the Fokker-Planck coefficient given approximately by

$$\alpha_{\rm FP}(\epsilon_\gamma, T_e) = \frac{\sigma_{\rm T} n_e \epsilon_\gamma^4}{m_e c} \frac{1 + f(T_e)/(1 + 0.02\epsilon_k)}{1 + 0.009\epsilon_k + 4.2 \times 10^{-6}\epsilon_k^2}, \tag{3.48}$$

where ϵ_k is ϵ_γ in keV and

$$f(T_e) = \frac{5}{2}\left(\frac{\theta_e}{m_e c^2}\right) + \frac{15}{8}\left(\frac{\theta_e}{m_e c^2}\right)^2\left(1 - \frac{\theta_e}{m_e c^2}\right).$$

In this approximation, the expectation of the energy change of a photon per unit time is given by

$$\langle(\epsilon_\gamma' - \epsilon_\gamma)\rangle = \frac{1}{\epsilon_\gamma^2}\left[\theta_e \frac{\partial \alpha_{\rm FP}(\epsilon_\gamma, T_e)}{\partial \epsilon_\gamma} - \alpha_{\rm FP}(\epsilon_\gamma, T_e)\right]. \tag{3.49}$$

Nonrelativistically, this reduces to

$$\langle(\epsilon_\gamma' - \epsilon_\gamma)\rangle = \sigma_{\rm T} n_e c\left(\frac{\epsilon_\gamma}{m_e c^2}\right)(4\theta_e - \epsilon_\gamma), \tag{3.50}$$

corresponding to a fractional photon energy change of $(4\theta_e - \epsilon_\gamma)/m_e c^2$ per Compton collision. Thus nonrelativistic Compton scattering is capable of e-folding the energy of a subthermal photon (i.e., $\epsilon_\gamma < kT_e$) in $\sim m_e c^2/(4\theta_e)$ collisions.

To very roughly estimate the quantity $\langle \Delta w_\parallel \rangle_{e\gamma}$ (the expectation value of the initial rate of change of the parallel component of an electron's velocity as it passes through a photon gas at temperature $T_\gamma = T_e$) which is required in equation (3.35), we note, using equation (3.50), that:

$$\left.\frac{\langle \Delta w_\parallel \rangle_{e\gamma}}{w}\right|_{w = v_e^{\rm th}} \approx \left.\frac{\frac{1}{2}\langle \Delta w^2{}_\parallel \rangle_{e\gamma}}{2}\right|_{w = v_e^{\rm th}}$$

$$\sim \frac{1}{2}\frac{n_\gamma}{n_e}\left.\frac{\langle(\epsilon_\gamma' - \epsilon_\gamma)\rangle}{\frac{3}{2}\theta_e}\right|_{\epsilon_\gamma = 3\theta_e} = n_\gamma \sigma_{\rm T} c \frac{\theta_e}{m_e c^2}. \tag{3.51}$$

e) *Electron Specific Heat*

The electron specific heat coefficient, α_e, defined as the ratio of the electron energy density to electron pressure, is given for a nondegenerate arbitrarily relativistic gas by (cf. Chiu 1968)

$$\alpha_e = \Phi\left[\frac{3K_3(\Phi) + K_1(\Phi)}{4K_2(\Phi)} - 1\right], \tag{3.52}$$

where $\Phi = m_e c^2/\theta_e$ and the K_i are modified Bessel functions of the second kind. A convenient numerical expression for α_e is

$$\alpha_e \approx \frac{3}{2}\left(1 + \frac{5}{4\Phi + 5}\right), \tag{3.53}$$

which is exact to first order in $1/\Phi$, goes to the correct relativistic limit and, in general, is accurate to better than 2 percent.

It is apparent that α_e goes from $\frac{3}{2} \rightarrow 3$ as θ_e goes from 0 to ∞ with substantial (i.e., $\gtrsim 10$ percent) relativistic corrections occurring for $\theta_e \gtrsim 50$ keV.

IV. THE EFFECTIVE PHOTON APPROXIMATION

a) General Formulation

In their present form, shock-structure equations (2.13)–(2.20) are quite cumbersome and do not lend themselves to either numerical solution or analytic interpretation. A key factor in their simplification is to note from § III*d* that the time required for a near-thermal photon (i.e., $\epsilon_\gamma \gtrsim 0.1\theta_e$) to be thermalized to $\sim\theta_e$ is typically quite short in an optically thick plasma at temperatures above a few keV. For example, a 1 keV photon requires only $\sim(m_e c^2/4\theta_e)\ln(\theta_e/\epsilon_\gamma) \approx 30$ Compton collisions to be thermalized at $\theta_e = 10$ keV. Since the postshock velocities ($v_1 \approx v_0/7$; see § V) under consideration range from $c/150$ to $c/15$ (as the shock energy ranges from 1 to 100 MeV nucleon^{-1}), such thermalization will occur as the matter is swept through 0.2 to 2 Compton lengths. As has been shown in the Monte-Carlo Compton scattering calculations described by Chapline and Stevens (1973), such thermalization results in the buildup of a Bose-Einstein distribution of photons, characterized by an "effective" photon *number* density, n_γ, and an effective temperature $T_\gamma \approx T_e$.

If ϵ_c is the lowest energy from which a photon can be thermalized over a "relevant" shock length scale, then from § III*a*, we see that the quantity $(\ln\lambda)^2 \equiv \ln^2(\epsilon_c/\theta_e)$ provides a rough measure of the importance of subthermal photons in cooling the electrons. Thus, if we find that relevant shock scales are indeed greater than or approximately equal to a Compton length as we expect in radiation-dominated shocks, the effect of inverse Compton cooling will be substantial for $\theta_e \gtrsim 5$–10 keV.

To make these considerations a logically rigorous basis for simplifying equations (2.13)–(2.20), we shall first explicitly make the following assumptions, and later show that the shock structures that result are self-consistent with them:

1. All but a negligible fraction of the energy in the radiation field can be characterized to sufficient accuracy by a Bose-Einstein distribution with effective photon density n_γ and temperature $T_\gamma \approx T_e$.
2. The creation rate of effective photons, $Q_\gamma^{\rm eff}$, can be taken as the integral over the photon emission spectrum down to some cutoff energy, ϵ_c, determined by the constraints of inverse bremsstrahlung, screening, and the photon thermalization time with respect to relevant shock time scales, as prescribed in § IV*b*.

Using this set of assumptions, which we shall term the effective photon approximation, we can reduce the multigroup treatment of the radiation field implied by equation (2.20) to the following relatively simple equation describing the creation and diffusion of effective photons:

$$\frac{d(n_\gamma v_e)}{dx} - \frac{d}{dx}\left(\frac{c}{3n_e\bar{\sigma}_c}\frac{dn_\gamma}{dx}\right) = Q_\gamma^{\rm eff}\,, \tag{4.1}$$

where

$$Q_\gamma^{\rm eff} = Q_{ei}^{\rm NR} + Q_{\rm RCB} + Q_{\rm RC} \tag{4.2}$$

and $\bar{\sigma}_c \approx \sigma_c(3\theta_e)$ is the mean Compton cross section. Also we find

$$E_\gamma = 3P_\gamma = 2.7 n_\gamma\theta_e\,, \tag{4.3}$$

$$S_\gamma = -\frac{9}{10}\frac{c}{n_e\bar{\sigma}_c}\frac{d}{dx}(n_\gamma\theta_e)\,. \tag{4.4}$$

Here we have adopted the blackbody specific-heat coefficient of 2.7 in equation (4.3) to achieve consistency with the final equilibrium state. The 10 percent error this introduces for a nondegenerate Bose-Einstein distribution (where $E_\gamma = 3n_\gamma\theta_e$) will be neglected.

b) Cutoff Energy for Effective Photon Emission

i) *Absorption*

Chapline and Stevens (1973) have examined the effect of Compton scattering on bremsstrahlung emission spectra by utilizing the Fokker-Planck approximation (cf. Cooper 1971). They find that low-energy radiation will be absorbed by inverse bremsstrahlung before it can be thermalized for photon energies below

$$\epsilon_B = 0.77\theta_e^{-5/4}\,(\text{keV})\left(\frac{n_e}{10^{20}\ \text{cm}^{-3}}\right)^{1/2}\text{keV}\,, \tag{4.5}$$

provided $\epsilon_B \ll m_e c^2$.

ii) *Screening*

In a plasma, bremsstrahlung emission occurring at impact parameters larger than the Debye length, $\lambda_D = (\theta_e/4\pi n_e e^2)^{1/2}$, will be suppressed by Coulomb screening. This effect will be important for a given photon energy, ϵ_γ, only if

$$\lambda_D \lesssim b_{\rm max} \approx \frac{\gamma^2\beta}{\epsilon_\gamma}\hbar c\,, \tag{4.6}$$

where $b_{\max}$ is the normal cutoff impact parameter for that photon energy (cf. Jackson 1962, eq. [15-28]), and

$$\gamma^2\beta \approx \frac{v_e^{\rm th}}{c}\left[1 - \left(\frac{v_e^{\rm th}}{c}\right)^2\right]^{-1}$$

where $v_e^{\rm th}$ is given by equation (3.40). We find that the photon energy, $\epsilon_{\rm sc}$, below which screening is important is given approximately by:

$$\epsilon_{\rm sc} \approx 5.2 \times 10^{-4}\alpha_e^{1/2}\left(\frac{n_e}{10^{20}\ {\rm cm}^{-3}}\right)^{1/2}\left(1 + \frac{\alpha_e\theta_e}{2m_ec^2}\right)^{1/2}\left(1 + \frac{\alpha_e\theta_e}{m_ec^2}\right) {\rm keV}\,. \tag{4.7}$$

Thus $\epsilon_{\rm sc}$ is typically $\lesssim 1$ eV, and exceeds ϵ_B for $\theta_e \gtrsim 160$ keV. It is often the case, however, that not enough time is available to thermalize a 1 eV photon to $\theta_e > 100$ keV, and thus the dynamical cutoff discussed in the next section usually dominates where screening would otherwise have been important.

iii) *Thermalization*

Since according to equation (3.50) a nonrelativistic, subthermal photon will be e-folded in energy in $\approx m_ec^2/(4\theta_e)$ Compton collisions, the lowest energy, ϵ_d, from which a photon can be thermalized in a dynamical time, τ_d, is:

$$\epsilon_d \approx 2.7\theta_e \exp\left(-4cn_e\sigma_{\rm T}\tau_d\theta_e/m_ec^2\right)\left[1 + \frac{\Delta\theta_e(\tau_d)}{\theta_e}\right], \tag{4.8}$$

where $\Delta\theta_e(\tau_d)$ is the mean change of temperature that a photon experiences during τ_d. In the shock models discussed in § V and VIII, τ_d will be taken as the time a photon at mean velocity, v_γ, takes to cross the photon number or electron temperature e-folding distance, whichever is smaller. The mean photon velocity is defined by (see eq. [4.1])

$$v_\gamma \equiv -\frac{c}{3n_e\bar{\sigma}_c n_\gamma}\frac{dn_\gamma}{dx} + v_e\,. \tag{4.9}$$

(See § V*d* for a discussion of shock-structure sensitivity to this choice of τ_d.)

iv) *Maximum Cutoff Energy*

When conditions are such that $\epsilon_d/\theta_e \approx 1$, we expect the effective photon approximation to become inaccurate. In this case, we can still obtain the proper bremsstrahlung energy loss rate from the electrons by not letting ϵ_c exceed $\epsilon_{\max}$, the cutoff energy at which

$$3\theta_e(Q_{ei}^{\rm NR} + Q_{\rm RCB}) = W_{ei}^{\rm NR} + W_{ei}^{\rm RC} + W_{ee}\,, \tag{4.10}$$

where the W's are the bremsstrahlung energy loss rates given in § III*a*. From the relations in § III*a*, we find

$$\lambda_{\max} \equiv \frac{\epsilon_{\max}}{\theta_e} \approx 0.6\,. \tag{4.11}$$

The effective photon cutoff energy, ϵ_c, is then taken as the maximum of ϵ_B, $\epsilon_{\rm sc}$, and ϵ_d, up to a maximum of $0.6\theta_e$.

V. RADIATION-DOMINATED SHOCK MODEL

a) Assumptions and Basic Equations

The radiation-dominated shock model is based on the general formalism of § II, with the following additional assumptions and restrictions:

1. The preshock internal energy is negligible compared with the shock energy.
2. The effect of electron-positron pairs is not crucial.
3. The ions and electrons move together with velocity v, and thus have the same density n.
4. The effective photon approximation is valid. (Note that this includes the assumption that the photon temperature, T_γ, is approximately equal to the electron temperature, T_e.)
5. The principal dissipation mechanism is radiative heat conduction.
6. Except at the leading edge of the shock, radiation pressure dominates matter pressure.

The validity and self-consistency of these assumptions in the context of the shock structures they generate is considered in § V*d* below. Using them, the shock-structure equations, (2.13)–(2.20), can be recast in the particularly simple form:

$$n_\gamma \theta_\gamma = n_0 v_0 m_H (v_0 - v)\,, \tag{5.1}$$

$$4v n_\gamma \theta_\gamma - \frac{cv}{n_0 v_0 \bar{\sigma}_c} \frac{d(n_\gamma \theta_\gamma)}{dx} = n_0 v_0 m_H (v_0^2 - v^2)/2\,, \tag{5.2}$$

$$\frac{d(n_\gamma v)}{dx} - \frac{d}{dx}\left[\frac{cv}{3 n_0 v_0 \bar{\sigma}_c} \frac{dn_\gamma}{dx}\right] = Q_\gamma^{\rm eff}\,, \tag{5.3}$$

$$n = \frac{n_0 v_0}{v}\,, \tag{5.4}$$

$$\tfrac{3}{2} n_0 v_0 \frac{d\theta_i}{dx} = -\frac{n_0 v_0}{v}\theta_i \frac{dv}{dx} + A_2 \theta_i^{5/2}\left(\frac{dv}{dx}\right)^2 + \left(\frac{v_0 n_0}{v}\right)^2 \frac{A_1}{\theta_e^{3/2}} 3(\theta_e - \theta_i)\,. \tag{5.5}$$

Here x is the spatial coordinate in the frame in which the shock is at rest; m_H is the mass of a hydrogen *atom*; n_0 is the preshock hydrogen number density; v_0 is the velocity of the shock relative to the unshocked material; n_γ is the number density of "effective" (i.e., thermalized) photons; $\theta_\gamma \equiv \frac{9}{10} kT_\gamma \approx \theta_e$; $\frac{9}{10}\theta_e \equiv kT_e$; $\theta_i \equiv kT_i$, where k is Boltzmann's constant and T_i is the ion temperature; c is the velocity of light; $\bar{\sigma}_c$ is the energy-averaged photon transport cross section due to Compton scattering; $Q_\gamma^{\rm eff}$ is the creation rate of effective photons, either by direct emission processes, or by Compton upscattering of subthermal photons; and finally, A_1 and A_2 are nearly constant coefficients related to electron-ion energy coupling and ion viscosity, respectively. $Q^{\rm eff}$, A_1, A_2, and $\bar{\sigma}_c$ are given by equations (4.2) and (3.45), and in §§ III*c* and IV*a*, respectively.

Note that the plasma momentum conservation equation (5.1) is now algebraic and describes a linear relationship between radiation pressure, $n_\gamma \theta_\gamma$, and v. Equation (5.2) is the plasma energy conservation equation, while equations (5.3) and (5.4) describe photon and matter particle continuity, and (5.5) is the ion heating equation. Due to its small coefficient, ion heat conduction has been neglected in equation (5.5), with the remaining terms on the right-hand side describing compressional work, viscous heating, and electron-ion coupling.

For future convenience, we define $E_0 \equiv \frac{1}{2} m_H v_0^2$, the initial energy per nucleon in the *shock* frame.

b) Analytic Solutions

By differentiating equation (5.1) and using it to eliminate θ_γ and n_γ from equation (5.2), we obtain a decoupled equation for v:

$$\frac{dv}{dx} = -\bar{\sigma}_c n_0 v_0 \frac{(7v - v_0)(v_0 - v)}{2vc}\,. \tag{5.6}$$

Using the boundary condition that the velocity gradient vanishes at $x = +\infty$, we immediately obtain the expected postshock conditions:

$$v_1 \equiv v(+\infty) = v_0/7\,, \tag{5.7}$$

$$\theta_1 \equiv \theta_\gamma(+\infty) = \tfrac{6}{7} n_0 \frac{m_H v_0^2}{n_\gamma(+\infty)}\,, \tag{5.8}$$

$$n_1 \equiv n(+\infty) = 7 n_0\,. \tag{5.9}$$

Equation (6) can then be integrated directly to find $x(v)$:

$$x = \frac{c}{21 \bar{\sigma}_c n_0 v_0}\left\{\ln\left[\frac{(v_0 - v)^7}{(7v - v_0) v_0^6}\right] - \ln\left[\frac{1}{3}\left(\frac{3}{7}\right)^7\right]\right\}, \tag{5.10}$$

where we have taken $v = 4v_0/7$ at $x = 0$.

Thus the velocity profile of the shock is *independent* of the details of radiative equilibration (see Fig. 4). Near the upstream limit ($v \to v_0$), and using equations (5.1) and (5.6), we see that the energy in the radiation field, $3n_\gamma\theta_\gamma$, e-folds in a length $\Delta \equiv c/(3\bar{\sigma}_c n_0 v_0)$. In the downstream limit ($v \to v_0/7$), the residual directed momentum in the ions e-folds in a length $\Delta/7$. A characteristic shock is then $\sim\Delta$ or $\sim c\sigma_T/3v_0\bar{\sigma}_c$ preshock Thompson lengths, where σ_T is the Thompson cross section.

To calculate the peak ion temperature occurring in the shock and thus the expected amount of nucleosynthesis, it is still necessary first to solve the photon continuity equation (5.3) and then the ion heating equation (5.5), which

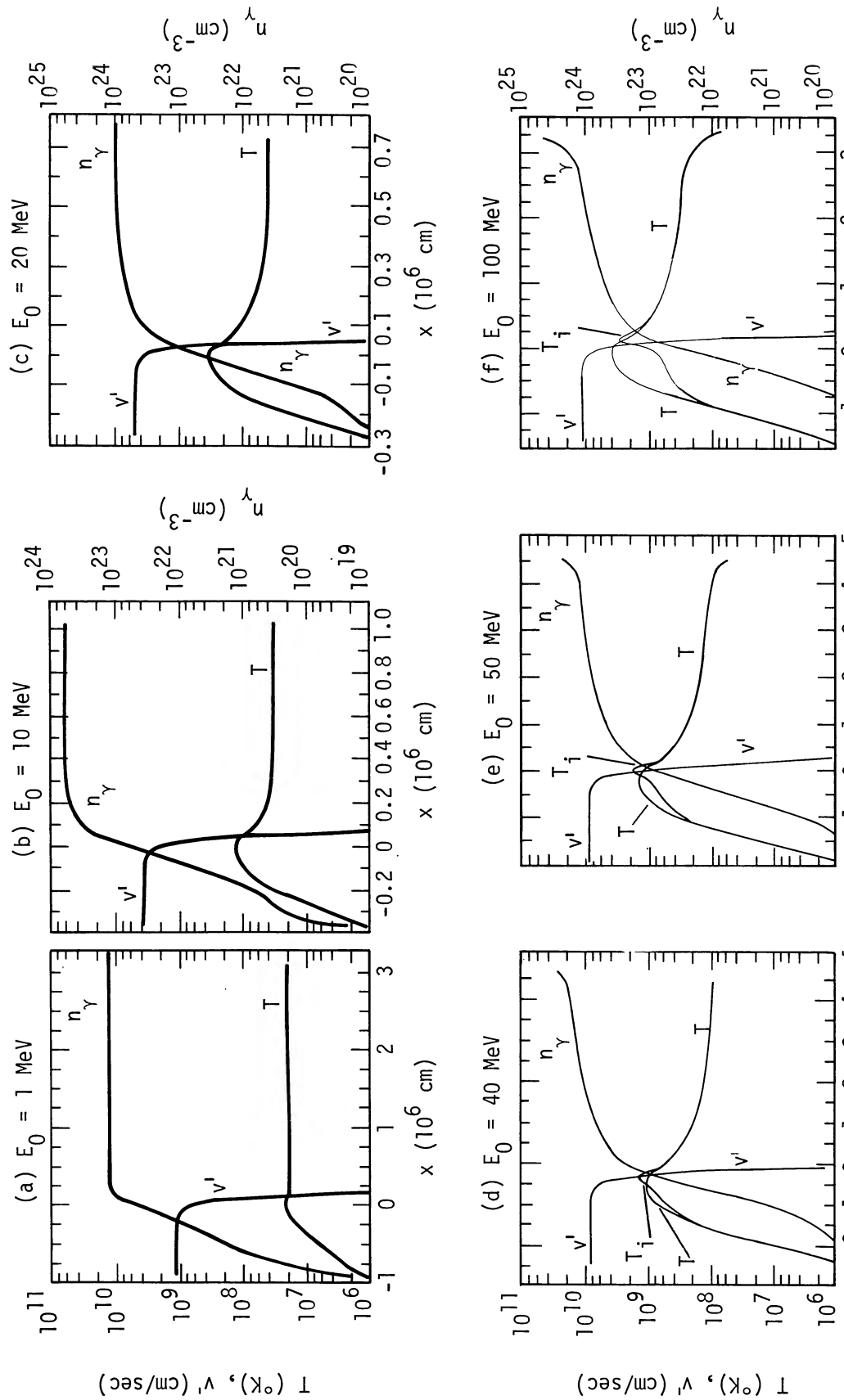

FIG. 4.—Radiation-dominated shock structures for a preshock number density of 10^{20} cm^{-3} and shock energy E_0, as indicated, shown in a frame moving with the shock front. A preshock temperature and photon number density of 10^6 K and 2.03×10^{19} cm^{-3}, respectively, were taken, although the results are not sensitive to this choice. Here $v' = v - v_0/7$, where v is the fluid velocity (directed to the right), v_0 is the preshock velocity, T is the common photon and electron temperature, n_γ is the effective photon number density, and T_i is the ion temperature, shown only when it differs from T. Note the progressive departure from radiative equilibrium as the shock energy is increased from 1 to 100 MeV.

in general must be done numerically. Some analytic insight can be gained, however, by using equations (5.6) and (5.1) to change the variable in (5.3) from x to v, yielding

$$(7v - v_0)^2(v_0 - v)^2 \frac{d^2 n_\gamma}{dv^2} + 8(7v - v_0)(v_0 - v)^2 \frac{dn_\gamma}{dv} + 6(7v - v_0)(v_0 - v)n_\gamma = -\frac{12vc}{n_0 v_0 \bar{\sigma}_c} Q_\gamma^{\text{eff}} . \quad (5.11)$$

Note that by doing this we have explicitly exhibited the singularities in the photon continuity equation by moving them from $\pm\infty$ to $v = v_0, v_0/7$.

Equation (5.11) can now be solved analytically for the case of a near-equilibrium radiation field (i.e. $f_E \ll 1$, where $f_E \equiv 1 - n_\gamma/bT_e^3$ is the radiation equilibrium parameter, and $b = 20.3\ \text{cm}^{-3}\ \text{K}^{-3}$ is the radiation equilibrium number density constant). T_γ and n_γ then become

$$T_\gamma = \left[\frac{10 n_0 v_0 m_H (v_0 - v)}{9kb(1 - f_E)}\right]^{1/4} , \quad (5.12)$$

$$n_\gamma = [10 n_0 v_0 m_H (v_0 - v)/9k]^{3/4}[b(1 - f_E)]^{1/4} . \quad (5.13)$$

For small f_E and $v_0 < c/2$, θ_γ will always be less than 50 keV, and so only the nonrelativistic bremsstrahlung photon source term will be important. Setting the $(1 - f_E)^{1/4}$ terms in equations (5.12) and (5.13) equal to unity and using equation (5.11) to solve for f_E yields

$$f_E(v) \approx \frac{1}{(n_0 v_0)^{1/8}} \left(\frac{m_H}{0.9k}\right)^{7/8} \frac{\bar{\sigma}_c b^{1/8}}{64 c J_0} v[v_0 - v]^{7/8}(7v - v_0)^2[g_2(\lambda)]^{-1} , \quad (5.14)$$

where, using equation (3.2), we have defined a bremsstrahlung photon emission coefficient $J_0 \equiv 5.692 \times 10^{-12}\ \text{K}^{1/2}\ \text{cm}^3\ \text{s}^{-1}$ and combined Gaunt factor $g_2(\lambda) \equiv g_1(\lambda)E_1(\lambda)$. Here $\lambda \equiv \epsilon_c/\theta_e$, where ϵ_c is the cutoff energy for effective photon emission; $g_1(\lambda)$ is the bremsstrahlung Gaunt factor given by equation (3.4); and $E_1(\lambda)$ is the first-order exponential integral function. The neglect of derivatives involving $(1 - f_E)$ in deriving equation (5.14) is a good approximation except for $v \lesssim 2v_0/7$, where the shock is very close to equilibrium and all gradients are small.

An approximate criterion for the consistency of our assumption of a near-equilibrium shock can be established by requiring that the maximum value of $f_E(v)$ be $\lesssim 1/2$ (with λ held constant), and can be written in the form

$$E_0 \lesssim 0.71(n_{20}{}^0)^{1/15}\left(\frac{g_2(\lambda)}{3}\right)^{8/15} \text{MeV} , \quad (5.15)$$

where $n_{20}{}^0 = n_0/10^{20}\ \text{cm}^{-3}$, and we have taken $\bar{\sigma}_c = \sigma_T$ since the resulting equilibrium temperatures are $\ll m_e c^2$, where m_e is the electron mass.

To determine ϵ_c we utilize the formalism of § IV, and note from equation (4.9) that for an equilibrium shock the mean photon velocity, v_γ^{eq}, is given by

$$v_\gamma^{\text{eq}} = \frac{-cv}{3n_0 v_0 \bar{\sigma}_c T_\gamma^3} \frac{dT_\gamma^3}{dv}\frac{dv}{dx} + v = \frac{v_0 + v}{8} , \quad (5.16)$$

while the photon e-folding length, $l_{\Delta\gamma}{}^{\text{eq}}$, is $\frac{1}{3} l_{\Delta t}{}^{\text{eq}}$, the temperature e-folding length; and using equation (5.10) we find that, for $v \gtrsim \frac{2}{7}v_0$,

$$l_{\Delta\gamma}{}^{\text{eq}} \approx \frac{cv}{9\bar{\sigma}_c n_0 v_0{}^2} , \quad (5.17)$$

implying

$$\tau_d{}^{\text{eq}} \equiv l_{\Delta\gamma}{}^{\text{eq}}/v_\gamma{}^{\text{eq}} = \frac{8cv}{9\bar{\sigma}_c n_0 v_0{}^2(v_0 + v)} . \quad (5.18)$$

The dynamic effective photon cutoff energy, ϵ_d, at which subthermal photons can no longer be thermalized in the dynamic time, $\tau_d{}^{\text{eq}}$, is then (see eq. [4.8])

$$\epsilon_d = 3.6\theta_e \exp\left[-\frac{32}{9}\left(\frac{\sigma_T}{\bar{\sigma}_c}\right)\frac{\theta_e}{m_e v_0(v_0 + v)}\right] . \quad (5.19)$$

For $E_0 = 1$ MeV, $n_0 = 10^{20}\ \text{cm}^{-3}$, and $\bar{\sigma}_c = \sigma_T$, we have at midshock ($v = \frac{4}{7}v_0$) that $\epsilon_d = 0.31$ keV ($\theta_e = 1.32$ keV); or for $n_0 = 10^{17}\ \text{cm}^{-3}$ that $\epsilon_d = 0.51$ keV ($\theta_e = 0.23$ keV). The corresponding inverse bremsstrahlung cutoffs are 0.54 keV and 0.15 keV, respectively, while those for screening are 6.4×10^{-4} keV and 2.0×10^{-5} keV. We thus find $\lambda = 0.41$ and 0.6, yielding $g_2(\lambda) = 1.65$ and 1.47, respectively. Criterion (5.15) thus becomes $E_0 \lesssim$

0.52 MeV and $E_0 \lesssim 0.31$ MeV for $n_0 = 10^{20}$ cm^{-3} and 10^{17} cm^{-3}, respectively. Thus shocks with $E_0 \lesssim 1$ MeV will be reasonably close to blackbody equilibrium over this density range.

The temperatures of such shocks will remain $\lesssim T_{eq}$, the final equilibrium temperature, given by

$$T_{eq} = 1.57[n_{20}{}^0 E_0\ (\mathrm{MeV})]^{1/4}\ \mathrm{keV}\ , \tag{5.20}$$

where $n_{20}{}^0 = n_0/10^{20}$ cm^{-3}. The final equilibrium photon density will be

$$n_\gamma{}^{eq} = 1.22 \times 10^{23}[E_0\ (\mathrm{MeV}) n_{20}{}^0]^{3/4}\ \mathrm{cm}^{-3}\ . \tag{5.21}$$

Evaluation of the terms in the ion heating equation (5.5) shows that, for temperatures of a few keV and the velocity gradients given by equation (5.6), electron-ion coupling dominates, and thus requires $\theta_i \approx \theta_e$.

c) *Numerical Solutions*

The photon continuity equation (5.3) can be solved in a stable fashion numerically, by using double-side boundary conditions and an appropriate back-substitution algorithm. The details of this method of numerical solution are given in Appendix A. These details are important since several straightforward ways of differencing equation (5.3) lead to unstable results.

The boundary conditions are taken as $n_\gamma(x_0) = n_\gamma{}^s$ and $n_\gamma(x_1) = n_\gamma{}^{eq}$, where x_0 and x_1 are the upstream and downstream boundaries of the calculation. The points x_0 and x_1 are then moved toward $-\infty$ and $+\infty$, respectively, until the solution stops changing significantly. The value of $n_\gamma{}^s$ is typically chosen either as $10^{-2} n_0$ or $bT_s{}^3$, where T_s is defined below, and the resulting shock structure is found to be quite insensitive to this choice, provided $n_\gamma{}^s \ll n_0$.

Once n_γ is known, the analytic equations (5.1) and (5.10) serve to determine v and θ_γ, except at the leading edge of the shock where matter pressure becomes important. In addition, at temperatures below a few keV, Compton scattering becomes less and less effective in maintaining $T_e \approx T_\gamma$. These points are discussed in more detail below, but in fact the shock structure is reasonably insensitive to where the upstream (i.e., $x \to -\infty$) boundary on n_γ is taken. In view of this, it is convenient to use the following procedure for choosing the upstream boundary point.

The matter-pressure terms are reinserted into the expression for the radiation temperature (see eq. [2.13]) with the assumption $T_\gamma \approx T_e \approx T_i$, yielding

$$T_\gamma = \frac{n_0 v_0 m_H (v_0 - v)}{(0.9 k n_\gamma + 2 n_0 v_0 k/v)}\ . \tag{5.22}$$

The upstream boundary point is then chosen so that the resulting temperature, T_s, is sufficient to ensure that Compton scattering will result in rapid temperature equilibration of newly created photons. Typically T_s is taken ~ 5 keV and $n_\gamma{}^s = 10^{-2} n_0$ for $E_0 \gtrsim 10$ MeV. The peak shock temperatures that result are found to agree within ~ 1 percent with calculations where T_s is chosen such that $n_\gamma{}^s = bT_s{}^3 \approx 0.1 n_0$. For $E_0 < 10$ MeV, adequate Compton thermalization can occur for $T_s \gtrsim 1$–2 keV, while at lower temperatures the number of near-thermal bremsstrahlung photons emitted over a characteristic shock scale is sufficiently great to ensure a near-equilibrium photon number (although the spectrum will probably be distorted). Such shock calculations are started using the $n_\gamma{}^s = bT_s{}^3 \approx 0.1 n_0$ condition.

Given the temperature and velocity, the ion heating equation (5.5) can be solved by taking $\theta_i(x_0) = \theta_e(x_0)$ and integrating downstream. The appropriate difference equation is given in Appendix B.

The Bose-Einstein radiation-dominated shock structures that result from the present model are shown in Figures 4 and 5 for typical values of E_0 and n_0. The abrupt rise of n_γ and corresponding fall in T apparent in some of these shock structures near the downstream boundary (e.g. Fig. 5*a*), is due to numerically forcing the shock to come to final equilibrium at a point x_1 not sufficiently far downstream, and is done so the shock can be zoned and plotted on a reasonable length scale. Test calculations show that this has essentially no effect on the structure of the shock outside the "flared" region. Figure 6 plots the peak temperature reached in the shock as a function of E_0 over the range 1–100 MeV nucleon^{-1}, and shows explicitly the effect of the various sources of radiation, as well as various characteristic temperatures. In these models $\bar{\sigma}_c = \sigma_T$, which is a reasonable approximation considering the temperatures involved. The effect of decreasing $\bar{\sigma}_c$ is to somewhat widen the shock and thus somewhat increase the degree of radiative equilibration (note that inverse Compton scattering involves σ_T, not $\bar{\sigma}_c$).

Before discussing the details of these results and the implications for nucleosynthesis of the relatively low temperatures involved in these shocks, it is necessary to determine under what conditions our model is valid. This is undertaken in the next section.

d) *Self-Consistency of the Radiation-Dominated Shock Solution*

i) *Sufficiency of Dissipation by Radiative Heat Conduction*

We wish to derive the value of the ratio of the radiation to matter pressure, $\xi \equiv P_\gamma/P_m$, below which radiation heat conduction is insufficient to prevent a shock discontinuity in the absence of viscosity. To this end, we introduce

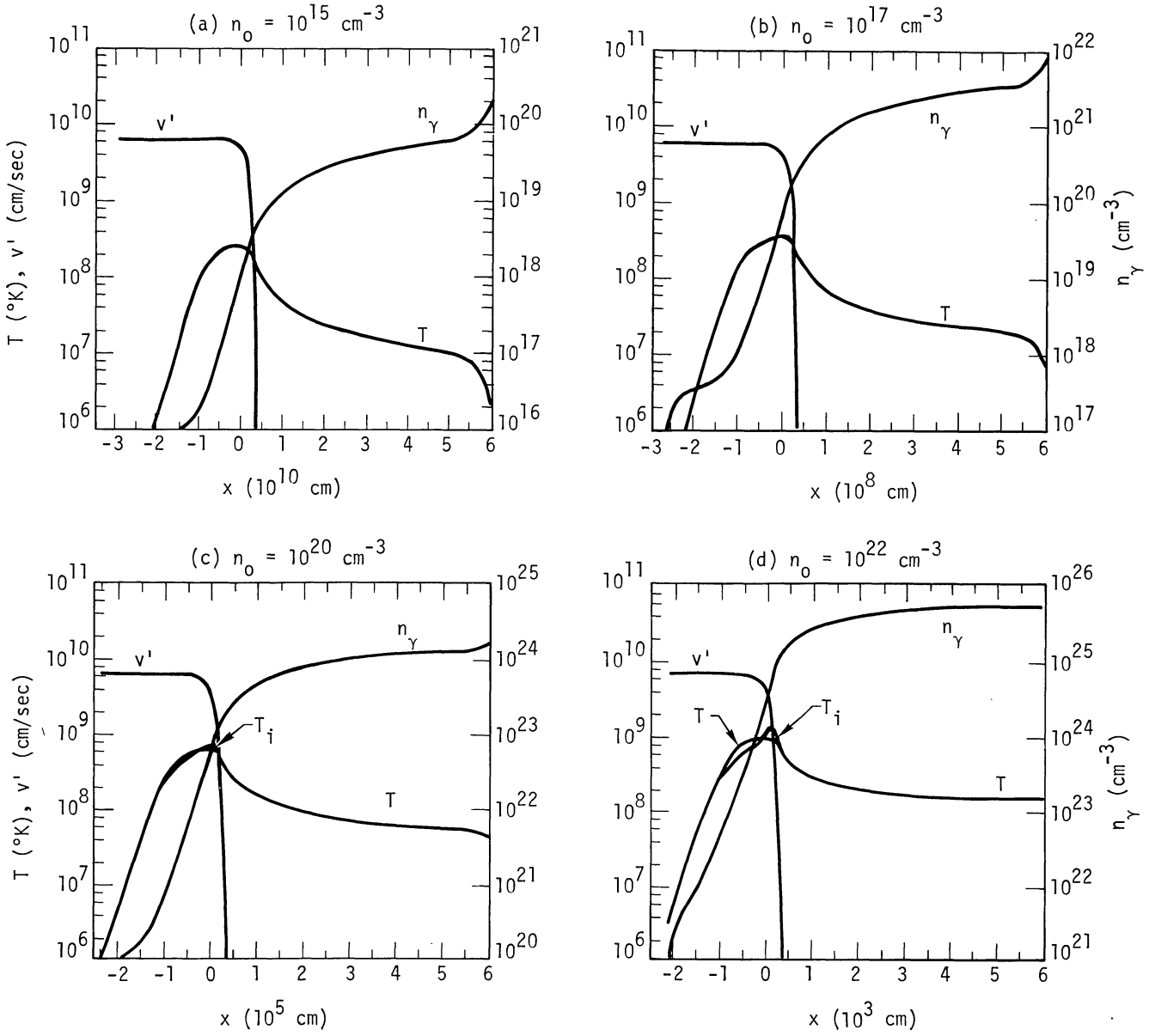

FIG. 5.—Radiation-dominated shock structures for a shock energy $E_0 = 30$ MeV and preshock density, n_0, as indicated. The preshock temperature, T_0, was taken as 2×10^4, 10^5, 10^6, and 3×10^6 K, respectively in parts (a)–(d), with the preshock radiation field considered in equilibrium. The notation is the same as for Fig. 4. Note that the lower density shocks are closest to radiative equilibrium, due mainly to the density dependence of the inverse bremsstrahlung low-energy cutoff.

matter thermal energy and pressure terms into the equations of momentum and energy conservation, (5.1) and (5.2), and utilize the variable $\eta = v/v_0$, yielding

$$P_m + P_\gamma = n_0 m_H v_0^2 (1 - \eta)\,, \tag{5.23}$$

$$\tfrac{5}{2}\eta P_m + 4\eta P_\gamma - \frac{c\eta}{n_0 v_0 \bar{\sigma}_c}\frac{dP_\gamma}{dx} = n_0 m_H v_0^2 (1 - \eta^2)/2\,, \tag{5.24}$$

where $P_\gamma = n_\gamma \theta_\gamma$ and $P_m = 2n_0 k \bar{T}_m/\eta$, and where $\bar{T}_m$ is the average of the electron and ion temperature. To determine if these equations can have a simultaneous solution, we note from substituting equation (5.23) into equation (5.24), that

$$\frac{c\eta}{n_0 v_0 \bar{\sigma}_c}\frac{dP_\gamma}{dx} = \left(\frac{7\eta - 1}{2}\right)P_\gamma + \left(\frac{4\eta - 1}{2}\right)P_m\,, \tag{5.25}$$

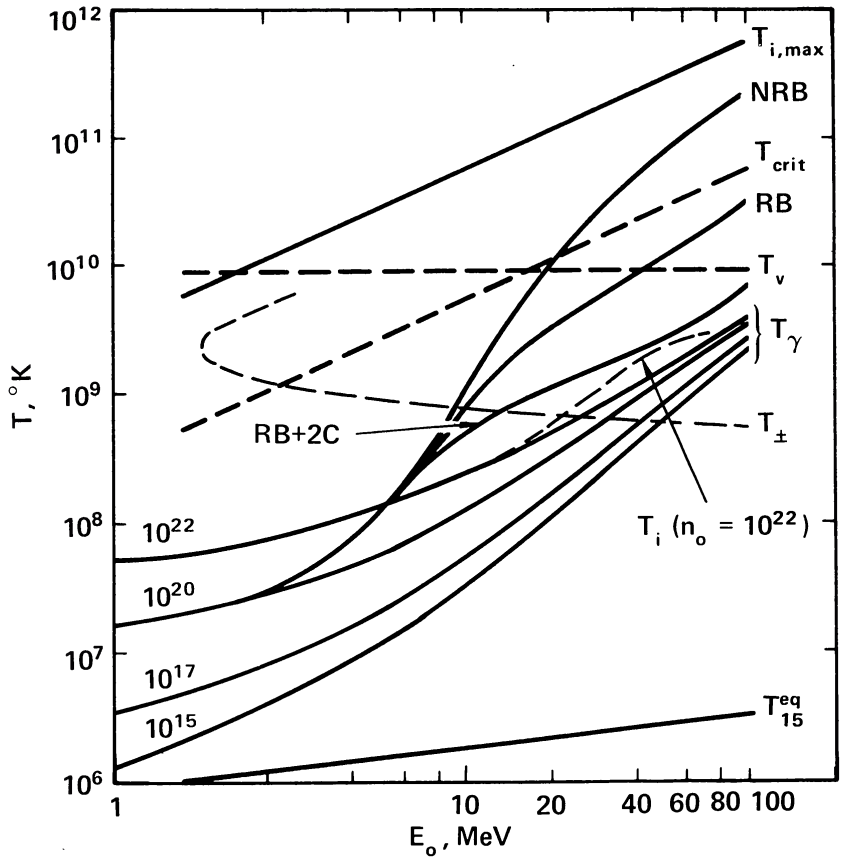

FIG. 6.—Peak and characteristic shock temperatures. The curves labeled NRB, RB, and RB+2C show the peak radiation temperature reached in the shock where only nonrelativistic bremsstrahlung, relativistic bremsstrahlung, and relativistic bremsstrahlung *and* radiative Compton scattering, respectively, are included in the calculation (and the average thermalizable bremsstrahlung photon energy is conservatively taken as $\frac{3}{2}kT_e$). These curves are plotted for density $n_0 = 10^{20}$ cm^{-3}, but except near equilibrium, the density dependence is quite weak. The curves labeled $T_\gamma(10^{15}$–$10^{22})$ are the peak radiation temperatures reached in a shock of the indicated density (in cm^{-3}) when all radiation effects including inverse Compton scattering are included, while the curve labeled $T_i(n_0 = 10^{22})$ shows the peak ion temperature associated with $T_\gamma(10^{22})$. $T_{i,max}$ is the ion temperature that would occur if all the shock energy were transformed into ion thermal energy; T_{crit} is the temperature (near the rear of the shock) below which photon diffusion can mediate the shock; T_v is the ion temperature above which ion viscosity is important over radiation-dominated shock velocity gradients; $T_\pm$ is the temperature at which the number density of pairs equals n_0; and $T_{eq}{}^{15}$ is the final equilibrium temperature at $n_0 = 10^{15}$ cm^{-3}.

and thus $dP_\gamma/dx > 0$ (for v_0 in the positive x direction) in the range $1 > \eta > \eta_1$. Here η_1 is the postshock value of η (i.e., the η for which

$$\left.\frac{dP_\gamma}{dx}\right|_{\eta_1} = 0$$

and $\eta < 1$). From equation (5.25) we see η_1 must satisfy the Hugoniot relation

$$\xi(\eta_1) = \frac{1 - 4\eta_1}{7\eta_1 - 1}, \tag{5.26}$$

resulting in fourfold compression across the shock in the absence of radiation [$\xi(\eta_1) = 0$], increasing toward sevenfold compression as $\xi(\eta_1) \to \infty$.

On the other hand, differentiating equation (5.23) with respect to x yields

$$\frac{1}{n_0 m_H v_0^2}\frac{dP_\gamma}{dx} = \frac{(2\eta - 1) + \eta\xi}{\eta(1 + \xi)}\left(-\frac{d\eta}{dx}\right) - \frac{2k}{m_H v_0^2 \eta}\frac{d\bar{T}_m}{dx}, \tag{5.27}$$

where for a physically realizable shock we require $d\eta/dx < 0$ (i.e., that the matter velocity decrease monotonically). Thus, to be consistent with the requirement derived from equation (5.25) that $dP_\gamma/dx > 0$, the right-hand side of equation (5.27) must be positive in the range $1 > \eta > \eta_1$. Physically this requirement amounts to the observation

that conservation of energy (eqs. [5.24] and [5.25]) requires energy transport by radiative diffusion in the $-x$ direction (and thus $dP_\gamma/dx > 0$), while the conservation of momentum (eq. [5.23]) determines the relation between P_γ and η. As long as $dP_\gamma/d\eta < 0$, the required magnitude of energy flux can be obtained by adjusting $d\eta/dx$, but this is no longer possible in a region where $dP_\gamma/d\eta > 0$, and thus a discontinuous jump in density and velocity will occur across such a region in the absence of other dissipation mechanisms. (See Zel'dovich and Raizer [1966, p. 477] for analogous arguments concerning electron heat conduction.)

To evaluate the right-hand side of equation (5.27) requires some assumption about $d\bar{T}_m/dx$. If $d\bar{T}_m/dx \leq 0$, then a *sufficient* condition that no discontinuity exists is

$$\xi \geq \frac{1 - 2\eta}{\eta} \quad \text{for} \quad 1 > \eta > \eta_1 . \tag{5.28}$$

This condition is most stringent when $\eta \to \eta_1$. Using the Hugoniot relation (5.26), we find that in this case equation (5.28) becomes

$$\xi_1 \geq 2 + \sqrt{6} \approx 4.45 . \tag{5.29}$$

It is interesting to note that for $\eta > 1/2$, essentially no radiation is required to prevent a discontinuity. However, if the amount of radiation is small, the gradients needed to obtain the necessary energy flux will become very large, and eventually other dissipation mechanisms will become important, even if they are not strictly needed to prevent a discontinuity. This situation will be considered in the next subsection.

It remains to consider the case when $d\bar{T}_m/dx > 0$. The Bose-Einstein model we are considering assumes $T_\gamma \approx T_e$, while we have found $T_i \approx T_e$. The range of validity of this assumption is considered below. Within this range, we take $\bar{T}_m \approx T_\gamma$, and observe that $d\bar{T}_m/dx > 0$ implies $dT_\gamma/dx > 0$, which implies that if $dP_\gamma/dx < 0$, then $dn_\gamma/dx < 0$. However, the character of the photon continuity equation (5.3) and its associated boundary conditions precludes dn_γ/dx from being negative as long as Q_γ^{eff} remains positive, which is the physical case of interest, and so no discontinuities arise.

Thus, within the framework of the present study, equation (5.28) is a generally sufficient criterion for no shock discontinuities to occur and is plotted in Figure 6 as T_{crit}. It might be noted that equations (5.28) and (5.29) are consistent with previous treatments (Belokon' [1959]; Zel'dovich and Raizer [1966, p. 543]) of the occurrence of discontinuities in shocks where the radiation field is assumed in equilibrium.

As has been pointed out by Zel'dovich and Raizer (1966, p. 546), a more intuitive, if less rigorous, approach to these questions is to note that ion-ion collisions can only substantially influence the shock when the ion sound velocity (at $\eta \approx \eta_1$) is above the velocity of the shock front relative to the postshock material, i.e. when (using eq. [5.23])

$$\frac{v_0}{7} \lesssim \left(\frac{5kT_i}{3m_i}\right)^{1/2} \approx \left(\frac{5}{49(1 + \xi)}\right)^{1/2} v_0 \tag{5.30}$$

or

$$\xi < 4 , \tag{5.31}$$

which is in good agreement with the previous results.

Numerical shock models in which both ion viscosity and radiative diffusion are taken into account will be treated in §§ VII and VIII and shown to be consistent with the above analytic results.

It should be noted that since our analysis has assumed that the shock wave has reached a steady state in its comoving frame (see § II*a*), solutions with oscillatory velocity profiles cannot arise, since such oscillations would tend to propagate as sound waves toward the front of the shock, and are thus unsteady. A discussion of this steady-state assumption and the unlikelihood of significant non–steady state effects is given in § IX*a*.

ii) *Non-Radiative Dissipation Mechanisms*

If the velocity or temperature gradients in a radiation-dominated shock steepen to the order of a few electron or ion mean-free-paths, nonradiative dissipation mechanisms such as ion viscosity and electron heat conduction will become important.

Quantitatively, we shall consider that ion viscosity plays a significant role in determining the shock structure when the viscous stress, P_v, becomes greater than one-fifth the radiation pressure, corresponding to the level at which matter pressure becomes important. This criterion can then be written

$$P_v = A_2\theta_i^{5/2}\left|\frac{dv}{dx}\right| > \tfrac{1}{5}P_\gamma = \tfrac{1}{5}n_0 v_0 m_{\text{H}}(v_0 - v) . \tag{5.32}$$

Using equations (5.6) and (5.1) and the main Coulomb term in equation (3.37), this criterion can be rewritten as

$$\theta_i \gtrsim 2.2\left(\frac{v}{7v - v_0}\right)^{2/5}\left(\frac{\sigma_{\text{T}}}{\bar{\sigma}_c}\frac{\ln \Lambda}{10}\right)^{2/5} \text{ MeV} , \tag{5.33}$$

where ln Λ is the Coulomb logarithm (Spitzer 1962). Taking $v_0/v = 7/4$, as is typical near the peak shock temperature, $\bar{\sigma}_c = \sigma_T$, ln $\Lambda = 10$, and $T_\gamma \approx T_i$, we find that viscous effects can only become important when $\theta_\gamma \gtrsim 1$ MeV. (Note, however, the limiting effects of nuclear scattering for $\theta_i \gtrsim 1$ MeV.) This criterion is plotted in Figure 6 as T_v. The exception to this, of course, is when the ratio of radiation to matter pressure falls below 4.45 at this temperature, causing the shock to steepen until viscosity generates the needed dissipation.

iii) *Charge Separation*

If the ions are stopped exclusively by the action of an electric field, the maximum electric field occurring in the shock will be given approximately by $\Sigma_{max} \approx E_0/(e\Delta)$, where Δ is the characteristic shock width and e is the protonic charge. Taking $\Delta = c/(3n_0v_0\bar{\sigma}_c)$ and using Poisson's equation, we find the net charge density, ρ, to be:

$$\frac{\rho}{en_0} \approx 4.7 \times 10^{-19}\left(\frac{\bar{\sigma}_c}{\sigma_T}\right)^2 n_{20}{}^0 E_0{}^2 \quad \text{(MeV)}\,. \tag{5.34}$$

Thus the maximum required charge separation is quite small, and using equation (5.4) we see that the difference between the ion and electron velocities is also negligibly small. As discussed below, however, the presence of electron-positron pairs can cause substantial differences between these velocities. In addition, if ions with a different charge-to-mass ratio from hydrogen are present at levels typical of Population I stars, the electric field is not sufficient to ensure that all species remain comoving. As will be shown in § VIII, however, viscous forces acting between ions serve to keep the resulting velocity differentials small.

iv) *Consistency of the Effective-Photon Approximation*

One expects the effective photon approximation to be valid provided $\lambda_d \equiv \epsilon_d/\theta_e \ll 1$. Examination of the numerical solutions shows this to be the case for temperatures $\gtrsim$ 1–5 keV, depending on the shock energy. Temperatures < 5 keV are typically found only near the leading edge of the shock and in the final postshock equilibrium region for shocks of low density and energy. Numerical sensitivity experiments show, however, that the bulk of the shock structure is little affected by conditions in these extreme regions.

The principal error involved in the effective photon approximation arises from the specification of the time available for photon thermalization, τ_d. By taking τ_d as the *smallest* relevant shock scale, we neglect soft photons which are thermalized only after times longer than τ_d, but still in time to help cool the downstream portion of the shock. The sharp increase in photon density across the shock, however, will tend to dilute this effect. In addition, this error toward lower photon density is consistent with the policy we have used in resolving uncertainties in the evaluation of $Q_\gamma{}^{eff}$ (see § III*a*), and results in the temperatures in radiation-dominated shock models being in fact approximate *upper* limits on the actual shock temperatures.

Since the electrons serve principally as intermediaries in transferring energy between the hot photons that have diffused upstream and newly created subthermal photons, we expect that their temperature will be a good measure of the effective photon temperature, and thus $T_e \approx T_\gamma$.

v) *Pair Effects*

From the results of § III*b*, we note that the number of electron-positron pairs will become significant somewhere in the regime $\theta_e = 60$–100 keV. The substantial changes these pairs make in the shock structure are treated in the next section. The critical temperature $T_\pm$ derived there for the onset of these changes is plotted in Figure 6.

e) *Discussion*

Comparison of the radiation-dominated shock structures presented in Figures 4 and 5, and summarized in Figure 6, with the results of § V*d* shows that throughout the range of our calculations, radiative heat transport provides sufficient dissipation to mediate the shock transition, and moreover does so over scale lengths sufficiently large that viscosity never becomes an important dissipation mechanism, and serves only to heat the ions mildly. It is evident that, while not required to avoid a viscous shock, inverse Compton scattering provides the dominant mechanism for cooling the electrons and thus reducing the peak ion temperatures by more than two orders of magnitude from those that could occur in a viscosity-dominated shock.

The density dependence of the peak shock temperatures is due primarily to the density dependence of the inverse bremsstrahlung cutoff, τ_B, defined in equation (4.5). This cutoff has the most effect in determining the effective photon emission rate at low shock energies where it is not usually dominated by the thermalization cutoff, τ_d, and this behavior is reflected in Figure 6. In the shock calculations where inverse Compton processes are neglected, the only residual density dependence is due to the factor f_E, which allows for inverse processes near radiative equilibrium, and the very small density dependence of ln Λ, the Coulomb logarithm that occurs in the ion viscosity and electron-ion coupling coefficients. The treatment of inverse Compton scattering used in the present study is substantially more accurate than the approximate treatment used in Weaver and Chapline (1974), primarily due to the use of the variable Gaunt factor $g_1(\lambda)$ in place of a constant "averaged" one ($g_1 = 2.71$). This results in a

reduction of the peak shock temperatures by 5–50 percent from the previous work, for the case where inverse Compton scattering is included.

The ion temperature is determined primarily by viscous heating and electron-ion coupling (see eq. [5.5]). For $\theta_e \lesssim 25$ keV, the *e-i* coupling is sufficiently strong to keep T_i essentially equal to T_e, while at higher temperatures the $T_e^{-3/2}$ dependence of this coupling together with the $T_i^{5/2}$ dependence of the ion viscosity allows moderate temperature differences to develop. Since radiative heat transport serves to convert the kinetic energy of the ions directly into electron and photon thermal energy, T_i tends to lag T_e in the upstream portion of the shock where the velocity gradients are small, and thus viscosity is negligible. The viscous heating that occurs near the center of the shock ($x = 0$) is usually sufficient to make $T_i > T_e$ there, a difference which is then quickly relaxed in the postshock region [see, e.g., Fig. 4(*e*)]. For $T_e \gtrsim 300$ keV, however, T_i lags T_e so much in the upstream region that the ion temperature never reaches the maximum electron temperature [see Fig. 4(*f*)]. The T_i curve in Figure 6 summarizes this behavior.

As predicted by the near-equilibrium analytic shock models of § V*b*, the shocks are close to equilibrium near $E_0 = 1$ MeV, particularly in the upper part of the density range, where fewer photons per electron are required for equilibration (see Figs. 4(*a*) and 6, and eq. [5.21]).

Comparison of the $T_\pm$ and T_γ curves in Figure 6 shows that pairs become important for radiation temperatures $\gtrsim 60$–70 keV and shock energies $\gtrsim 30$–50 MeV nucleon^{-1}. As will be discussed, the general effect of this transition is to increase the degree of radiative equilibrium and thus lower the peak shock temperature relative to the radiation-dominated model. At the same time the source of dissipation is expected to shift from radiative heat transport to ion-lepton Coulomb friction.

We thus conclude that the ion temperature remains below ~ 400 keV for shock energies up to 100 MeV nucleon^{-1} in the radiation-dominated case, and (as we will show in § VI) below ~ 100–200 keV when the effect of pairs is taken into account. Since spallation thresholds ($Z > 1$) are ~ 8 MeV nucleon^{-1}, the amount of nuclear spallation that will take place in these shocks is quite small, and thus essentially no deuterium will be produced. Indeed, the $n\tau$ products characteristic of the temperature peaks of these shocks (where τ is the time duration) are only of the order of 10^{15}–10^{17} cm^{-3} s, which for $T_i \sim 100$–400 keV, will only suffice to burn whatever beryllium, boron, and perhaps lithium, might have been present originally (see Fowler, Caughlan, and Zimmerman 1975). Deuterium, tritium, and ^{3}He will not be appreciably burned unless they have a mass fraction of at least several percent.

Before accepting these conclusions, it is desirable to investigate whether other self-consistent shock-structure solutions can be found (especially one corresponding to a high temperature viscous shock), as has been suggested by Colgate (1975*a*), and indeed whether the self-consistency of the low-temperature radiation-dominated solutions is stable against perturbations. To do this it is necessary to explicitly include the effects of viscosity in our calculations. This is carried out in §§ VII and VIII.

VI. EFFECT OF ELECTRON-POSITRON PAIRS ON SHOCK STRUCTURE

The number density of pairs created in a characteristic radiation-dominated shock width, Δ, by photons moving with mean velocity $v_\gamma \approx v_0/4$ is

$$N_p = \frac{Q_{\gamma\gamma}{}^{\pm}}{v_\gamma}\frac{c}{3v_0 n_0 \bar{\sigma}_c} = 96.0\left(\frac{n_\gamma}{n_0}\right)^2\left(\frac{\sigma_T}{\bar{\sigma}_c}\right)(1 + 0.782\Phi^{-1})^{7/2}\Phi^3 e^{-2\Phi}\frac{n_0}{E_0\,(\mathrm{MeV})}, \tag{6.1}$$

where we have obtained $Q_{\gamma\gamma}{}^{\pm}$, the rate of photon-photon pair creation, from equation (3.14); and $\Phi = m_e c^2/kT$. From § III*b*, we have that the number density $n^{\pm}$ of electron-positron pairs in relative equilibrium with a Bose-Einstein distribution with photon density n_γ is

$$n^{\pm} \approx 0.50\Phi^2 K_2(\Phi) n_\gamma \xrightarrow[\Phi \gg 1]{} 0.63\Phi^{3/2} e^{-\Phi} n_\gamma \tag{6.2}$$

where $K_2(\Phi)$ is the second-order modified Bessel function of the second kind. For example, $n^{\pm} \approx 0.04 n_\gamma$ at $kT = 100$ keV. Combining equations (6.1) and (6.2) and assuming $v_\pm \approx v$ (see below), we find that γ-γ pair creation is sufficiently fast to cause the pair density to be in relative equilibrium for

$$E_0\,(\mathrm{MeV}) \leq 1.52 \times 10^4\left(\frac{n_\gamma}{100 n_0}\right)\left(\frac{\sigma_T}{\bar{\sigma}_c}\right)\Phi^{3/2} e^{-\Phi}(1 + 0.782/\Phi)^{7/2}. \tag{6.3}$$

For $\theta_e = 50$ keV, and $\bar{\sigma}_c = \sigma_T$, we find the pairs will be in relative equilibrium for $E_0 \lesssim 23(n_\gamma/100 n_0)$ MeV; for $\theta_e = 75$ keV, for $E_0 \lesssim 435(n_\gamma/100 n_0)$ MeV; and for $\theta_e = 100$ keV, for $E_0 \lesssim 1750(n_\gamma/100 n_0)$ MeV. Thus for the energies of present interest (i.e., $E_0 \lesssim 100$ MeV), the pairs can be considered to be in relative equilibrium whenever their density is at all significant (i.e., $\gtrsim n_0$).

By combining equations (5.1) and (6.2) we can derive the condition for $n_\pm \gtrsim n_0$ as

$$E_0\,(\mathrm{MeV}) \gtrsim 0.95\Phi^{-5/2} e^{\Phi}, \tag{6.4}$$

where Φ is evaluated at $v/v_0 = 4/7$ (i.e., essentially at the peak shock temperature). Since the density of pairs is extremely temperature-dependent for $\theta_e \lesssim 200$ keV, the temperature, $T_\pm$, at which $n_+ = n_0$ (derived from eq. [6.4]), is a good criterion for when pair effects can become important, and is plotted in Figure 6.

A principal effect of the pairs is to support a current tending to short out the shock electric field and thus weaken the electron-ion coupling, lengthen the shock scale, and allow more time for radiative equilibration. At the same time, however, the presence of pairs increases the opacity as well as the photon production rate, which tends to reduce the scale of the shock, while leaving the degree of equilibrium unchanged. Which effect dominates depends on the pair conductivity, and on the magnitude of the direct ion-lepton coupling via Coulomb friction.

While accurate solution of the resulting shock structure seemingly must be done numerically, a fairly plausible pair-dominated shock can be sketched out.

Using the facts that the total current through the shock must vanish and the fractional charge density must be exceedingly small (i.e., Debye length $\ll$ shock width), we find that

$$v_e = v_i\left(1 - \frac{J_\pm}{en_0v_0}\right), \tag{6.5}$$

where $J_\pm \equiv en_+(v_e - v_+)$ is the current due to the presence of pairs and v_+ and n_+ are the positron velocity and density. Approximately adopting the classical plasma conductivity given by Spitzer (1962) to a pair gas by multiplying it by a factor $\sqrt{(2)}n_+/n_{e^-}$, we find

$$\frac{J_\pm}{en_0v_0} \approx 3.56 \times 10^{-4}\theta_e^{3/2}\,(\text{keV})\,E_0\,(\text{MeV})\,\frac{n_+}{n_{e^-}}\frac{\bar{\sigma}_c}{\sigma_T}\frac{10}{\ln\Lambda}\frac{\Sigma_x}{\Sigma_{\max}}, \tag{6.6}$$

where Σ_x is the electric field, n_{e^-} the total e^- density, and $\Sigma_{\max}$, the maximum electric field that can occur in the absence of pairs (see § V*d*). We see that for $\theta_e \gtrsim 60$ keV, $E_0 \gtrsim 30$ MeV, $n_+ \approx n_{e^-}$, and $\Sigma \approx \Sigma_{\max}$, that $J_\pm/en_0v_0$ is $\gtrsim 1$. Since the velocities in equation (6.5) cannot be negative, a self-consistent solution of equation (6.6) will be reached in which $\Sigma_x < \Sigma_{\max}$ and $J_\pm/en_0v_0 \approx 1$. Physically, one expects that without the aid of a strong electric field the electrons will be approximately comoving with the radiation field, and most of the shock dissipation will occur via resistive heating of the pairs and Coulomb friction between the ions and leptons.The relative contribution of these effects can be estimated by calculating the ratio of the classical Coulomb stopping distance l_{ei} (derived from Spitzer 1962) to the distance over which the reduced electric field can stop the ions. This ratio is given by

$$\frac{l_{ei}}{E_0/e\Sigma_x} = 1.26 \times 10^{-4}\theta_e^{3/2}\,(\text{keV})\,E_0\,(\text{MeV})\left|\frac{v_0}{v_i - v_e}\right|\frac{\bar{\sigma}_c}{\sigma_T}\frac{10}{\ln\Lambda}\frac{n_0}{n_e}\frac{\Sigma_x}{\Sigma_{\max}}. \tag{6.7}$$

For $J_\pm/en_0v_0 \approx 1$ appropriate when $\Sigma \ll \Sigma_{\max}$, we find from equation (6.6) that

$$\frac{l_{ei}}{E_0/e\Sigma_x} = 0.35\frac{n_{e^-}}{n_+}\left|\frac{v_0}{v_i - v_e}\right|\frac{n_0}{n_e}. \tag{6.8}$$

It thus appears that electron-ion Coulomb friction will provide the dominant dissipation when more than a few pairs per nucleon are present. The scale of the shock, $\Delta_\pm$, is then l_{ei} with $v_0/(v_i - v_e) \approx 1$, i.e.,

$$\Delta_\pm = 0.7\Phi^{-4}e^\Phi\frac{10}{\ln\Lambda}\frac{\bar{\sigma}_c}{\sigma_T}\Delta, \tag{6.9}$$

which holds when $n_e/n_0 \gg 1$ and $\theta_e/m_ec^2 < 1$ and provided the classical e^+e^- conductivity and stopping lengths assumed above are applicable.

Two stream instabilities between the ions and electrons or the electrons and positrons may, however, lead to anomalously small values of l_{ei} and the plasma conductivity. Idealized linear theory (Stringer 1964) predicts the existence of stable counterstreaming for $|v_i - v_e| \lesssim 1.2(\theta_e/m_e)^{1/2}$ when $T_e \approx T_i$. For $\theta_e \gtrsim 60$ keV where pairs become important, we thus require $E_0 \gtrsim 160$ MeV to reach an unstable regime for $|v_i - v_e| \approx v_0$. Further, McKee (1970) has shown in one-dimensional numerical simulations that the *e-i* two-stream instability leads to heating $\sim m_e|v_i - v_e|^2$, which is a factor m_i/m_e too small to mediate a collisionless shock. Thus classical two-stream instabilities do not appear to play a crucial role in the shock structures of present interest.

Returning to equation (6.9), we see that, due to the rapid rise in pair number with temperature below 200 keV, the absolute size of the shock will be smaller than it would have been without pairs, decreasing to a minimum of $\sim 0.2\Delta$ at 100 keV and then expanding. When the size of the shock is measured in Compton lengths, however, the shock width with pairs increases monotonically and always remains more than that of a shock from which pairs have been artificially excluded. The pair shock's radiation field will thus be seemingly better equilibrated and will reach a lower peak temperature than the pairless shock, although one must solve the problem self-consistently, allowing for the sharp decrease of pair number with temperature. The probable outcome is that the temperature will remain below $\sim$100–200 keV for $E_0 < 100$ MeV nucleon^{-1}. Using the criterion of § V*d*, we see that this is too low a temperature for ion viscosity to become important even over the reduced shock scales. In addition, ion viscosity will be damped by ion-lepton collisions.

We are thus led to the overall picture of a pair-dominated shock where a relatively cool radiation-pair field stops the incoming electrons fairly abruptly near the front of the shock, while the ions are stopped gradually by the pairs, heating and regenerating the radiation-pair field in the process. This scenario is in some respects similar to the equilibrium pair-dominated shocks suggested by Colgate (1969) to occur in the mantles of compact supernovae ($n_0 \approx 10^{28}$ cm^{-3}, $T_{eq} \approx 500$ keV, $E_0 > 16$ MeV) and to be involved in cosmic-ray production.

VII. SHOCK MODELS WITH VISCOSITY

a) One-Fluid Viscous Shocks without Radiation

Specializing the shock-structure equations (2.13)–(2.20) to the case of a single fluid containing no radiation or pairs, we obtain, after some rearrangement,

$$n_0 v_0 kT - \mu v \frac{dv}{dx} = m n_0 v_0 (v_0 - v) v + P_0 v \,, \tag{7.1}$$

$$\alpha n_0 v_0 kT - \kappa \frac{dT}{dx} = \tfrac{1}{2} m n_0 v_0 (v_0 - v)(v_0 - v + 2\epsilon_0 v_0) + \alpha_0 P_0 v_0 \,, \tag{7.2}$$

$$n = n_0 v_0 / v \,. \tag{7.3}$$

Here n is the particle number density; v is the velocity of the fluid relative to the shock; n_0 and v_0 are the preshock values of n and v; T is the temperature; x is the spatial coordinate in the rest frame of the shock; μ and κ are the coefficients of viscosity and heat conduction; α, the specific heat coefficient, is defined as the ratio of energy density to pressure; m is the particle mass; k is Boltzmann's constant; P_0 and α_0 are the preshock pressure and α-value, respectively; and $\epsilon_0 \equiv P_0 / m n_0 v_0^2$.

Models of the type represented by equations (7.1)–(7.3) have been studied by several authors (cf. Zel'dovich and Raizer 1966). For clarity and continuity, and to develop methods applicable to the more general shock problem, we shall independently derive some of the properties of this model, for the case of constant μ and κ.

It is convenient to first cast equations (7.1)–(7.3) into the dimensionless form

$$\tau - \eta\delta \frac{d\eta}{d\zeta} = \eta(1 - \eta) + \eta\epsilon_0 \,, \tag{7.4}$$

$$\alpha\tau - \frac{d\tau}{d\zeta} = \tfrac{1}{2}(1 - \eta)(1 - \eta + 2\epsilon_0) + \alpha_0\epsilon_0 \,, \tag{7.5}$$

$$\frac{n}{n_0} = \frac{1}{\eta} \,, \tag{7.6}$$

where

$$\eta \equiv \frac{v}{v_0} \,, \qquad \delta \equiv \frac{\mu k}{m\kappa} \,, \qquad \zeta \equiv \frac{x n_0 v_0 k}{\kappa} \,, \qquad \tau \equiv \frac{kT}{m v_0^2} \,. \tag{7.7}$$

The Hugoniot relations governing conditions on either side of the shock are obtained as usual by setting the gradients in equations (7.4) and (7.5) to zero. By construction the preshock solution is $n = n_0$, $\eta = 1$, $\tau = \epsilon_0$. For the case of constant α, the postshock conditions (denoted by the subscript 1) are found directly to be (independent of the constancy of μ and κ)

$$\eta_1 = \frac{1 + 2(1 + \alpha)\epsilon_0}{2\alpha + 1} \rightarrow \begin{cases} \dfrac{1 + 5\epsilon_0}{4} \,, & \alpha = \tfrac{3}{2} \,, \\ \dfrac{1 + 8\epsilon_0}{7} \,, & \alpha = 3 \,, \end{cases} \tag{7.8}$$

$$\tau_1 = \frac{(1 + 2(1 + \alpha)\epsilon_0)(2\alpha - \epsilon_0)}{(2\alpha + 1)^2} \rightarrow \begin{cases} \dfrac{(1 + 5\epsilon_0)(3 - \epsilon_0)}{16} \,, & \alpha = \tfrac{3}{2} \,, \\ \dfrac{(1 + 8\epsilon_0)(6 - \epsilon_0)}{49} \,, & \alpha = 3 \,, \end{cases} \tag{7.9}$$

$$\frac{n_1}{n_0} = \frac{1}{\eta_1} \,. \tag{7.10}$$

For nonconstant α, the Hugoniot relations can be solved quadratically and then iterated to find η_1 and τ_1.

For the special case $\delta = 1/(\alpha + 1)$ (α constant), equations (7.4)–(7.6) can be solved analytically. (This was first shown by Becker 1922.) This is a not unreasonable approximation for single-species gases or *single*-component plasmas. Indeed, $\delta \approx 0.36$ for the latter case, although μ and κ are then highly temperature-dependent. Adding equation (7.4) to (7.5) and making the above substitution, we find

$$(\alpha + 1)\tau + \tfrac{1}{2}\eta^2 - \frac{1}{\alpha + 1}\frac{d}{d\zeta}[(\alpha + 1)\tau + \tfrac{1}{2}\eta^2] = (\alpha + 1)\epsilon_0 + \tfrac{1}{2}. \tag{7.11}$$

Making the substitution $h \equiv (\alpha + 1)\tau + \frac{1}{2}\eta^2$, we see that equation (7.11) is a standard first-order differential equation having the solution

$$h = h_0 + De^{(\alpha+1)\zeta}, \tag{7.12}$$

where $h_0 \equiv (\alpha + 1)\epsilon_0 + \frac{1}{2}$ is the upstream value of h, and D is an undetermined constant. Unless $D = 0$, the exponential term in equation (7.12) will blow up at the downstream limit, while the Hugoniot relations show h_0 to also be the correct downstream value of h. We therefore conclude that $h = h_0$ throughout the shock. Using this result, we find from equation (7.4) and (7.8) that

$$-\frac{d\eta}{d\zeta} = \frac{(1 - \eta)(\eta - \eta_1)(2\alpha + 1)}{2\eta} = \frac{(\alpha + 1)}{\eta}\frac{d\tau}{d\zeta}, \tag{7.13}$$

which can be integrated to find ζ:

$$\zeta = \frac{1}{\alpha - (1 + \alpha)\epsilon_0}\ln\left[\frac{(1 - \eta)}{(\eta - \eta_1)^{\eta_1}}\right] + \zeta_0, \tag{7.14}$$

where ζ_0 is a constant fixing the location of the shock. Asymptotically,

$$\begin{aligned} 1 - \eta &\approx \exp[(\alpha - (1 + \alpha)\epsilon_0)\zeta], && \zeta \to -\infty, \\ \eta - \eta_1 &\approx \exp\left[-\frac{1}{\eta_1}(\alpha - (1 + \alpha)\epsilon_0)\zeta\right], && \zeta \to +\infty. \end{aligned} \tag{7.15}$$

Equation (7.14) is singular for $\epsilon_0 = \alpha/(1 + \alpha)$, which is just the point where v_0 equals the initial adiabatic sound speed, c_s^0, and, retracing our steps, we find $d\eta/d\zeta = 0$ as expected. In general, the upstream Mach number, M, is given by

$$M \equiv \frac{v_0}{c_s^0} = \left[\frac{\alpha}{(1 + \alpha)\epsilon_0}\right]^{1/2}. \tag{7.16}$$

It is interesting to note that the velocity profile given by equation (7.14) is identical to that in the radiation-dominated shock model when $\epsilon_0 = 0$ and $\alpha = 3$ (see eq. [5.21]), although the relation between τ and η is different.

Taking another special case, we can investigate the role of viscosity by setting $\delta = 0$ and seeing if continuous shock solutions can be obtained. Differentiating equation (7.4) and using equation (7.5) to eliminate $d\tau/d\zeta$, we find

$$-\frac{d\eta}{d\zeta} = \frac{2\alpha + 1}{2}\frac{(1 - \eta)(\eta - \eta_1)}{(1 - 2\eta + \epsilon_0)}. \tag{7.17}$$

This solution is singular for $\eta = \eta_c \equiv (1 + \epsilon_0)/2$, and we thus expect a shock discontinuity unless $\eta_1 > \eta_c$, which occurs only for weak shocks with

$$\epsilon_0 < \frac{2\alpha - 1}{2\alpha + 3} \quad \text{or} \quad M < \left[\frac{(2\alpha + 3)\alpha}{(2\alpha - 1)(\alpha + 1)}\right]^{1/2}. \tag{7.18}$$

For $\alpha = \frac{3}{2}$, this criterion becomes $M = \sqrt{\frac{9}{5}} \approx 1.34$.

Thus ordinary heat conduction is usually insufficient to mediate a strong shock, and some other dissipation mechanism (typically viscosity) is required to prevent a discontinuity. Note, however, that no discontinuity occurs for $\alpha \leq \frac{1}{2}$, a case which might correspond to a highly Fermi-degenerate medium (if the Fermi energy is subtracted in the α calculation—alternately such a case could be considered a "weak" shock). This fact, together with the large heat conduction coefficient typically associated with such media, might dramatically increase the scale of the shock relative to a viscous mean-free-path estimate. The possible implications of this for carbon-detonation supernovae are being investigated.

In general, the physical content of criterion (7.18) is that, in the absence of viscosity, relatively little increase in the energy density near the back ($\eta \approx 1$) of a shock is required to provide pressure balance [scales as $(1 - \eta)$ from eq. (7.4)], while the material there is being rapidly compressed ($\sim 1/\eta$). For strong shocks, this usually results in a

negative temperature gradient and thus the inability to provide the required heat flux toward the front of the shock. Weak or low α thermal conduction shocks are possible because they are not sufficiently compressed to encounter this difficulty. Also, as we have discussed analytically in § V*d* and will treat numerically in the next subsection, strong shocks with sufficiently high radiation pressure may be mediated solely by radiative heat conduction, basically since the radiation field does not take part in the final sharp compression. Note also that the radiation field can transport energy *against* a temperature gradient if a sharp enough gradient in photon number exists to compensate.

Returning to the radiationless case at hand, we wish now to solve the basic viscous shock equations, (7.1)–(7.3), numerically in the case of arbitrary δ (but constant μ and κ, and $\alpha = \frac{3}{2}$). This can be done in a stable and convenient fashion by differencing equations (7.1) and (7.2) in the manner given in Appendix C and solving the resulting equations simultaneously for v^{i+1} and T^{i+1} at point x^{i+1} in terms of the variables at point x^i. The form of the special case solution (7.12) suggests that such an integration will be stable only if carried out in the $-x$ direction, i.e., from the back to the front of the shock, for otherwise the unwanted exponential solution will exponentiate off the noise inevitable in any finite difference scheme. This is indeed observed to the case.

In order to begin such an integration, one needs an asymptotic solution for the downstream limit for T in terms of v. To obtain such a solution, we make the substitutions $\epsilon \equiv \eta - \eta_1$ and $\epsilon_\tau \equiv \tau_1 - \tau$ in equations (7.4) and (7.5). Using the Hugoniot relations (7.8)–(7.10) and neglecting terms higher than first order in ϵ and ϵ_τ, we obtain

$$-\epsilon_\tau - \frac{\delta}{4}(1 + 5\epsilon_0)\frac{d\epsilon}{d\zeta} = \frac{\epsilon}{2}(1 - 3\epsilon_0)\,, \tag{7.19}$$

$$-\tfrac{3}{2}\epsilon_\tau + \frac{d\epsilon_\tau}{d\zeta} = \frac{\epsilon}{4}(\epsilon_0 - 3)\,. \tag{7.20}$$

The form of these equations and the methods of nonlinear mechanics (cf. Minorsky 1947; Jaffrin and Probstein 1964) suggest trying exponential solutions in the form

$$\epsilon = Be^{\lambda\zeta}\,, \qquad \epsilon_\tau = Ce^{\lambda\zeta}\,, \tag{7.21}$$

where B, C, and λ are undetermined constants. Making these substitutions and solving for C/B yields

$$\frac{\epsilon_\tau}{\epsilon} = \tfrac{1}{4}\{[(1 - 3\epsilon_0 + 3\eta_1\delta)^2 - 16\tau_1\delta]^{1/2} - 1 - 3(\eta_1\delta - \epsilon_0)\}\,, \tag{7.22}$$

The shock integration is then started by choosing $\epsilon \ll 1$ ($\equiv \epsilon_s$) at $x = 0$ and then finding ϵ_τ from equation (7.22). Numerically, we find that using this asymptotic solution leads to the appropriate upstream boundary conditions.

The results of such numerical integrations are shown in Figure 7 for the case of strong shocks with various values of δ. Note that the majority of the velocity change takes place over a few viscous lengths ($\lambda_\mu \equiv \mu/mn_0v_0$) near the back of the shock while thermal conduction has preheated the incoming material over a distance $\lambda_\kappa \equiv \lambda_\mu/\delta$. The analytic solution for the special case $\delta = 0.4$ agrees precisely with the numerical calculation. It is also clear from Figures 7(*a*) and 7(*b*) that heat conduction does not play an essential role in the formation of a viscous shock.

b) Viscous Shock Models with Specified Radiation Fields

To study the effects of radiation on viscous shocks, we reintroduce the radiation pressure, energy density, and heat transport terms into equations (7.1)–(7.2), yielding

$$(1 + \chi\eta)n_0v_0kT - \mu v\frac{dv}{dx} = mn_0v_0(v_0 - v)v + P_0v\,, \tag{7.23}$$

$$(\tfrac{3}{2} + 3\chi\eta)n_0v_0kT - \lambda_0n_0vkT\frac{d\chi}{dx} - \kappa'\frac{dT}{dx} = \tfrac{1}{2}mn_0v_0(v_0 - v)(v_0 - v + 2\epsilon_0v_0) + \alpha_0P_0v_0\,, \tag{7.24}$$

where

$$\chi \equiv \frac{9}{10}\frac{n_\gamma}{n_0}\,, \qquad \kappa' \equiv \kappa + \chi\eta\lambda_0v_0n_0k\,, \qquad \lambda_0 \equiv \frac{c}{v_0}\frac{1}{n_0\bar{\sigma}_c}\,, \tag{7.25}$$

and

$$P_0 = (1 + \chi_0)n_0kT_0\,, \qquad \alpha_0 = \frac{3/2 + 3\chi_0}{1 + \chi_0}\,. \tag{7.26}$$

Here χ_0 is the preshock value of χ, $\bar{\sigma}_c$ is the photon energy transport mean free path, c is the speed of light, and the specific heat coefficient for the matter has been taken as $\frac{3}{2}$. In addition, our assumption of constant μ and κ will be retained.

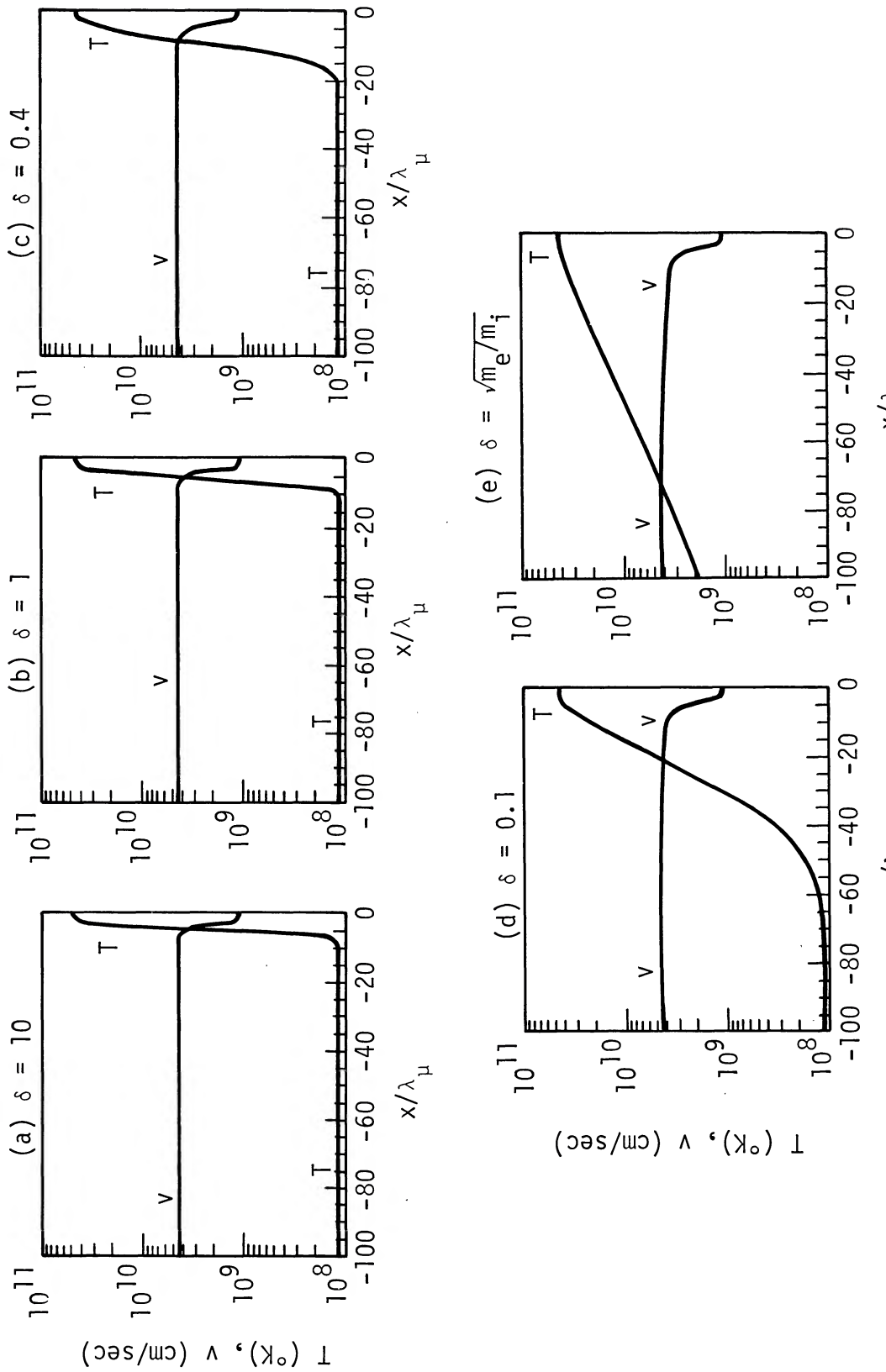

FIG. 7.—One-fluid viscous shocks for various values of the dimensionless ratio $\delta \equiv \mu k/mn$, where μ and κ are the coefficients of viscosity and heat conduction, respectively, m is the mass of the shocked particles, and k is Boltzmann's constant. The position of the shock, shown here in its comoving frame, is fixed by specifying that the fluid velocity v (directed to the right) at $x = 0$ be $\epsilon_s v_0$ above its asymptotic postshock value, where $\epsilon_s = 10^{-4}$ and v_0 is the preshock velocity. T is the temperature, and the spatial coordinate, x, is measured in units of the characteristic viscous length $\lambda_\mu \equiv \mu/mn_0v_0$, where n_0 is the preshock number density. While the specific cases shown are for a shock energy $E_0 = 10$ MeV, $n_0 = 10^{20}$ cm^{-3}, and a preshock temperature, T_0, of 1.16×10^8 K, the results can be readily scaled to any strong shock of the same Mach number. Note that the width of the velocity transition is largely independent of δ and always $\sim \lambda_\mu$, indicating that the transition is viscosity-mediated and insensitive to the effects of heat conduction. The temperature transition length, on the other hand, is $\sim \lambda_\kappa \equiv \kappa/kn_0v_0$, but is lower-bounded by λ_μ. An almost purely viscous shock is shown in (*a*), while (*c*) and (*e*) are characteristic of a monotonic gas and an effectively one-fluid hydrogen plasma, respectively.

In dimensionless form these equations become

$$(1 + \chi\eta)\tau - \eta\delta\frac{d\eta}{d\zeta} = \eta(1 - \eta + \epsilon_0)\,, \tag{7.27}$$

$$(\tfrac{3}{2} + 3\chi\eta)\tau - A\eta\tau\frac{d\chi}{d\zeta} - (1 + \chi\eta A)\frac{d\tau}{d\zeta} = \tfrac{1}{2}(1 - \eta)(1 - \eta + 2\epsilon_0) + \alpha_0\epsilon_0\,, \tag{7.28}$$

where $A \equiv \lambda_0/\lambda_\kappa$. In the present section, we shall assume $\chi(x)$ is a known function.

The main analytic result of this model, the ability of radiation to mediate a strong shock, has already been discussed in a slightly different form in § V*d*, and we will concentrate here on the methods necessary to obtain specific numerical solutions.

As is obvious from the radiation-dominated shocks shown in Figure 4, the photon number gradient, $d\chi/d\zeta$, will not in general vanish at the same downstream region as the velocity and pressure gradients. Instead, an extended radiation relaxation region will typically occur after the shock proper, in which increasing photon number balances a declining temperature to maintain constant pressure. It is numerically convenient to separate these two regions by choosing an $x \equiv x_s$ such that

$$\left.\frac{d\eta}{d\zeta}\right|_{x_s} \ll 1\,.$$

For the purposes of calculating the structure of the shock proper, the downstream radiation conditions are taken as $\chi_1 \equiv \chi(x_s)$ and $\chi_1' \equiv (d\chi/d\zeta)_{x_s}$; and $(d\chi/d\zeta)_{x\to-\infty}$ is assumed to become negligible.

Pseudo-Hugoniot relations can then be obtained by first assuming $d\eta/d\zeta \to 0$ in equation (7.27). Differentiating the result, we find immediately that $d\Pi/d\zeta$ also $\to 0$, where $\Pi \equiv (1 + \chi\eta)\tau$. We then find the pseudo-downstream conditions (denoted by subscript 1) to be described by the relations

$$(1 + \chi_1\eta_1)\tau_1 = \eta_1(1 - \eta_1 + \epsilon_0)\,, \tag{7.29}$$

$$(\tfrac{3}{2} + 3\chi_1\eta_1)\tau_1 - \eta_1\tau_1\chi_1'\frac{(A - 1)}{1 + \chi_1\eta_1} = \tfrac{1}{2}(1 - \eta_1)(1 - \eta_1 + 2\epsilon_0) + \alpha_0\epsilon_0\,. \tag{7.30}$$

The second term in equation (7.30) represents residual dissipation occurring at the relaxation layer interface, and is typically small. Indeed, if this term becomes too large, meaningful solutions of equations (7.29)–(7.30) for η_1 and τ_1 do not exist, implying that our arbitrary association of shock and radiation field by our choice of x_s was nonphysical. Typically, however, reasonable values of τ_1 and χ_1 are readily found by using equation (7.29) to eliminate τ_1 from equation (7.30) and then iterating.

To find pseudo-downstream asymptotic solutions, we proceed as before, except that instead of ϵ_τ we introduce the expansion variable $\epsilon_\pi \equiv \Pi_1 - \Pi$ where $\Pi_1 \equiv (1 + \chi_1\eta_1)\tau_1$. We obtain the relation

$$\left(\frac{\epsilon_\pi}{\epsilon}\right)^2 A\mu_1 + \frac{\epsilon_\pi}{\epsilon}[A\mu_1(1 - 2\eta_1 + \epsilon_0) + A\mu_1\chi_1\tau_1 + \eta_1\delta(\alpha_1 - \eta_1 c_\kappa)]$$
$$+ [(1 - 2\eta_1 + \epsilon_0)A\mu_1\chi_1\tau_1 - \eta_1\delta(1 - \eta_1 + \epsilon_0 - \Pi_1 c_\kappa)] = 0\,, \tag{7.31}$$

where

$$\alpha_1 \equiv \frac{3/2 + 3\chi_1\eta_1}{1 + \chi_1\eta_1}\,, \qquad \mu_1 \equiv \frac{1 + \chi_1\eta_1 A}{A(1 + \chi_1\eta_1)}\,, \qquad c_\kappa \equiv \frac{A(1 - \mu_1)}{1 + \chi_1\eta_1}\chi_1'\,. \tag{7.32}$$

This relation can be readily solved quadratically with the positive value of the square-root term being physical. The quantity ϵ_τ is then related to ϵ_π and ϵ by the expression

$$\epsilon_\tau = \frac{\epsilon_\pi + \tau_1\chi_1\epsilon}{1 + \chi_1\eta_1}\,. \tag{7.33}$$

We can now quantize our earlier specification of x_s by choosing $\eta(x_s) = \eta_1 + \epsilon_s$, where $\epsilon_s \ll 1$ and is typically taken 10^{-3}. We can then find $\tau(x_s)$ by making use of equation (7.33) and thus have a starting point for the numerical integration of the shock model equations (7.23)–(7.24).

The difference scheme adopted for equations (7.23)–(7.24) is given in Appendix C. Due to the change in character of the shock equations as radiation pressure becomes dominant, most straightforward difference schemes are either intrinsically numerically unstable in one or more limits or require an exceedingly fine x-mesh to be convergent. The method adopted, however, appears to satisfactorily resolve these difficulties.

Figure 8 shows the shock structures that result from assuming that the radiation/matter pressure ratio ($\xi \equiv \chi\eta$)

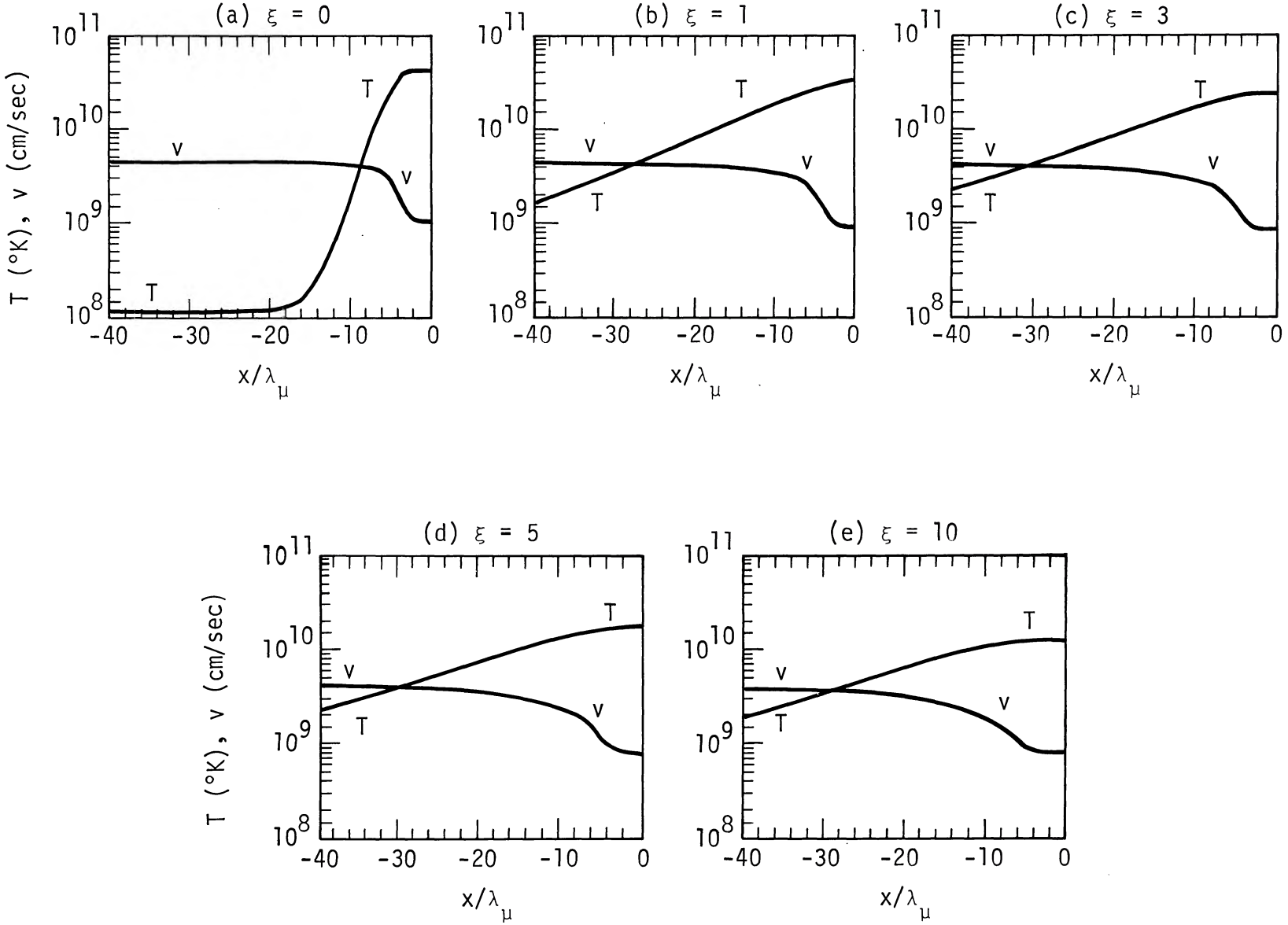

FIG. 8.—Shocks with constant radiation/matter pressure ratios, ξ. The notation is the same as for Fig. 7, and the shock parameters are $E_0 = 10$ MeV, $n_0 = 10^{20}$ cm^{-3}, $T_0 = 1.16 \times 10^8$ K, $\delta = 0.4$, $\epsilon_s = 10^{-4}$, and $A \equiv \lambda_0/\lambda_\kappa = 20$, where λ_0 is the characteristic preshock radiation diffusion length, and δ and λ_κ do not include radiative effects. Note that as ξ is increased from 0 to 10 in the sequence (*a*)–(*e*), a shock with a velocity transition of $\sim\lambda_\mu$, is broadened into a shock with a velocity transition $\sim\lambda_0 v/v_0$, the radiation diffusion length. Thus, unlike heat conduction by matter, radiative heat conduction can mediate a strong shock over a sufficiently large distance that viscous effects are small.

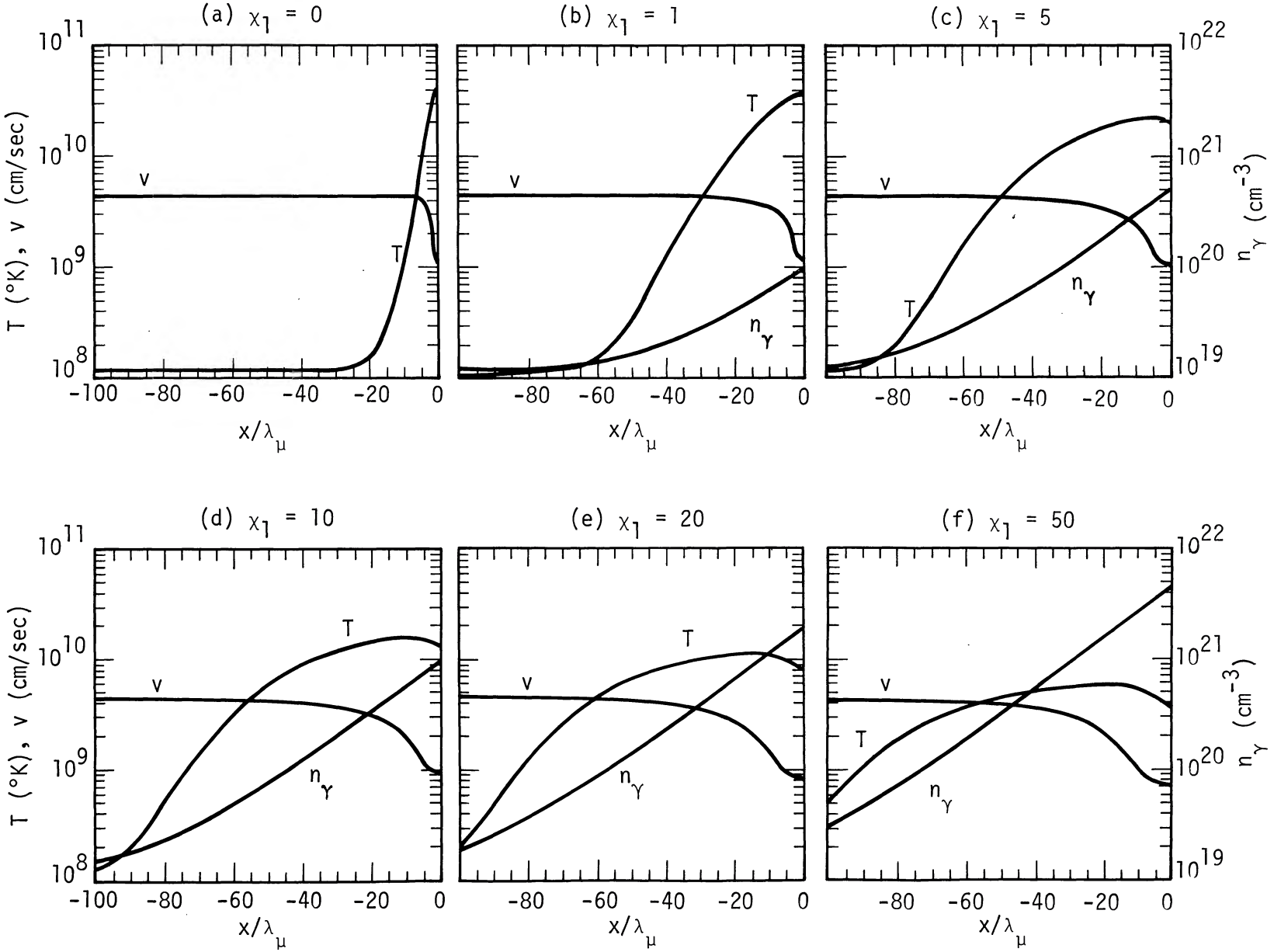

FIG. 9.—Shocks with exponential radiation fields. The notation is the same as in Figs. 7 and 8, with the shock parameters being $E_0 = 10$ MeV, $n_0 = 10^{20}$ cm^{-3}, $T_0 = 1.16 \times 10^8$ K, $\delta = 0.4$, $\epsilon_s = 10^{-3}$, and $A = 20$. The radiation field exponentiates with the mean radiation diffusion length $\lambda_0/3$ and is given by $\chi \equiv 9n_\gamma/10n_0 = \chi_0 + (\chi_1 - \chi_0) \exp(3x/\lambda_0)$, where n_γ is the photon number density, $\chi_0 = 0.09$, and the graphs are parametrized in terms χ_1, the value of χ at $x = 0$. Note that as χ_1 is varied from 0 to 50, a hot viscous shock is transformed into a cool radiation-dominated shock with a characteristic temperature peak. The transformation occurs for $\chi = 3$–5 (in the region of the maximum velocity gradient), in agreement with the analytic limits.

remains constant across the shock, while Figure 9 shows the results when χ is taken to be an exponentially increasing function of x given by

$$\chi(x) = \chi_0 + (\chi_1 - \chi_0) \exp(3x/\lambda_0) . \tag{7.34}$$

The transition from a viscous to radiation-dominated shock is seen to occur for $\chi = 3$–5 (in the region of the maximum velocity gradient), in agreement with our analytic limits. Specifically, the scale of the velocity gradient undergoes a transition from $\sim\lambda_\mu$ to $\sim\lambda_0\eta$. In addition, the shocks with exponential radiation fields already exhibit the temperature maximum typical of the nonequilibrium radiation-dominated shocks of § V.

VIII. GENERAL EFFECTIVE PHOTON SHOCK MODEL

a) Formulation of the Model

We are now in a position to consolidate our results into a model containing both explicit viscosity and a realistic treatment of the radiation field based on the effective photon approximation. We shall refer to this as the general effective photon shock model, and base it on the general assumptions of § II, while in addition assuming essentially comoving ions and electrons, the absence of crucial pair effects, and the validity of the effective-photon approximation. The assumption of a pure hydrogen medium will be relaxed below.

The shock-structure equations (2.13)–(2.20) then take the form

$$(1 + \tau_R + \chi\eta)n_0v_0kT - \mu v\frac{dv}{dx} = mn_0v_0(v_0 - v)v + P_0v , \tag{8.1}$$

$$(\tfrac{3}{2}\tau_R + \alpha_e + 3\chi\eta)n_0v_0kT - \tfrac{9}{10}\lambda_0vkT\frac{dn_\gamma}{dx} - \kappa'\frac{dT}{dx} = \tfrac{1}{2}mn_0v_0(v_0 - v)(v_0 - v + 2\epsilon_0v_0) + \alpha_0P_0v_0 , \tag{8.2}$$

$$\frac{d}{dx}(n_\gamma v) - \frac{d}{dx}\left[\frac{v\lambda_0}{3}\frac{dn_\gamma}{dx}\right] = Q_\gamma^{\text{eff}} , \tag{8.3}$$

$$\tfrac{3}{2}n_0v_0k\frac{dT_i}{dx} = -\frac{n_0v_0}{v}kT_i\frac{dv}{dx} + A_2(kT_i)^{5/2}\left(\frac{dv}{dx}\right)^2 + \left(\frac{n_0v_0}{v}\right)^2\frac{A_1}{(kT)^{3/2}}3k(T - T_i) , \tag{8.4}$$

$$n = n_e = n_i = \frac{n_0v_0}{v} , \tag{8.5}$$

where $\tau_R \equiv T_i/T$, and

$$P_0 = (2 + \chi_0)n_0kT_0 , \qquad \alpha_0 = \frac{3(1 + \chi_0)}{2 + \chi_0} , \tag{8.6}$$

$$\kappa' = \kappa_e + \chi\eta\lambda_0v_0n_0k . \tag{8.7}$$

Here T_i is the ion temperature; T is the common electron and radiation temperature; n and n_0 refer to the current and preshock electron or ion number density; n_γ is the effective photon density; v is the common electron and ion velocity; m is the mass of a hydrogen atom; α_e is the specific heat coefficient for electrons; A_1 and A_2 are coefficients related to electron-ion energy coupling and ion viscosity, respectively [$\mu = A_2(kT_i)^{5/2}$]; Q_γ^{eff} is the creation rate of effective photons; κ_e is the electron heat conduction coefficient; and, except as noted in equations (8.6) and (8.7), the remaining notation is the same as in § II. A_1, α_e, and Q_γ^{eff} are given by equations (3.45), (3.52), and (4.2), respectively, while A_2 and κ_e are given in § III*c*.

As before, we have neglected ionic heat conduction, due to its small coefficient and since, as was shown in § VII*a*, it has little effect on the velocity profile and only moderately ($\delta \approx 0.36$) broadens the temperature profile of a viscous *ion* shock.

To cast equations (8.1)–(8.2) into dimensionless form, it is convenient to introduce $\zeta' \equiv x/\lambda_x$, where λ_x is an arbitrary constant length. (Note that the heat conduction length, λ_κ, is no longer suitable because of its large [$\sim(kT)^{5/2}$] temperature dependence.) We then obtain

$$(1 + \tau_R + \chi\eta)\tau - \eta\delta'\frac{d\eta}{d\zeta'} = \eta(1 - \eta + \epsilon_0) , \tag{8.8}$$

$$(\tfrac{3}{2}\tau_R + \alpha_e + 3\chi\eta)\tau - A'\eta\tau\frac{d\chi}{d\zeta'} - \delta_\kappa\frac{d\tau}{d\zeta'} = \tfrac{1}{2}(1 - \eta)(1 - \eta + 2\epsilon_0) + \alpha_0\epsilon_0 , \tag{8.9}$$

where

$$\delta' \equiv \frac{\mu}{mn_0v_0\lambda_x} , \qquad A' = \frac{\lambda_0}{\lambda_x} , \qquad \delta_\kappa = \frac{\kappa'}{n_0v_0k\lambda_x} . \tag{8.10}$$

Final Hugoniot relations are then found by setting all gradients to zero and requiring the radiation field to be in equilibrium, yielding

$$2\tau_f + \chi_q \eta_f \tau_f^4 = \eta_f(1 - \eta_f + \epsilon_0)\,, \tag{8.11}$$

$$(\alpha_{ef} + \tfrac{3}{2})\tau_f + 3\eta_f \chi_q \tau_f^4 = \tfrac{1}{2}(1 - \eta_f)(1 - \eta_f + 2\epsilon_0) + \alpha_0 \epsilon_0\,, \tag{8.12}$$

where

$$\chi_q \equiv \frac{9}{10}\frac{b}{n_0}\left(\frac{mv_0^2}{k}\right)^3$$

and the subscript f denotes a final downstream value. (The subscript 1 will be used below to denote pseudo-downstream variable values.) These relations can be readily quadratically iterated to find τ_f and η_f, and $\chi_f = \chi_q \tau_f^3$.

Pseudo-Hugoniot relations are obtained in the same manner as described in the previous section, with the definition of Π generalized to $\Pi \equiv (1 + \tau_R + \chi\eta)\tau$, yielding

$$\Pi = \eta(1 - \eta + \epsilon_0)\,, \tag{8.13}$$

$$\alpha\Pi - (1 - \mu')A'\eta\tau\frac{d\chi}{d\zeta'} = \tfrac{1}{2}(1 - \eta)(1 - \eta + 2\epsilon_0) + \alpha_0\epsilon_0\,, \tag{8.14}$$

where

$$\mu' \equiv \frac{\delta_\kappa}{A'(1 + \tau_R + \chi\eta)}\,, \qquad \alpha = \frac{\frac{3}{2}\tau_R + \alpha_e + 3\chi\eta}{1 + \tau_R + \chi\eta}\,. \tag{8.15}$$

By construction, these conditions describe any point in the radiation relaxation region characterized by $d\Pi/d\zeta'$, $d\eta/d\zeta' \approx 0$, and can be solved iteratively if $d\chi/d\zeta'$, χ, and τ_R are known at that point. Here the relatively small amount of dissipation arising from the slow variation of τ_R in the relaxation layer due to *e-i* relaxation, and of η due to the change in α during radiative equilibration, has been neglected.

To fix the location of the shock we shall choose a particular point $x = x_s$ near the upstream boundary of this region, by specifying that the true value of $\eta(x_s)$ differ from the value deduced from pseudo-Hugoniot relations (8.13)–(8.15) by a small amount ϵ_s. We find $T(x)$ and $v(x)$ by using equations (8.1)–(8.2) to integrate upstream and equations (8.13)–(8.15) to find conditions downstream of x_s. To do this we first need to assume initial values for $\tau_R(x)$ and $n_\gamma(x)$. Once values for $T(x)$ and $v(x)$ are found, equations (8.3) and (8.4) are sequentially solved to find new values for $\tau_R(x)$ and $n_\gamma(x)$. The whole process is then iterated until it converges.

To begin the upstream integration to find T and v, we still require an asymptotic starting solution. Following the same procedure as before, we find ϵ_π can be obtained by quadratically solving the relation

$$\left(\frac{\epsilon_\pi}{\epsilon}\right)^2 A'\mu_1' + \left(\frac{\epsilon_\pi}{\epsilon}\right)[A'\mu_1'(1 - 2\eta_1 + \epsilon_0) + A'\mu_1'\chi_1\tau_1 + \eta_1\delta_1'(\alpha_1 - \eta_1 c_\kappa')]$$
$$+ [(1 - 2\eta_1 + \epsilon_0)A'\mu_1'\chi_1\tau_1 - \eta_1\delta_1(1 - \eta_1 + \epsilon_0 - \Pi_1 c_\kappa')] = 0\,, \tag{8.16}$$

where:

$$c_\kappa' \equiv \frac{A'(1 - \mu_1')(d\chi/d\zeta')_1}{1 + \tau_{R_1} + \chi_1\eta_1}\,, \qquad \alpha_1 = \frac{\frac{3}{2}\tau_{R_1} + \alpha_{e_1} + 3\chi_1\eta_1}{1 + \tau_{R_1} + \chi_1\eta_1}\,. \tag{8.17}$$

Here τ_1, η_1, and related 1-subscripted quantities have been obtained from the pseudo-Hugoniot relations at point x_s. We then find

$$\epsilon_\tau = \frac{\epsilon_\pi + \chi_1\tau_1\epsilon}{1 + \tau_{R_1} + \chi_1\eta_1}\,. \tag{8.18}$$

The photon continuity equation (8.3) and ion temperature equation (8.4) are solved by methods very similar to those used in Paper II for the photon-dominated model, except that dv/dx is evaluated explicitly from the preceding solution for $v(x)$. The photonic boundary conditions ($n_\gamma = \frac{10}{9}n_0\chi_f \equiv \eta_\gamma^{eq}$ as $x \to \infty$ and $n_\gamma = bT_0^3$ or $10^{-2}n_0$ as $x \to -\infty$) are taken at points far enough upstream and downstream as to have negligible effect on the bulk of the shock. The ion heating equation is integrated from upstream to downstream starting from the condition $\tau_R = 1$.

The explicit difference scheme used for equations (8.1)–(8.4) is given in Appendix D. Typically, runs involving $\sim$1000 mesh points converge in 10–15 overall iterations.

b) Effect of the Presence of Helium and High-Z Ion Species

The envelope of a normal Population I star contains $\sim$25 percent by weight of helium and $\sim$2 percent higher-Z material. Since these ions have different Z/A ratios from hydrogen, a given electric field is not sufficient to keep all

species comoving with the electrons. Instead, the electric field will act to keep an "average" ion comoving, while individual ion species develop drift velocities whose magnitude is limited principally by ion-ion collisions.

Quantitatively, we find that to maintain pseudo-charge neutrality,

$$\sum_i n_i Z_i = \sum_i \frac{n_i^0 v_0}{v_i} Z_i = \frac{n_e^0 v_0}{v_e}, \tag{8.19}$$

and assuming the electric field to be the dominant force accelerating the ions, we find

$$e \frac{n_e^0 v_0}{v_e} \Sigma_x = \sum_i m_i n_i^0 v_0 \frac{dv_i}{dx}. \tag{8.20}$$

Here n_i, n_i^0, v_i, Z_i, and m_i are the number density, preshock number density, velocity, atomic number, and mass of ion species i; v_e and n_e^0 are the electron velocity and initial electron number density; and e is the protonic charge. Differentiating equation (8.20) by time and using it to rewrite equation (8.21) gives

$$\Sigma_x = \left[\sum_i A_i \frac{n_i^0}{n_e^0} \frac{dv_i}{dx} \Big/ \sum_i Z_i \frac{n_i^0 v_e}{n_e^0 v_i} \frac{dv_i}{dx}\right] \frac{m_p}{e} v_e \frac{dv_e}{dx} \equiv \left\langle \frac{A}{Z} \right\rangle \frac{m_p}{e} v_e \frac{dv_e}{dx}, \tag{8.21}$$

where $A_i \equiv m_i/m_p$, and m_p is the proton mass.

To use our present model to estimate the magnitude of the ion drift velocities and resultant ion heating, we shall restrict our attention to a hydrogen-helium plasma, and assume that the helium drift velocity, $v_{\rm drift}$, relative to the protons, is in approximate steady state (i.e. $dv_e/dx \approx dv_i/dx = dv/dx$) and $v_{\rm drift} \ll v_0$. (This latter assumption is found to be self-consistent over a wide range of parameters.) This allows us to approximate the insensitive factor $\langle A/Z \rangle$, as

$$\left\langle \frac{A}{Z} \right\rangle \approx \frac{\sum_i A_i n_i^0}{\sum_i Z_i n_i^0}. \tag{8.22}$$

From Burgers (1960) and § III*d* we find that the force on the α-particles, $F_{\alpha p}$, due to collisions with the protons is given by

$$F_{\alpha p} = f n_\alpha n_p v_{\rm drift}, \tag{8.23}$$

where in cgs units

$$f \approx 8.23 \times 10^{-49} \ln \Lambda (kT_i)^{-3/2}, \tag{8.24}$$

provided $v_{\rm drift} < v_i^{\rm th}$, the ion thermal velocity. Here $\ln \Lambda$ is the Coulomb logarithm (see eq. [3.30]). Requiring the Coulomb drag force to compensate the differing electric forces on the α's and p's sufficiently to give them roughly equal accelerations, we find

$$\frac{e n_p \Sigma_x - f n_p n_\alpha v_{\rm drift}}{m_p n_p} = \frac{2 e n_\alpha \Sigma_x + f n_p n_\alpha v_{\rm drift}}{m_\alpha n_\alpha}, \tag{8.25}$$

and solving for $v_{\rm drift}$, we have

$$v_{\rm drift} = \frac{e(m_\alpha - 2m_p)\Sigma_x}{f(n_p m_p + m_\alpha n_\alpha)} \approx \frac{2m_p}{n_p + 2n_\alpha} \frac{v}{f} \frac{dv}{dx}. \tag{8.26}$$

The rate of ion heating from Coulomb dissipation, $H_{\alpha p}$, is then given by

$$H_{\alpha p} = F_{\alpha p} v_{\rm drift} = \frac{n_\alpha n_p}{(n_p + 2n_\alpha)^2} \frac{4 m_p^2 v^2}{f} \left(\frac{dv}{dx}\right)^2. \tag{8.27}$$

Inserting $H_{\alpha p}$ on the right-hand side of the ion heating equation (8.4) and relating $n = n_0 v_0/v$ to n_p in such a way as to keep the initial mass density constant (i.e., $n_p = n - 4n_\alpha$), we can approximately include helium effects in our shock model, without extensive modifications. The price we pay for this convenience is to slightly (for small helium number fractions) underestimate the electron-ion density ratio. The resulting apparent overestimate of photon creation rates is almost exactly compensated for by the fact that per-particle bremsstrahlung rates are $(Z_\alpha/Z_p)^2 = 4$ times larger for α-particles than for protons, which we do not include in our calculation of radiative emission.

For $E_0 > 1$ MeV and the densities of current interest, the final equilibrium shock temperature is sufficiently high with respect to the temperature at which most high-Z atoms are stripped that the number of photons produced by bound-bound and bound-free processes (even assuming radiative equilibrium up to the stripping temperature) is three or more orders of magnitude below the equilibrium photon number (see eq. [5.20] and Clayton 1968, p. 224). Also, we find numerically, as in § V, that the peak shock temperatures are not sensitive to the preshock temperature

and photon number, provided these are small compared to their postshock values. The principle radiative effect of the high-Z ions is a $\lesssim 10$ percent augmentation of the electron-ion bremsstrahlung rate, which we shall neglect.

c) *Results and Discussion*

The shock structures that result from this model are shown in Figures 10 and 11 for various values of n_0 and $E_0 \equiv \frac{1}{2}mv_0^2$. The calculations involved were started "hot," with essentially no radiation in the region of the shock. As can be seen, they have in all cases[2] relaxed to radiation-dominated shocks very similar (typically within 3–5%) to those calculated in § V, and the discussion of the salient features of these shocks given there still applies in detail.

Figure 12 explores the effects of the presence of helium for a 40 MeV nucleon^{-1} shock, and is seen to result in only modest ion heating even for a 50 percent mass fraction ($Y = 0.5$). For lower energies, electron-ion coupling and ion-ion Coulomb friction are sufficiently strong that there is virtually no effect. At higher energies pairs become important, and as we have seen, all species will be decelerated principally via ion-lepton Coulomb friction.

To search for stable "hot-ion" shocks of the type predicted by Colgate (1975*a*), runs were made in which radiation emission was reduced by a factor of 100, resulting, as expected, in hot viscous shocks. When these had converged, the radiation emission rate was returned to normal and the structure allowed to relax. This always resulted in reaching the same radiation-dominated shock structures obtained above. An example of this process is shown in Figure 13. Note, in particular, that when the radiative rates are returned to their full values, radiation diffuses forward and changes the shock structure in such a way as to allow increased diffusion. The ensuing radiation diffusion wave engulfs the hot-ion shock, broadening and cooling it into a radiation-dominated shock. Figure 14 shows some of the typical intermediate hot-ion shocks. Note that, even with emission reduced by a factor of 100, the residual amount of radiation is still sufficient to keep $T_e \ll T_i$ near the center of the shock. In most cases, reducing radiation emission by a factor of 10 is not sufficient to cause a hot-ion shock.

IX. DISCUSSION AND ASTROPHYSICAL IMPLICATIONS

a) *Prospects for Deuterium Production in Supernovae*

We have shown under fairly general assumptions that strong shocks in the density regime 10^{15}–10^{22} cm^{-3} and energy regime 1 to ~ 40 MeV nucleon^{-1} will be nonequilibrium radiation-dominated and reach peak temperatures below ~ 70 keV, while low-temperature ($\lesssim 200$ keV) pair-dominated shocks are likely to prevail in the ~ 40–100 MeV nucleon^{-1} energy range (see §§ V*e*, VI, and VIII*c*). As was discussed in § V, these temperatures are far too low for any significant production of neutrons via spallation to take place, thus precluding the postshock synthesis of deuterium by neutron captures on protons. We conclude that, if light elements are produced in supernovae, it will be under circumstances and physical conditions other than those we have assumed. With this in mind, it is useful to review both our general assumptions and the context in which the shocks have been set.

i) *Energy and Density Regime*

The density regime was chosen to be that typical of the envelope of a red-giant star, but there seems no basic physical reason why our models cannot be extended upward in density until the onset of Fermi degeneracy, the breakdown of the assumption that the inverse bremsstrahlung cutoff is $\ll m_e c^2$, or the onset of sufficiently relativistic electron temperatures that the physical parameters calculated in § III become qualitatively suspect (i.e., $kT_e \gg m_e c^2$). Above $n_0 = 10^{22}$ cm^{-3}, however, the final postshock equilibrium temperature is $\gtrsim 10$ keV for $E_0 > 3$ MeV, so any deuterium produced is likely to be burned up before the postshock region can be sufficiently cooled by expansion over typical red-giant length scales (e.g., for a 10^{12} cm radius and a $0.1c$ expansion velocity, we have $n\tau = 2 \times 10^{25}$ cm^{-3} s, while $\langle \sigma v \rangle_{DD}(10 \text{ keV}) = 1.2 \times 10^{-18}$ cm^3 s^{-1} and $\langle \sigma v \rangle_{PD}(10 \text{ keV}) = 1.6 \times 10^{-23}$ cm^3 s^{-1} [Fowler, Caughlan, and Zimmerman 1975]).

Again, while no basic physical approximation breaks down for $n_0 < 10^{15}$ cm^{-3}, the capture time for neutrons on protons is $> 10^4$ seconds, compared with a mean neutron decay time of 10^3 seconds, and thus deuterium production will be negligible (Colgate 1974).

For energies below 1 MeV nucleon^{-1}, little nuclear spallation will occur even in a hot-ion shock, while shock energies > 100 MeV nucleon^{-1} must of energetic necessity occur only in a small mass fraction of a supernova. Physically, very low energy shocks are likely to be in radiative equilibrium (in part due to bound-bound and bound-free processes) and to eventually become viscosity-dominated when the equilibrium radiation pressure drops below 4.45 times the matter pressure (see eq. [5.29]). At energies above 100 MeV nucleon^{-1}, higher radiative transfer

[2] Specifically, runs were made for $n_0 = 10^{15}$, 10^{17}, 10^{20}, and 10^{22} cm^{-3} and $E_0 = 1$, 10, 30, 50, 100 MeV. (The initial temperature T_0, was chosen so that $\chi_0 \approx 0.1$ in radiative equilibrium; $\epsilon_s = 10^{-3}$, $\bar{\sigma}_c = \sigma_T$, and Y, the helium mass fraction, is zero unless otherwise specified. As discussed in Paper II and below, the shock structure is insensitive to these parameters. As also noted above, the "flaring" that occasionally occurs in the T and n_γ curves near the downstream boundary is due to numerically forcing the shock to come to final equilibrium at a point not sufficiently far downstream, and is done so that the shock can be zoned and plotted on a reasonable length scale. Test calculations again show that this has essentially no effect on the structure of the shock outside the flared region.)

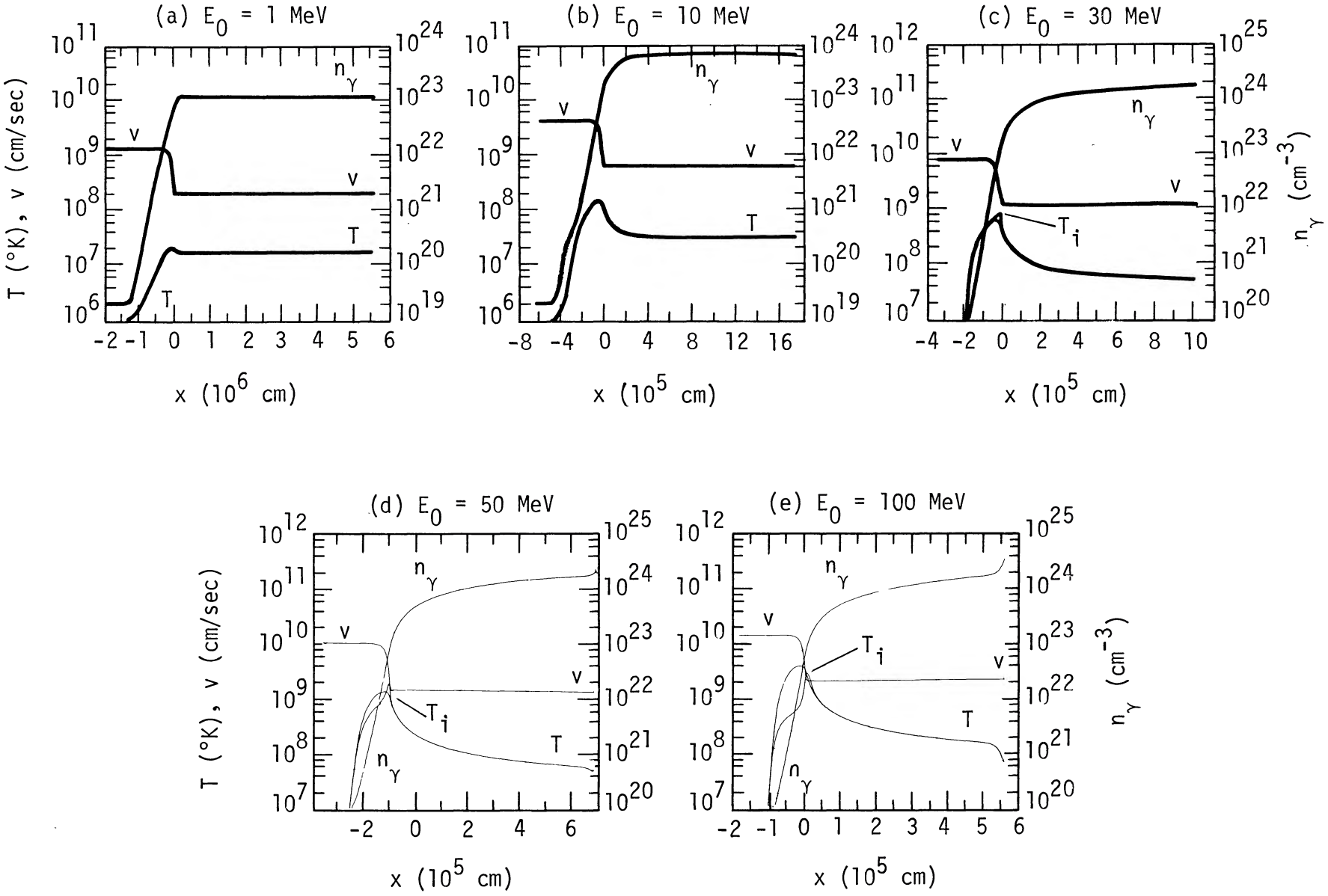

FIG. 10.—Strong shock structures including viscous effects for a preshock number density, n_0, of 10^{20} cm^{-3} and shock energy, E_0, as indicated. The preshock material is taken to be in radiative equilibrium with a temperature $T_0 = 10^6$ K, and as usual, the results are insensitive to this choice. The shocks are shown in their comoving frame where v is the fluid velocity (directed to the right), T and T_i are the common electron-radiation and ion temperatures, respectively, and n_γ is the effective photon number density. Note the close similarity of those shock to the radiation-dominated model shocks of Fig. 4.

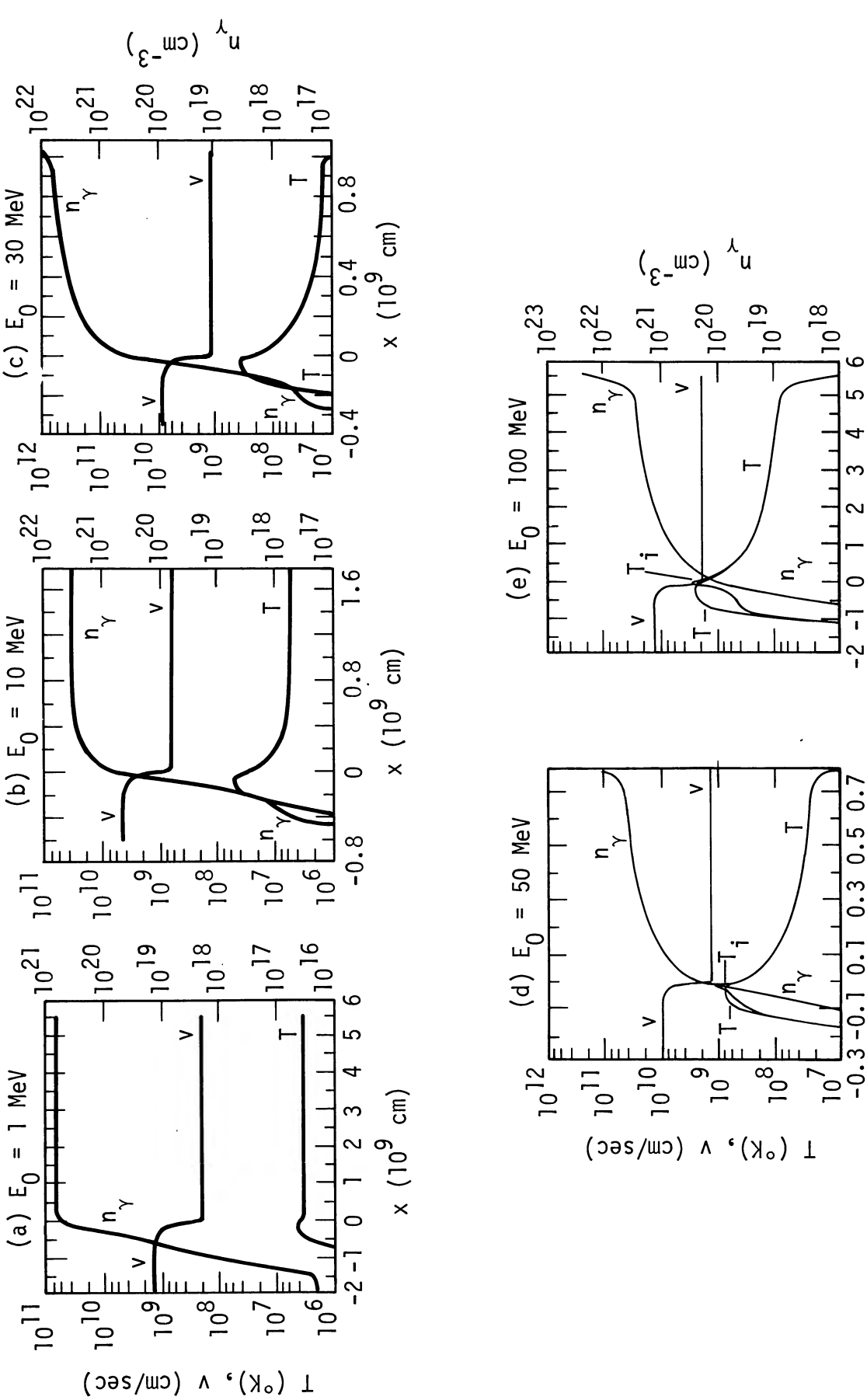

FIG. 11.—Strong shock structures including viscous effects for $n_0 = 10^{17}$ cm^{-3}, as a function of shock energy. The notation is the same as for Fig. 10, with $T_0 = 10^5$ K. These shock structures are also nearly identical to their radiation-dominated model counterparts.

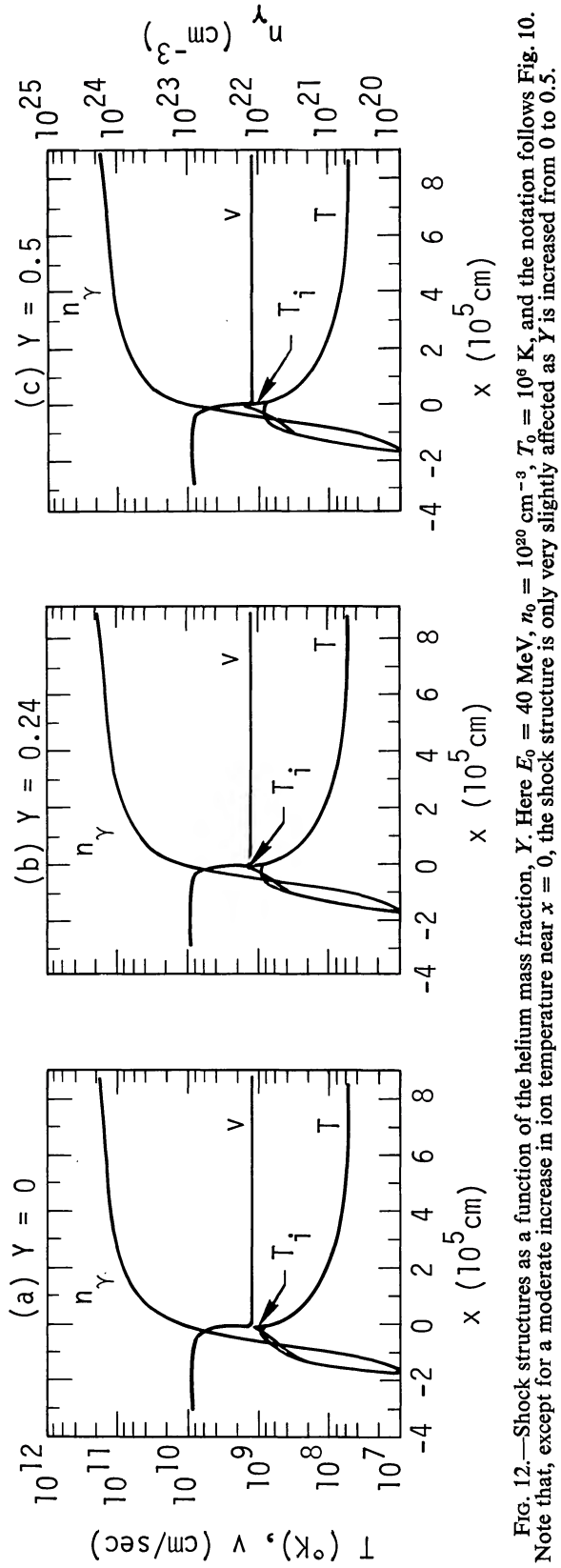

FIG. 12.—Shock structures as a function of the helium mass fraction, Y. Here $E_0 = 40$ MeV, $n_0 = 10^{20}$ cm^{-3}, $T_0 = 10^6$ K, and the notation follows Fig. 10. Note that, except for a moderate increase in ion temperature near $x = 0$, the shock structure is only very slightly affected as Y is increased from 0 to 0.5.

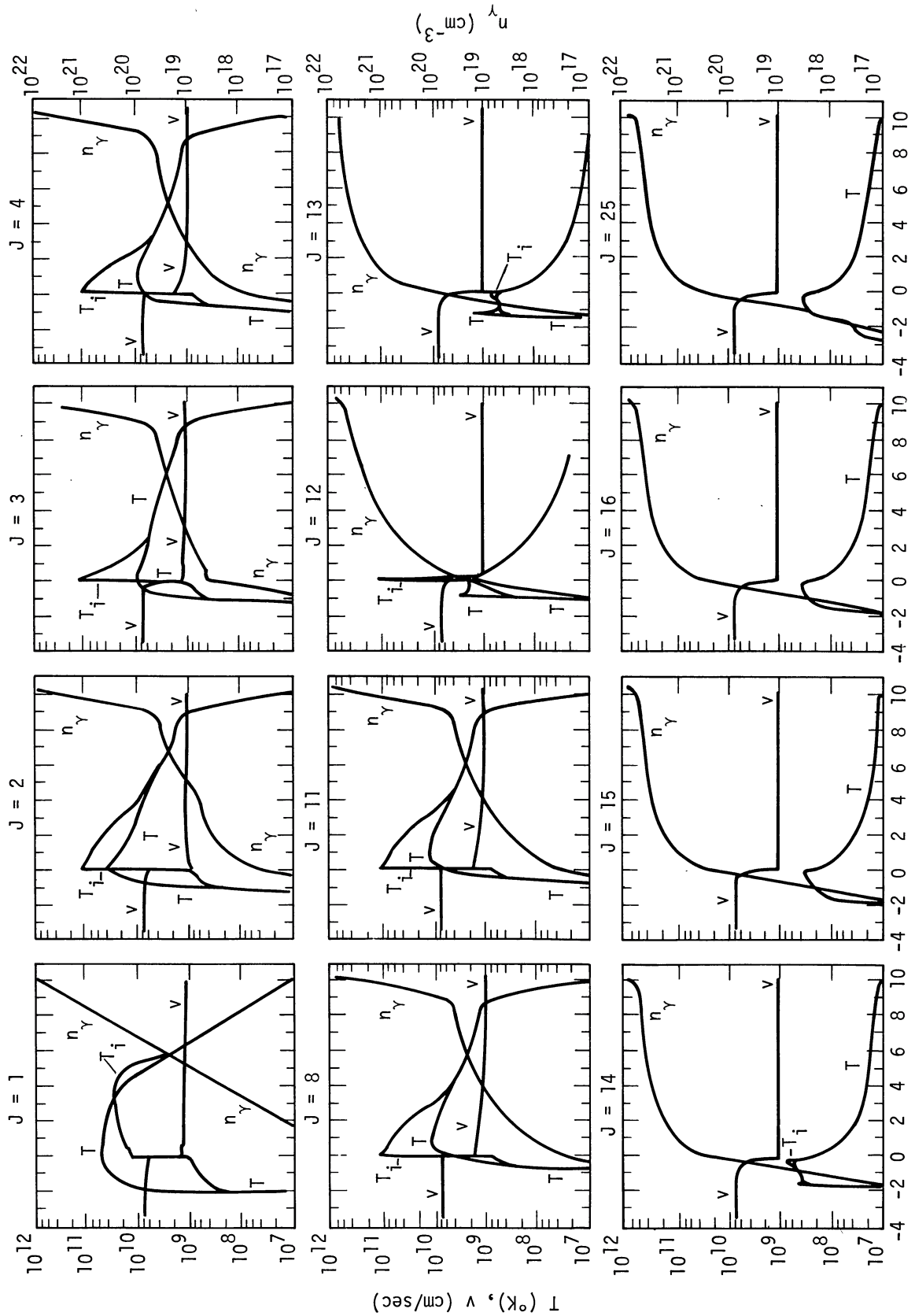

FIG. 13.—Relaxation of a hot-ion shock to a radiation-dominated shock ($E_0 = 30$ MeV, $n_0 = 10^{17}$ cm^{-3}, $Y = 0.25$, $T_0 = 10^5$ K; see Fig. 10 for notation). The frame labeled $J = 1$ shows the initial shock configuration. In frames 2–11, the radiative rates are reduced by a factor of 100, and the initial structure is seen to relax to a hot-ion shock. In frames 12–25, the radiative rates are restored to normal, and the hot-ion shock is rapidly transformed into a radiation-dominated shock identical to that of Fig. 11(*c*) except for a very slightly higher ion temperature at $x = 0$ due to the presence of helium.

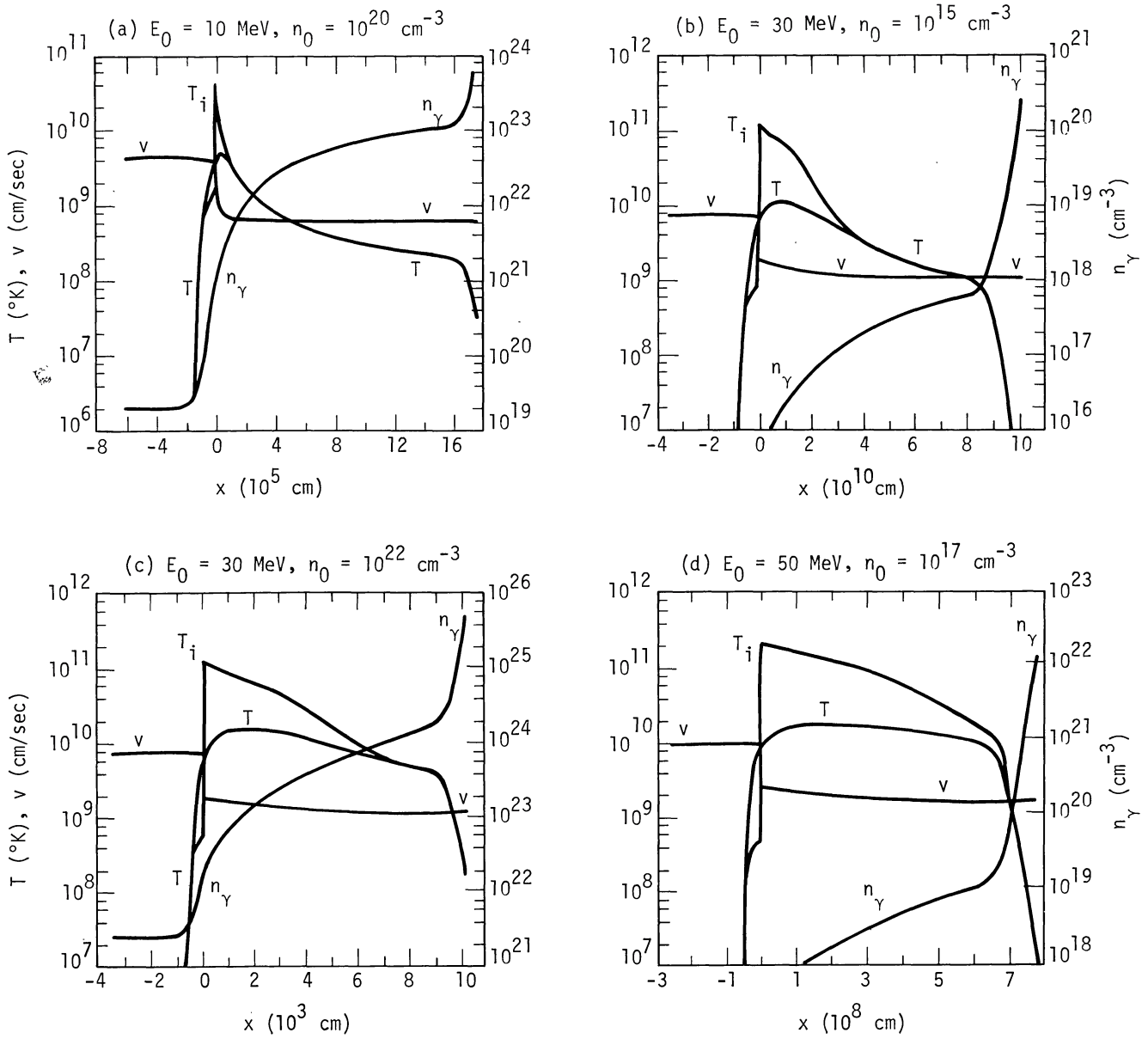

FIG. 14.—Typical hot-ion shocks produced by artificially lowering radiative emission rates a hundredfold. The notation follows that of the previous figures. Note the characteristic very sharp ion viscosity-dominated velocity transition resulting in ion temperatures $\sim E_0$, followed by a long relaxation layer in which the ion thermal energy is slowly transferred through the electrons to the radiation field.

moments (e.g., radiative momentum *transport*) become important since v_0 is no longer $\ll c$, and in addition relativistic kinematics must be employed (Johnson and McKee 1971).

ii) *Optical Thickness*

The assumption of optical thickness for shocks giving rise to a cosmologically significant amount of deuterium can be shown to be reasonable by the following argument.

Assume that the average radius of a presupernova star is less than 10^{14} cm (Iben's 1973 model of an evolved 7 $M_\odot$ star with a carbon-oxygen core, for example, has a radius of 3.5×10^{13} cm). Then the mass, M_{OT}, contained in its outer 30 preshock Thompson lengths ($30l_T$) is

$$M_{OT} = \frac{120\pi R^2 m}{\sigma_T} \leq 4.8 \times 10^{-3} M_\odot . \tag{9.1}$$

Since (1) 30 l_T is a greater distance than radiation can diffuse in a shock passage time for shock energies >1 MeV; (2) the fraction of the interstellar medium recycled in supernova explosions is believed to be not more than 10 percent (cf. Reeves 1974); and (3) the average ejected-mass-weighted supernova event is thought to eject $\gtrsim 10\ M_\odot$ (partly on nucleosynthetic grounds; see Arnett and Schramm 1973); we conclude that the amount of helium initially present in supernova shocks in nonoptically thick regimes represents an interstellar *mass* fraction of at most 1.2×10^{-5} (assuming the shocked material starts with normal cosmic abundance). Even assuming that *all* of the shocked helium is converted to deuterium, such shocks would still fail by about a factor of 2 to reproduce the observed interstellar deuterium *mass* fraction of 2×10^{-5} (Rogerson and York 1973). Such total conversion is extremely unlikely, however, since the ratio of the hydrodynamic rarefaction time to the mean time for a neutron to be captured by a proton is $\lesssim 10^{-3}$ under these conditions (cf. Colgate 1974). Thus significant optically thin deuterium production appears unlikely in supernovae.

iii) *Assumption of Steady State*

Similar arguments can be made to qualitatively justify the assumption that the density regime through which the shock propagates is sufficiently wide that the shock has reached a near-steady-state condition. This follows since 30 l_T, equivalent to $\sim 90\ v_0/c$ characteristic radiation-dominated shock lengths, is a more than adequate distance to recreate all the radiation in the shock and thus probably to relax any significant structural transients.

Colgate (1975*a* and private communication) has suggested that, since the sound speed in the "hot-ion precursor" (assuming it can be formed) is higher than in the completely relaxed postshock gas, such a precursor may be able to run away from any photon diffusion front that lies behind it. While it is true that the precursor sound speed is larger by $\sim\sqrt{2}$, the velocity of the hot-ion shock ($v_0/4$) is still *subsonic* with respect to the radiation-dominated sound velocity ($2\sqrt{(2)}v_0/7$). Thus any disturbance in the radiation-dominated fluid will catch up with the ion shock, and so a steady-state radiation-relaxation layer will exist in the frame of the shock, and have a structure determined by the equations given and solved above.

An exception to such a steady state, however, would occur if there existed in or behind the shock a *continuing* source of sound waves. Such waves could only effect the shock structures calculated here if the velocity perturbations they cause are a significant fraction of v_0 (and thus significantly perturb the temperature and radiative equilibration rate) and if their wavelength is comparable to or smaller than the shock width (for otherwise, it would only be necessary to periodically correct n_0 and v_0). Seemingly, the only energy source large enough to drive such sound waves is the energy of the shock itself, presumably via the hydrodynamic or electromagnetic instabilities. Indeed, electromagnetic instabilities are known to mediate "collisionless" shocks in very low density plasmas such as the solar wind (cf. Tidman and Krall 1971). In the present case, however, such instabilities appear unlikely due to the relatively high density, the small Debye length, the large electron velocities compared to ion velocities, and the damping effects of radiation transport (see §§ V*d* and VI). Hydrodynamic instabilities, such as the Rayleigh-Taylor instability, may well be important in disrupting the large-scale symmetry of a supernova shock-wave front (Falk and Arnett 1973; Chevalier 1976), but are likely to be strongly damped by radiation transport on scales of the order of a shock width. Thus there seem to be no presently known instabilities capable of playing an important role in supernova shock waves.

iv) *Sensitivity to Radiative Rates*

As noted in § VIII*c* a 10- to 100-fold reduction in radiative rates is required to produce a hot-ion shock. Numerical sensitivity experiments suggest, however, that the present treatment of the radiative rates is accurate to within a factor of 2, with most of the uncertainty arising from the specification of the dynamical cutoff, τ_d, due to inverse Compton scattering, in § IV. Note that the most *conservative* reasonable assumptions were made in evaluating these radiative rates.

A multigroup treatment of the radiation field in the form indicated by equation (2.20) is probably required for more accurate results, and is being undertaken in connection with the neutron-star accretion problem (see § IX*b*). It is evident, however, that the present level of accuracy is sufficient to settle the deuterium production question. With respect to errors in the relativistic corrections to the bremsstrahlung rate, we note that the use of Gould's (1975) quadrupole *e-e* bremsstrahlung rates instead of those given by Maxon (1972) typically makes only ~ 2 percent difference in the calculated shock structures.

v) *Navier-Stokes Treatment of Dissipation*

Since radiation-dominated shocks typically extend over several Compton lengths, sources of dissipation that are nonlinear in the gradients of the physical parameters are unlikely to become important, and so a kinetic or Monte Carlo treatment of the shock structure does not appear necessary. It is interesting to note, however, that strong hot-ion viscous shocks occurring over ~ 2 ion-ion mean free paths can show several interesting nonhydrodynamic effects. In particular, two-dimensional Monte Carlo calculations of shocks made up of hard spheres (Bird 1967) show that such shocks are a factor of 1.5–2 broader than predicted by the Navier-Stokes relations, have higher longitudinal than lateral temperatures, and show a secondary peak in the high-energy tail of the longitudinal velocity distribution corresponding to particles that have been backscattered *against* the general flow while approxi-

mately retaining the absolute magnitude of the flow velocity. This last effect, though probably diminished in a realistic plasma due to the *usual* (i.e., nonnuclear) predominance of low-angle scatters, may have interesting implications for nucleosynthesis if circumstances are found in which hot-ion shocks *can* occur.

vi) *Hot-Ion Shock Nucleosynthesis*

Calculations of shock-wave nucleosynthesis (Epstein, Arnett, and Schramm 1974) based on the hot-ion shock model of Colgate (1974) show overproduction of Li, Be, and B relative to deuterium. While the details of these results depend on the initial composition, and the revised hot-ion shock structures recently proposed by Colgate (1975*a*) may reduce some of the abundance discrepancies, no natural resolution has yet emerged.

Such problems with hot-ion shock nucleosynthesis are, of course, completely consistent with the cool, radiation-dominated shocks found in the present study.

vii) *Conclusion*

The conclusion thus seems reasonably forced that the production of a cosmologically significant amount of deuterium is unlikely to occur in supernova shock waves. The only currently viable and "nonexotic" means for the production of the presently existing deuterium appears to be its formation via the $p + n \rightarrow D + \gamma$ reaction in the primordial big bang (Gott *et al.* 1974). As is well known, present models of such a process require a low-density and thus open universe if subsequent deuterium burnup is to be avoided.

b) Other Astrophysical Applications

While the shock structures in this study were calculated principally to evaluate the prospects for supernova deuterium synthesis, the concepts and results can also be applied to other astrophysical situations involving strong shocks.

i) *Supernova Cosmic-Ray Production*

Colgate and Johnson (1960) have postulated that cosmic rays are produced as the shock formed in the envelope of a Type I supernova explosion is accelerated to extreme relativistic energies as it traverses the steep density gradient near the surface of the compact star ($\lesssim 10^9$ cm in radius) thought to be involved in such an explosion. The composition of these cosmic rays is clearly critically dependent on the temperatures reached in such relativistic shocks. The initial calculations were made under the assumption of complete radiative equilibrium and resulted in temperatures ≤ 500 keV.

It was in this context that the original suggestion was made that sufficiently strong shocks would very probably exhibit a high-temperature "precursor," either in the form of a hot-ion viscous shock, or more probably a non-equilibrium radiation-dominated shock (cf. Weaver *et al.* 1974). While a detailed treatment of the relativistic shock structure is beyond the scope of the present study, naïve extension of our nonrelativistic results leads to temperatures greatly in excess of 1 MeV. Indeed a preliminary pair-dominated shock model yields a peak temperature of > 100 MeV for a shock with a relativistic γ of 15, despite the bootstrap effect operating between pair-production via the $\gamma\gamma \rightarrow e^+e^-$ reaction and radiative Compton scattering. (Multiple radiative Compton scattering and multiple bremsstrahlung, however, were not included and may serve to limit these temperatures.) Even if the peak radiation temperatures remain ~ 1 MeV, both pair and radiation-dominated models predict that the ions will stream through the radiation/pair field so that a typical photon will appear to have an energy of $\sim 3\gamma$ MeV. Thus at least some spallation of high-Z nuclei in cosmic rays produced by $\gamma > 10$ shock waves appears likely. More detailed calculations are clearly needed to confirm this conclusion, however, and will be the subject of a later paper.

In such calculations, time-dependent effects related to the breakout of the radiation field and the shock thickness becoming of the order of an atmospheric scale height are likely to become important. One interesting point in this respect is that the presence of pairs in the high temperature "precursor" will serve to "dam in" the postshock radiation, and thus allow the shock to propagate to a lower optical depth than would otherwise have been the case (see Colgate 1975*b* for a discussion of the situation in the case of radiative/pair equilibrium). The magnitudes of these effects are uncertain, and indeed it is possible that Rayleigh-Taylor instabilities will ensue.

ii) *Accretion onto Neutron Stars*

The deceleration of material accreting onto a neutron star at energies ~ 50–100 MeV nucleon^{-1} has been studied by several authors (Zel'dovich and Shakura 1969; Alme and Wilson 1973; Shapiro and Salpeter 1974), and is proposed to involve either electron-ion Coulomb friction or strong plasma instabilities. A key question in such a process is whether or not a standing accretion shock forms in the infalling material *above* the surface of the neutron star, following which the postshock material is adiabatically compressed up to its final surface density. The results of this study suggest that a radiation-dominated shock of this type could be formed fairly readily, especially if accretion is occurring at a rate near the Eddington limit. Indeed, if the accretion shock lies $\gtrsim 30$ Compton lengths deep in the accreting material, the shock structures calculated in this study should be directly applicable. In the more likely case of a less optically thick shock, a multigroup treatment of the radiation field in terms of flux-limited diffusion (see § IIIc) and allowing for higher radiative moments such as momentum transport is required,

and is currently being pursued. In such a shock, radiation loss will compete with reduced inverse Compton cooling to determine the shock temperature and thus the characteristics of the emitted radiation spectrum.

iii) *Formation of Protogalaxies*

Shock compression arising from collisions between perturbations in the early universe is thought to be important in the formation of regions sufficiently dense to resist being dispersed by the general expansion of the universe and thus become protogalaxies (Silk 1974). If the perturbations involved are optically thin, the radiation loss rate and thus the structure of the shock will be important in determining the velocity and extent of its propagation. The shock-structure treatment being developed for neutron-star accretion shocks appears applicable to such cases. If the shock energies and resulting temperatures are sufficiently high, the possibility of nuclear processing, including light-element formation, should not be overlooked.

I would like to thank my advisor, Joseph Silk, and George Chapline and Lowell Wood of the Lawrence Livermore Laboratory for their joint guidance and encouragement of this study. I would also like to thank Stirling Colgate and Edward Teller for their interest and support, and George Zimmerman, Chris McKee, and Richard Epstein for a number of useful discussions. The support of the Fannie and John Hertz Foundation throughout the course of my graduate study is gratefully acknowledged, as is the hospitality of the Lawrence Livermore Laboratory.

APPENDIX A

I. LIST OF SYMBOLS

The principal symbols and subscripts employed in this study are listed below with their units and defining equation where applicable. Notation peculiar to the Appendices or figure legends, as well as briefly used notation, is not included.

II. SYMBOLS

A: Ratio of radiative to matter heat conduction lengths ($\equiv \lambda_0/\lambda_\kappa$).
A_i: Mass of species i in proton mass units.
A': $\equiv \lambda_0/\lambda_x$.
A_1 (ergs$^{3/2}$ cm^3 s^{-1}): Electron-ion coupling parameter (3.45).
A_2 (ergs$^{-3/2}$ cm^{-3} s): Viscosity parameter [$\equiv \mu_i (kT_i)^{-5/2}$].
b (20.3 cm^{-3} K^{-3}): Radiation equilibrium number density constant.
C: Radiation field degeneracy parameter [see (A19)].
c (cm s^{-1}): Velocity of light.
c_κ: see (7.32).
c_κ': see (8.17).
$c_s^{\,o}$ (cm s^{-1}): Preshock sound speed.
$D_\gamma(\epsilon_\gamma)$ (cm^2 s^{-1}): Radiation diffusion coefficient.
$E_x^{\,i}$ (ergs cm^{-2} s^{-1}): x energy component of stress-energy tensor.
E_0 (MeV): Initial shock energy ($\equiv m_H v_0^2/2$).
E_1: First-order exponential integral function.
E_γ (ergs cm^{-3}): Total radiation energy density.
$\mathscr{E}^{ij}$ (ergs cm^{-3} s^{-1}): Energy transfer rate from species j to i.
$\mathscr{E}_{ei}'$ (ergs cm^{-3} s^{-1}): Nonelectrical energy transfer rate from ions to electrons.
e (ergs$^{1/2}$ cm$^{1/2}$): Protonic charge.
f_E: Equilibrium parameter (3.10).
f_{ei}: Electron-ion coupling relativistic correction factor (3.46).
g_1: Bremsstrahlung Gaunt factor defined by (3.3).
g_2: Combined bremsstrahlung Gaunt factor [$g_2(\lambda) \equiv g_1(\lambda)E_1(\lambda)$].
$H_{\alpha p}$ (ergs cm^{-3} s^{-1}): Coulomb friction heating between protons and α-particles.
$\hbar$ (ergs s): Planck's constant/2π.
J_{ei}^{NR} (cm^{-3} s^{-1} ergs^{-1}): Nonrelativistic bremsstrahlung emission spectrum.
J_0 ($\equiv 5.692 \times 10^{-12}$ K$^{1/2}$ cm^3 s^{-1}): Bremsstrahlung emission coefficient [see (3.2)].
$J_\pm$ (ergs$^{1/2}$ cm$^{-3/2}$ s^{-1}): Net current density in the *pair* fluid [$\equiv en_+(v_e - v_+)$].
j_e (ergs$^{1/2}$ cm$^{-3/2}$ s^{-1}): Current density due to the electron-positron fluid.
K_i: Modified Bessel functions of the second kind of order i.
k (ergs K^{-1}): Boltzmann's constant.
l_c (cm): Compton length ($\equiv 1/\sigma_c n_e$).
l_{ei} (cm): Stopping length for ions in an electron gas.
l_T (cm): Thompson length ($\equiv 1/\sigma_T n_e$).

ln Λ: Coulomb logarithm (3.30).
M: Mach number; see (7.16).
$M_\odot$ (g): Solar mass.
m (g): Mass of shocked particle species, usually m_H.
m_e, m_H, m_i, m_p, m_α (g): Electron, hydrogen, ion, proton, helium mass.
n (cm^{-3}): Common electron, proton number density.
n^i (cm^{-3}): Number density of component i.
n_e, n_i, n_p, n_α, n_+, n_{e^-}, $n^\pm$ (cm^{-3}): Number density of electrons, ions, protons, α-particles, positrons, negatrons, and pairs.
n_0 (cm^{-3}): Preshock number density.
n_{20}: $n_0/10^{20}$ cm^{-3}.
$n_\gamma(\epsilon_\gamma)$ (cm^{-3} ergs^{-1}): Number density of photons with energy ϵ_γ per unit energy.
n_γ^{eq} (cm^{-3}): Equilibrium photon number density (5.21).
n_γ^s (cm^{-3}): Upstream starting photon density.
$n\tau$ (cm^{-3} s): Number density–confinement time product.
P_m (ergs cm^{-3}): Matter pressure.
P_{xx}^i (ergs cm^{-3}): xx pressure component of the stress-energy tensor.
P_0 (ergs cm^{-3}): Preshock pressure.
P_γ (ergs cm^{-3}): Radiation pressure.
$\mathscr{P}^{ij}$ (dynes cm^{-3}): Momentum transfer rate from species j to i.
$\mathscr{P}_{ei}'$ (dynes cm^{-3}): Nonelectrical momentum transfer rate from ions to electrons.
$Q_\gamma(\epsilon_\gamma)$ (cm^{-3} s^{-1} ergs^{-1}): Photon emission rate at ϵ_γ per unit energy.
$Q(\epsilon_c, \theta_e)$ (cm^{-3} s^{-1}): Total photon emission rate down to an $\epsilon_\gamma = \epsilon_c$ cutoff.
Q_γ^{eff} (cm^{-3} s^{-1}): Effective photon emission rate.
Q_{ei}^{NR}, Q_{RCB}, Q_{RC} (cm^{-3} s^{-1}): Effective photon emission rates due to nonrelativistic bremsstrahlung, relativistic corrections to bremsstrahlung, and radiative Compton scattering.
$Q_{\gamma\gamma}^\pm$ (cm^{-3} s^{-1}): Pair production rate due to the $\gamma\gamma \rightarrow e^+e^-$ reaction.
$Q_\pm$ (cm^{-3} s^{-1}): Total pair production rate.
r_0 (cm): Classical electron radius.
S_0 (ergs cm^{-2} s^{-1}): Preshock internal energy flux.
S_γ (ergs cm^{-2} s^{-1}): Total radiative energy flux relative to the electrons.
$S_\gamma(\epsilon_\gamma)$ (cm^{-2} s^{-1}): Radiative energy flux relative to the electrons per unit photon energy at ϵ_γ.
T (K): Common radiation and electron temperature.
T_e, T_i, T_γ, $\bar{T}_m$ (K): Electron, ion, radiation, and mean matter temperatures.
T_S, T_0, T_{eq} (K): Upstream starting, initial, and final equilibrium (5.20) temperatures.
T_v, $T_\pm$: Critical temperatures for the onset of viscous and pair effects.
t_{sjk} (s): Transport collision period (3.27).
v (cm s^{-1}): Common electron and ion velocity.
v^i (cm s^{-1}): Velocity of species i.
v_e, v_i, v_+, v_γ (cm s^{-1}): Electron, ion, positron, and effective photon velocities.
v_{drift}: Relative velocity between α-particles and protons.
v_j^{th} (cm s^{-1}): Thermal velocity of species j (3.25).
v_s (cm s^{-1}): Starting velocity for shock integration.
v_0 (cm s^{-1}): Preshock fluid velocity in the shock frame.
W_{ei}^{NR}, W_{ei}^{RC}, W_{ee} (ergs cm^{-3} s^{-1}): Energy loss rates due to nonrelativistic bremsstrahlung, relativistic e-i bremsstrahlung corrections, and electron-electron bremsstrahlung.
w (cm s^{-1}): Velocity of a particle.
x (cm): Spatial coordinate.
x_s (cm): Starting value of x for shock integration.
x_0, x_1 (cm): Upstream and downstream boundary points.
Y: Helium mass fraction.
Z_i: Number of protonic charges contained in particle i.
α: Ratio of energy density to pressure; fine structure constant.
α_0: Preshock value of α.
α_e, α_j: Ratio of energy density to pressure for electrons and species j.
γ: Relativistic $\gamma \equiv (1 - v^2/c^2)^{-1/2}$.
Δ: Characteristic radiation-dominated shock width ($\equiv cl_c/3v_0$).
$\Delta_\pm$: Characteristic pair-dominated shock width (6.9).
δ: Ratio of viscous to matter heat conduction lengths (7.7).
$\delta' \equiv \lambda_\mu/\lambda_x$.
$\delta_\kappa \equiv \lambda_\kappa/\lambda_x$.
ϵ: Dimensionless velocity difference ($\equiv \eta - \eta_1$).

ϵ_c (ergs): Low-energy cutoff for effective photon emission.
ϵ_B, ϵ_{sc}, ϵ_d (ergs): Radiation emission cutoff energies due to inverse bremsstrahlung, screening, and dynamical considerations.
ϵ_s: Starting value of ϵ.
ϵ_0: Dimensionless preshock pressure ($\equiv P_0/mn_0v_0^2$).
ϵ_τ, ϵ_π: Dimensionless pressure differences ($\epsilon_\tau \equiv \tau_1 - \tau$, $\epsilon_\pi \equiv \pi_1 - \pi$).
ϵ_γ (ergs): Photon energy.
ζ: Dimensionless distance ($\equiv x/\lambda_\kappa$).
ζ': Dimensionless distance ($\equiv x/\lambda_x$).
η: Dimensionless velocity ($\equiv v/v_0$).
θ_e, θ_i (ergs) $\equiv kT_e$, kT_i.
θ_γ (ergs) $\equiv 0.9\ kT_\gamma$.
κ (ergs cm^{-1} s^{-1} K^{-1}): Heat conduction coefficient.
κ' (ergs cm^{-1} s^{-1} K^{-1}): Heat conduction coefficient including radiative processes (7.25).
κ_e, κ_i (ergs cm^{-1} s^{-1} K^{-1}): Electron and ion heat conduction coefficients.
λ: Low-energy radiative cutoff parameter ($\equiv \epsilon_c/\theta_e$).
λ_D (cm): Debye length [$\equiv(\theta_e/4\pi n_e e^2)^{1/2}$].
λ_j (cm): Transport mean free path for species j; see (3.26).
λ_{jk} (cm): Transport mean free path for species j with respect to species k.
λ_{max}: Maximum cutoff parameter (4.11).
λ_x (cm): Convenient scale length.
λ_0 (cm): Radiation diffusion scale length (7.25).
λ_κ (cm): Matter heat conduction scale length ($\equiv \kappa/kn_0v_0$).
λ_μ (cm): Viscous scale length ($\equiv \mu/mn_0v_0$).
μ (ergs cm^{-3} s): Viscosity coefficient.
μ_e, μ_i (erg cm^{-3} s): Electron and ion viscosity coefficients.
μ_j (ergs): Chemical potential of species j.
μ_1: See (7.32).
μ': See (8.15).
ξ: Ratio of radiation to matter pressure.
Π: Dimensionless pressure [$\equiv(1 + x\eta)\tau$].
ρ (ergs$^{1/2}$ cm$^{-5/2}$): Net charge density.
ρ_e (ergs$^{1/2}$ cm$^{-5/2}$): Charge density of the electron-positron fluid.
Σ_x (ergs$^{1/2}$ cm$^{-3/2}$): x component of electric field.
Σ_{max} (ergs$^{1/2}$ cm$^{-3/2}$): Maximum shock electric field [$\equiv E_0/(e\Delta)$].
σ (cm^2): Reaction or scattering cross section.
$\sigma_c(\epsilon_\gamma)$ (cm^2): Compton transport cross section at photon energy ϵ_γ.
$\bar{\sigma}_c$ (cm^2): Mean Compton transport cross section.
σ_T (cm^2): Thompson cross section ($8\pi r_0^2/3$).
$\langle\sigma v\rangle$ (cm^3 s^{-1}): Density-normalized reaction rate.
τ: Dimensionless temperature (7.7); also $\tau \equiv \theta_e/m_ec^2$ in § III.
τ_d (s): Dynamical time scale.
τ_R: Ion-electron temperature ratio ($\equiv T_i/T$).
Φ: $\equiv m_ec^2/kT$.
χ: Dimensionless radiation number density ($\equiv 0.9\ n_\gamma/n_0$).

III. SUBSCRIPTS AND SUPERSCRIPTS

0: Preshock value.
1: Postshock or pseudo-downstream value.
ER: Extreme relativistic.
e: Electron value.
f: Final postshock value.
i, p: Ion or proton value.
NR: Nonrelativistic.
γ: Photon value.

APPENDIX B

NUMERICAL SOLUTION METHODS: RADIATION-DOMINATED SHOCK MODEL

The photon continuity equation (5.3) can be written in the form

$$D_1\frac{d^2n_\gamma}{dx^2} + D_2\frac{dn_\gamma}{dx} + D_3n_\gamma = -Q\left(1 - \frac{n_\gamma}{n_{eq}}\right), \tag{B1}$$

where

$$D_1 = \frac{cv}{3n_0v_0\bar{\sigma}_c}, \qquad D_2 = \frac{v^2 - 8v_0v + v_0^2}{6v}, \qquad D_3 = \frac{(7v - v_0)(v_0 - v)}{2vc} n_0v_0\bar{\sigma}_c, \tag{B2}$$

$$n_{eq} \equiv bT_e^3, \qquad Q \equiv \frac{Q_\gamma^{eff}}{1 - n_\gamma/n_{eq}}. \tag{B3}$$

Utilizing a three-point difference scheme on an unequally spaced mesh of points x^i ($i = 1, N$), equation (B1) can be differenced in the form

$$\frac{2D_1^i}{\Delta^i}[\Delta x^{i-1/2}(n_j^{i+1} - n_j^i) - \Delta x^{i+1/2}(n_j^i - n_j^{i-1})] + \frac{D_2^i}{\Delta^i}[(\Delta x^{i-1/2})^2(n_j^{i+1} - n_j^i) + (\Delta x^{i+1/2})^2(n_j^i - n_j^{i-1})]$$

$$+ D_3 n_j^i = -Q_{j-1}^i\left(1 + \frac{3n_{j-1}^i}{n_{eq_{j-1}}^i} - \frac{4n_j^i}{n_{eq_{j-1}}^i}\right), \tag{B4}$$

where i superscripts denote evaluation at point x^i and j subscripts, evaluation at the jth iteration, and where

$$\Delta x^{i-1/2} = x^i - x^{i-1}, \qquad \Delta x^{i+1/2} = x^{i+1} - x^i, \tag{B5}$$

$$\Delta^i = \Delta x^{i+1/2}(\Delta x^{i-1/2})^2 + \Delta x^{i-1/2}(\Delta x^{i+1/2})^2. \tag{B6}$$

The form of the factor multiplying Q_{j-1}^i was derived by linearizing

$$\left(\frac{n_\gamma}{n_{eq}}\right)_j^i \quad \text{about} \quad \left(\frac{n_\gamma}{n_{eq}}\right)_{j-1}^i$$

making use of equation (5.1).

Solving equation (B4) and n_j^i, we find:

$$n_j^i = \frac{n_j^{i+1}(\Delta^i)^{-1}[2D_1^i\Delta x^{i-1/2} + D_2^i(\Delta x^{i-1/2})^2] + n_j^{i-1}(\Delta^i)^{-1}[2D_1^i\Delta x^{i+1/2} - D_2^i(\Delta x^{i+1/2})^2] + Q_{j-1}^i(1 + 3n_{j-1}^i/n_{eq_{j-1}}^i)}{2D_1^i(\Delta x^{i+1/2} + \Delta x^{i-1/2})/\Delta^i + D_2^i[(\Delta x^{i-1/2})^2 - (\Delta x^{i+1/2})^2]/\Delta^i - D_3^i + 4Q_{j-1}^i/n_{eq_{j-1}}^i}, \tag{B7}$$

and define for convenience the coefficients P_1^i, P_0^i, and C^i, so that

$$n_j^i \equiv P_1^i n_j^{i+1} + P_0^i n_j^{i-1} + C^i. \tag{B8}$$

Now let

$$n_j^i = \alpha_j^i n_j^{i+1} + \beta_j^i, \tag{B9}$$

$$n_j^{i-1} = \alpha_j^{i-1} n_j^i + \beta_j^{i-1}. \tag{B10}$$

Here the α_j^i and β_j^i are termed back-substitution coefficients and can be found recursively by substituting equations (B9) and (B10) into equation (B8) in the form

$$\alpha_j^i = \frac{P_1^i}{(1 - P_0^i\alpha_j^{i-1})}, \qquad \beta_j^i = \frac{P_0^i\beta^{i-1} + C^i}{(1 - P_0^i\alpha_j^{i-1})}, \tag{B11}$$

with the boundary conditions that

$$\alpha^{(2)} = P_1^{(2)}, \qquad \beta^{(2)} = P_0^{(2)}n^{(1)} + C^{(2)}, \tag{B12}$$

where we have assumed all quantities are known at $x^{(1)}$.

Having found all the back-substitution coefficients for $i = 2, N - 1$, we can then use equation (B10) together with the assumed known value of $n^{(N)}$ to solve recursively for the unknown n_j^i. Since Q_{j-1}^i and $n_{eq_{j-1}}^i$ rely on previous knowledge of n_{j-1}^i, we must begin our calculation by assuming initial values for the photon density distribution ($n_{(1)}^i$), and then iterating the back-substitution procedure described above until the results converge. Typically, 400 mesh points and 20 iterations are sufficient to achieve an accurate, converged solution.

The ion heating equation (5.5) can be rewritten in the form

$$\frac{d\theta_i}{dx} = H_{comp}\theta_i + H_{visc}\theta_i^{5/2} + H_{ei}(\theta_e - \theta_i), \tag{B13}$$

where

$$H_{comp} = -\frac{2}{3}\frac{1}{v}\frac{dv}{dx}, \qquad H_{visc} = \frac{2}{3}\frac{A_2}{n_0v_0}\left(\frac{dv}{dx}\right)^2, \qquad H_{ei} = 2\frac{n_0v_0}{v^2}\frac{A_1}{\theta_e^{3/2}}, \tag{B14}$$

with dv/dx following analytically from equation (5.6), and θ_e from the solution of the photon continuity equation. Explicitly differencing equation (B13) and linearizing the $\theta_i^{5/2}$ term gives the difference equation

$$\frac{\theta_i^{i+1} - \theta_i^i}{\Delta x^{i+1/2}} = (\theta_i^i)^{3/2} H_{\rm visc}{}^{i+1/2}\left(\tfrac{5}{4}\theta_i^{i+1} - \tfrac{1}{4}\theta_i^i\right) + H_{\rm comp}{}^{i+1/2}\left(\frac{\theta_i^{i+1} + \theta_i^i}{2}\right) + H_{ei}{}^{i+1/2}\left(\theta_e{}^{i+1/2} - \tfrac{1}{2}\theta_i^{i+1} - \tfrac{1}{2}\theta_i^i\right), \tag{B15}$$

where $\theta_e{}^{i+1/2} = \frac{1}{2}(\theta_e{}^{i+1} + \theta_e{}^i)$. This can be solved directly for θ_i^{i+1}, yielding

$$\theta_i^{i+1} = \frac{\theta_i^i + \Delta x^{i+1/2}\left[-\frac{1}{4}H_{\rm visc}{}^{i+1/2}(\theta_i^i)^{5/2} + \frac{1}{2}H_{\rm comp}{}^{i+1/2}\theta_i^i + H_{ei}{}^{i+1/2}\left(\theta_e{}^{i+1/2} - \frac{1}{2}\theta_i^i\right)\right]}{1 - \Delta x^{i+1/2}\left[\frac{5}{4}H_{\rm visc}{}^{i+1/2}(\theta_i^i)^{3/2} + \frac{1}{2}H_{\rm comp}{}^{i+1/2} - \frac{1}{2}H_{ei}{}^{i+1/2}\right]}. \tag{B16}$$

Given $\theta_i^{(1)}$, equation (B16) then yields the remaining θ_i^i. The integration is stable provided $\theta_i^{(1)}$ is taken at the upstream boundary of the shock ($x = x_0$).

APPENDIX C

NUMERICAL SOLUTION METHODS: SIMPLE VISCOUS SHOCK MODELS

Equations (7.1)–(7.2) are differenced in the form

$$n_0 v_0 k\,\frac{T^i + T^{i+1}}{2} - \mu v^i\,\frac{v^{i+1} - v^i}{\Delta x^{i+1/2}} = m n_0 v_0\left[(v_0 - 2v^i)\,\frac{v^{i+1}}{2} + \frac{v_0 v^i}{2}\right] + P_0\left(\frac{v^i + v^{i+1}}{2}\right), \tag{C1}$$

$$\alpha n_0 v_0 k\,\frac{T^i + T^{i+1}}{2} - \kappa\,\frac{T^{i+1} - T^i}{\Delta x^{i+1/2}} = \tfrac{1}{2}m n_0 v_0[(v^i - v_0)v^{i+1} + v_0(v_0 - v^i)] + \alpha_0 P_0 v_0 + \tfrac{1}{2}m n_0 v_0{}^2\epsilon_0[2v_0 - v^i - v^{i+1}], \tag{C2}$$

where the notation of Appendix B has been adopted. T^{i+1} and v^{i+1} are then readily found provided T^i and v^i are known. The integration is started by means of the asymptotic solution derived in § VII*a*, and must proceed from downstream to upstream to be stable.

By multiplying equation (7.23) by $\alpha \equiv (\frac{3}{2} + 3\chi\eta)/(1 + \chi\eta)$, and subtracting the result from equation (7.24), we derive an equation for the required shock dissipation in the form

$$\alpha\mu v\,\frac{dv}{dx} - \lambda_0 v k T n_0\,\frac{d\chi}{dx} - \kappa'\,\frac{dT}{dx} = \tfrac{1}{2}m n_0 v_0[v_0 - v(1 + 2\alpha) + 2(1 + \alpha)\epsilon_0 v_0][v_0 - v] + \epsilon_0(\alpha_0 - \alpha)m n_0 v_0{}^3. \tag{C3}$$

Equations (7.23) and (C3) are then differenced as

$$\left[2 + \frac{\chi^{i+1/2}(v^{i+1} + v^i)}{v_0}\right] n_0 v_0 k T^i - 2\mu v^i\,\frac{(v^{i+1} - v^i)}{\Delta x^{i+1/2}} = m n_0 v_0[v^i v_0 + v^{i+1}v_0 - 2v^i v^{i+1} + 2v^i v_0\epsilon_0], \tag{C4}$$

$$2\alpha^i\mu v^i\,\frac{v^{i+1} - v^i}{\Delta x^{i+1/2}} - \lambda_0 n_0 v^i k(T^{i+1} + T^i)\left(\frac{d\chi}{dx}\right)^{i+1/2} - 2(\kappa')^i\,\frac{(T^{i+1} - T^i)}{\Delta x^{i+1/2}}$$
$$= m n_0 n_0[v_0 - v^{i+1}(1 + 2\alpha^i) + 2(1 + \alpha^i)\epsilon_0 v_0][v_0 - v^i] + 2\epsilon_0(\alpha_0 - \alpha^i)m n_0 v_0{}^3. \tag{C5}$$

Since χ^i is known at all points, these equations can be readily integrated starting from the downstream asymptotic solutions derived in § VII*b*.

APPENDIX D

NUMERICAL SOLUTION METHODS: EFFECTIVE PHOTON SHOCK MODEL

The difference equations used to solve equations (8.1)–(8.2) are given by

$$\left[1 + \tau_R{}^i + \chi^{i+1/2}\,\frac{(v^{i+1} + v^i)}{2v_0}\right] n_0 v_0 k T^i - \mu^i v^i\,\frac{(v^{i+1} - v^i)}{\Delta x^{i+1/2}} = m n_0 v_0\left[v_0\,\frac{(v^{i+1} + v^i)}{2} - v^i v^{i+1}\right] + P_0 v^i, \tag{D1}$$

$$2\alpha^i\mu^i v^i\,\frac{v^{i+1} - v^i}{\Delta x^{i+1/2}} - \lambda_0 n_0 v k(T^{i+1} + T^i)\left(\frac{d\chi}{dx}\right)^{i+1/2} - 2(\kappa')^i\,\frac{(T^{i+1} - T^i)}{\Delta x^{i+1/2}}$$
$$= m n_0 v_0[v_0 - v^{i+1}(1 + 2\alpha^i) + 2(1 + \alpha^i)\epsilon_0 v_0](v_0 - v^i) + 2\epsilon_0(\alpha_0 - \alpha^i)m n_0 v_0{}^3, \tag{D2}$$

where

$$\frac{1}{\alpha} \equiv \frac{1 + \tau_R + \chi\eta}{\alpha_e + \frac{3}{2}\tau_R + 3\chi\eta} . \tag{D3}$$

As in Appendix C, we have first transformed the energy-conservation equation (8.2) into an expression for the required shock dissipation before differencing. These equations are then integrated upstream by the method described in § VIII.

The photon continuity equation (8.3) is solved in the manner described in Appendix B, except that the D_i coefficients in equation (B1) are defined in more general form

$$D_1{}^i = \frac{\lambda_0}{3} v^i , \qquad D_2{}^i = -v^i + \frac{\lambda_0}{3}\left(\frac{dv}{dx}\right)^i , \qquad D_3{}^i = -\left(\frac{dv}{dx}\right)^i . \tag{D4}$$

The ion heating equation, (8.4), is differenced as

$$\begin{aligned} \tfrac{3}{2} n_0 v_0 k T^{i+1/2} \frac{(\tau_R{}^{i+1} - \tau_R{}^i)}{\Delta x^{i+1/2}} + \tfrac{3}{2} n_0 v_0 k \left(\frac{dT}{dx}\right)^{i+1/2} \left(\frac{\tau_R{}^{i+1} + \tau_R{}^i}{2}\right) \\ = -\frac{n_0 v_0}{v^{i+1/2}} k T^{i+1/2} \left(\frac{dv}{dx}\right)^{i+1/2} \left(\frac{\tau_R{}^{i+1} + \tau_R{}^i}{2}\right) + A_2{}^i (k T^{i+1/2})^{5/2} \left[\left(\frac{dv}{dx}\right)^{i+1/2}\right]^2 (\tau_R{}^i)^{5/2} \\ + \left(\frac{n_0 v_0}{v^{i+1/2}}\right)^2 \frac{3 A_1{}^i}{(k T^{i+1/2})^{1/2}} \left[1 - \frac{(\tau_R{}^{i+1} + \tau_R{}^i)}{2}\right] + (\tau_R{}^{-3/2} H_{\alpha p})^{i+1/2} (\tau_R{}^i)^{3/2} , \end{aligned} \tag{D5}$$

and integrated from the upstream to the downstream limit with the boundary condition that $\tau_R = 1$ at the upstream boundary.

The iterative solution of these equations requires that the zoning be sufficiently fine that only a small change in the variables takes place across a zone. It is thus sometimes convenient, though not necessary, to limit the ratio of λ_μ/λ_0 (typically to $\gtrsim 10^{-3}$) in order to reduce the number of zones required.

REFERENCES

Abramowitz, M., and Stegun, I. A., ed. 1964, *Handbook of Mathematical Functions* (Washington: Government Printing Office).
Alme, M. L., and Wilson, J. R. 1974, *Ap. J.*, **186**, 1015.
Arnett, W. D., and Schramm, D. N. 1973, *Ap. J. (Letters)*, **184**, L47.
Becker, R. 1922, *Zs. f. Phys.*, **8**, 321.
Belokon', V. A. 1959, *Soviet Phys.—JETP*, **9**, 235.
Bird, G. A. 1967, *J. Fluid Mech.*, **30**, 479.
Bond, J. W., Watson, K. M., and Welch, J. A. 1965, *Atomic Theory of Gas Dynamics* (Reading, Mass.: Addison-Wesley).
Burgers, J. M. 1960, in *Plasma Dynamics*, ed. F. H. Clauser (Reading, Mass.: Addison-Wesley), pp. 119–186.
Chapline, G. F., and Stevens, J. 1973, *Ap. J.*, **184**, 1041.
Chevalier, R. A. 1976, preprint submitted to *Ap. J.*
Chiu, H.-Y. 1968, *Stellar Physics* (Waltham, Mass.: Blaisdell).
Clayton, D. D. 1968, *Principles of Stellar Evolution and Nucleosynthesis* (New York: McGraw-Hill).
Colgate, S. A. 1969, in *Proc. 11th Intern. Conf. Cosmic Rays* (Budapest: Akademiai Kiado).
———. 1973, *Ap. J. (Letters)*, **181**, L53.
———. 1974, *Ap. J.*, **187**, 321.
———. 1975*a*, *ibid.*, **195**, 493.
———. 1975*b*, in *Origin of Cosmic Rays*, ed. J. L. Osborne and A. S. Wolfendale (Dordrecht: Reidel), pp. 425, 447.
Colgate, S. A., and Johnson, M. H. 1960, *Phys. Rev. Letters*, **5**, 235.
Cooper, G. 1971, *Phys. Rev. D*, **3**, 2312.
———. 1974, *J. Quant. Spectrosc. and Rad. Trans.*, **14**, 887.
Drummond, J. E. 1961, *Plasma Physics* (New York: McGraw-Hill), p. 319.
Epstein, R. I., Arnett, W. D., and Schramm, D. N. 1974, *Ap. J. (Letters)*, **190**, L13.
Falk, S. W., and Arnett, W. D. 1973, *Ap. J. (Letters)*, **180**, L65.
Fediushin, B. K. 1952, *Zh. Eksper. i Teoret. Fiz.*, **22**, 140.
Fowler, W. A., Caughlan, G. R., and Zimmerman, B. A. 1975, *Ann. Rev. Astr. and Ap.*, **13**, 69.
Gott, J. R., Gunn, J. E., Schramm, D. N., and Tinsley, B. M. 1974, *Ap. J.*, **194**, 543.
Gould, R. J. 1975, preprint.
Hoyle, F., and Fowler, W. A. 1973, *Nature*, **241**, 384.
Iben, I. 1973, in *Explosive Nucleosynthesis*, ed. D. N. Schramm and W. D. Arnett (Austin: University of Texas Press), p. 115.
Jackson, J. D. 1962, *Classical Electrodynamics* (New York: Wiley).
Jaffrin, M. Y., and Probstein, R. F. 1964, *Phys. Fluids*, **7**, 1658.
Jauch, J. M., and Rohrlich, F. 1955, *Theory of Photons and Electrons* (Cambridge: Addison-Wesley).
Johnson, M. H., and McKee, C. F. 1971, *Phys. Rev. D*, **3**, 858.
Landau, L. D., and Lifshitz, E. M. 1959, *Fluid Mechanics* (London: Pergamon).
Mandl, F., and Skyrme, T. H. R. 1952, *Proc. Roy. Soc. Ser. A*, **215**, 497.
Maxon, S. 1972, *Phys. Rev. A*, **5**, 1630.
McKee, C. F. 1970, Ph.D. thesis, University of California, Berkeley.
Minorsky, N. 1947, *Introduction to Non-Linear Mechanics* (Ann Arbor: Edwards Brothers), pp. 9–23.
Quigg, C. 1968, *Phys. Fluids*, **11**, 461.
Ram, M., and Wang, P. Y. 1971, *Phys. Rev. Letters*, **26**, 476.
Reeves, H. 1974, *Ann. Rev. Astr. and Ap.*, **12**, 437.
Rogerson, J. B., Jr., and York, D. G. 1973, *Ap. J. (Letters)*, **186**, L95.
Shapiro, S. L., and Salpeter, E. E. 1975, *Ap. J.*, **198**, 671.
Shklovsky, I. S. 1968, *Supernovae* (New York: Interscience).
Silk, J. I. 1974, in *IAU Symposium 63, Confrontation of Cosmological Theories with Observational Data*, ed. M. S. Longair (New York: Reidel), p. 175.
Spitzer, L. 1962, *Physics of Fully Ionized Gases* (New York: Interscience).
Stone, S. 1971, UCRL-73424 (Lawrence Livermore Laboratory).
———. 1973, UCRL-75101 (Lawrence Livermore Laboratory).
Stone, S., and Nelson, R. G. 1966, UCRL-14918-T (Lawrence Livermore Laboratory).
Stringer, T. E. 1964, *Plasma Phys.*, **6**, 267.

Tidman, D. A., and Krall, N. A. 1971, *Shock Waves in Collisionless Plasmas* (New York: Wiley-Interscience).
Weaver, T. A. 1976, *Phys. Rev. A*, **13**, 1563.
Weaver, T. A., and Chapline, G. F. 1974, *Ap. J. (Letters)*, **192**, L57.
Weaver, T. A., Chapline, G. F., Wood, L. L., and Silk, J. I. 1974, *Bull. Am. Phys. Soc.*, **6**, 274.
Zel'dovich, Ya. B., and Raizer, Yu. P. 1966, *Physics of Shock Waves and High-Temperature Hydrodynamic Phenomena* (New York: Academic).
Zel'dovich, Ya. B., and Shakura, N. I. 1969, *Soviet Astr.—AJ*, **13**, 175.

THOMAS A. WEAVER: L-75, Lawrence Livermore Laboratory, University of California, P.O. Box 808, Livermore, CA 94550